UNIVERSITÀ DEGLI STUDI DI TORINO

DIPARTIMENTO DI NEUROSCIENZE

DOTTORATO DI RICERCA IN NEUROSCIENZE

CICLO XXXIII

TITOLO DELLA TESI: Spinocerebellar ataxia 38: the role of Elovl5 in central and peripheral nervous system

TESI PRESENTATA DA: Ilaria Balbo

TUTOR: Prof. Filippo Tempia

COORDINATORE DEL DOTTORATO: Prof. Andrea Calvo

ANNI ACCADEMICI: 2017-2021

SETTORE SCIENTIFICO-DISCIPLINARE DI AFFERENZA: BIO/09

ABSTRACT

ELOVL5 (ELOngation of Very Long-chain fatty acids) encodes for an enzyme necessary to synthetize omega-3 and omega-6 very long polyunsaturated fatty acids (PUFAs), which are precursors for longer PUFAs, including arachidonic acid (ARA, ω6), docosahexaenoic acid (DHA, ω3) and their derivatives. It belongs to a family of multi-pass transmembrane proteins (ELOVL1-7) which rose discreet interest in recent years because of the link found with various nervous system diseases, including movement and cognitive disorders. Missense mutations of *ELOVL5* cause the spinocerebellar ataxia (SCA) type 38, a recently discovered rare form of ataxia which, besides gait abnormalities, aphagia, aphasia and nystagmus, affects patients with hyposmia, peripheral neuropathy and cerebellar atrophy. In three decades from the diagnosis, patients are not able to feed themselves anymore nor to walk. The administration of DHA as therapeutical approach has been shown to just slow down the progression, but not to ameliorate patient lifestyle. Recently, studies on *Elovl5*$^{-/-}$ mice demonstrated that this model well represents SCA38. In fact, compared to control littermates, this mouse model shows the same symptoms and the same pathological features also showed by SCA38 patients. This PhD thesis is aimed at deepening the knowledge on the role of Elovl5 in the central nervous system (CNS) and in the peripheral nervous system (PNS), by assessing the consequences of its loss in these mice with a targeted deletion of the gene. Since very little is known about the precise localization of this enzyme in brain, *Elovl5* expression in mouse CNS slices and different cell cultures was assessed. We found that *Elovl5* is highly expressed by neurons in the central nervous system, especially in cerebellum, vestibular nuclei and olfactory bulb, in agreement with the main symptoms of SCA38. *Elovl5* is also expressed by oligodendrocytes, Schwann cells and microglia. This is in line with the finding, in *Elovl5*$^{-/-}$ mice, of alterations of myelin sheaths structure, detected by electron microscopy, accompanied by impairment of action potential conduction in peripheral nerves. At central level, *Elovl5* loss did not greatly alter cerebellar circuits functionality, except for a slight impairment in neurotransmitter release by glutamatergic fibers during high frequency activity. In addition, both endocannabinoid-dependent synaptic plasticity and action potential propagation along Purkinje cell axons were altered, partially explaining the motor impairment observed in *Elovl5*$^{-/-}$ mice. Rebalancing the lipidic profile by a diet containing PUFAs downstream of Elovl5, ameliorated motor performance of *Elovl5*$^{-/-}$ mice. Although this administration is not enough to induce structural amelioration in cerebellar atrophy. These

findings showed alterations in both neuronal and glial cells functioning and could partially explain the motor impairment observed in *Elovl5*$^{-/-}$ mice and SCA38 patients. These data taken together provide a more accurate understanding of Elovl5 physiological role in CNS and PNS and give a more detailed insight on the pathological alterations caused by its loss. Moreover, the preliminary results obtained by rebalancing the diet in *Elovl5*$^{-/-}$ mice suggest that an early-started and complete diet supplementation could counteract the progression of the SCA38 and might be used as a guideline for an optimized clinical trial.

INDEX

CHAPTER 1 – INTRODUCTION

1.1 The cerebellum

1.1.1 The cerebellar anatomy

1.1.2 Cytoarchitecture of the cerebellum

1.1.3 Purkinje cells: the central players in cerebellar circuitry

1.1.4 Cerebellar circuitry

1.1.5 Synaptic plasticity in the cerebellum

1.1.6 The cerebellum and the motor learning

1.2 Hereditary ataxias

1.2.1 Autosomal dominant spinocerebellar ataxias

1.2.2 Spinocerebellar ataxia 38

1.2.3 SCA38 therapeutic approach

1.2.4 Elovl5$^{-/-}$ mice as a model for the study of SCA38

1.3 ELOVL family genes

1.3.1 ELOVL5

1.3.2 Other ELOVL family genes and their associations with human diseases

1.4 Polyunsaturated fatty acids (PUFAs)

1.4.1 PUFAs synthesis

1.4.2 PUFA transport into brain

1.4.3 PUFAs physiological functions in brain

AIM OF THE THESIS

CHAPTER 2 – MATHERIALS AND METHODS

2.1 Animals

2.1.1 Mice feeding

2.1.2 Genotyping mice

2.2 Immunohistochemistry, immunofluorescence and electron microscopy

2.2.1 Tissue preparation

2.2.2 Immunofluorescence reactions

2.2.3 Immunohistochemistry

2.2.4 Images Acquisition and Processing

2.2.5 High resolution light microscopy and transmission electron microscopy

2.3 RNA and protein quantification

2.3.1 Magnetic-Activated Cell Sorting (MACS) Isolation of Oligodendrocytes and Cell Culture Procedures

2.3.2 Quantitative RT–PCR

2.3.3 Western blot assay

2.4 Electrophysiological recordings

2.4.1 Current clamp recordings

2.4.2 PC intrinsic membrane excitability

2.4.3 Responses of PCs to PF stimulation

2.4.4 mGlu1-mediated slow EPSC

2.4.6 Synaptically induced suppression of excitation (SSE)

2.4.7 Long-term depression (LTD)

2.4.8 Responses of PCs to CF stimulation

2.4.9 Antidromic action potential conduction

2.4.10 Caudal nerve conduction velocity

2.5 Lipidic analysis

2.5.1 Liquid chromatography–tandem mass spectrometry analysis

2.6 Behavioral study

2.6.1 Balance beam test

2.7 Statistical Analysis

CHAPTER 3 – RESULTS

3.1 Elovl5 Expression in the Central Nervous System of the Adult Mouse (Balbo et al., 2021)

3.1.1 Elovl5 Gene Expression in the Central Nervous System

3.1.2 Elovl5 Protein Distribution in Brain Regions

3.1.2.1 Elovl5 distribution in the telencephalon

3.1.2.2 Elovl5 presence in diencephalon

3.1.2.3 The expression of Elovl5 in brainstem

3.1.2.5 Elovl5 in the cerebellum

3.1.2.6 Elovl5 localization in spinal cord

3.1.3 Elovl5 Expression in Glial Cells

3.2 Elovl5 is required for proper action potential conduction along peripheral myelinated fibers (Hoxha et al., 2021)

3.2.1 ELOVL5 expression in peripheral myelin

3.2.2 Structural alterations of sciatic nerve of Elovl5$^{-/-}$ mice

3.2.3 Increased nodal gap and paranode length in sciatic nerves of Elovl5$^{-/-}$ mice

3.2.4 Reduced action potential propagation in peripheral axons of Elovl5$^{-/-}$ mice

3.2.5 Myelin proteins in sciatic nerve of Elovl5$^{-/-}$ mice

3.2.6 Phospholipid profile of Elovl5$^{-/-}$ sciatic nerve

3.3 The role of Elovl5 in cerebellar circuitry

3.3.1 Preserved intrinsic properties of PCs in Elovl5$^{-/-}$ mice
3.3.2 Conserved excitatory postsynaptic current of PF-PC synapse in Elovl5$^{-/-}$ mice
3.3.3 Conserved excitatory postsynaptic current of CF-PC synapse in Elovl5$^{-/-}$ mice
3.3.4 mGlu1-mediated slow EPSC is conserved in Elovl5$^{-/-}$ mice
3.3.5 Altered short-term plasticity endocannabinoid-dependent in Elovl5$^{-/-}$ mice
3.3.6 Maintained long term-depression in Elovl5$^{-/-}$ mice
3.3.7 Quantification of axon terminals
3.3.8 Increased nodal gap and paranode length in cerebellar axon of Elovl5$^{-/-}$ mice
3.3.9 Reduction of action potential antidromic propagation in Elovl5$^{-/-}$ mice

3.4 PUFA-enriched diet supplementation as possible therapeutic approach for SCA38
3.4.1 Progression of motor impairment with PUFA precursors diet
3.4.2 Effects of the administration of a complete PUFA diet since birth
3.4.3 Effects of the administration of a complete PUFA diet at later ages
3.4.4 Effects of the complete PUFA diet on the cerebellar morphological parameters

CHAPTER 4 – DISCUSSION

4.1 Elovl5 expression in the Central Nervous System is region- and cell-type specific (Balbo et al., 2021)

4.2 Elovl5 presence is essential for proper action potential propagation in peripheral myelinated fibers (Hoxha et al., 2021)

4.3 Elovl5 loss influences the correct function of the cerebellar circuitry

4.4 PUFA-enriched diet supplementations as a possible therapeutic approach for SCA38

CHAPTER 5 – GENERAL CONCLUSIONS AND FUTURE PERSPECTIVES

CHAPTER 6 – REFERENCES

CHAPTER 1 - INTRODUCTION

1.1 The cerebellum

1.1.1 The cerebellar anatomy

The cerebellum is a region of the brain located below the occipital lobe and dorsal to the brainstem, in the posterior cranial fossa and covered by the *tentorium cerebelli*. It is separated from the pons by the fourth ventricle, while it is connected to the brainstem by three bundles of fibers called cerebellar peduncles: the superior, the middle and the inferior cerebellar peduncles (Standrings, 2015). The cerebellum is composed of an outer part of grey matter, called cerebellar cortex, which overlays an inner part of white matter with lots of convolutions, forming structures called *folia* that cross the cerebellum from one side to the other. Deeper fissures divide the cerebellum into three lobes. The primary fissure separates the anterior from the posterior lobe while the posterolateral fissure delineates a much smaller lobe called the flocculonodular lobe. Moreover, superficial fissures divide every lobe into smaller lobules **(Fig. 1)**. It is also possible to distinguish three main longitudinal regions: a midline vermis and two lateral hemispheres that can be divided into intermediate and lateral portions (Kandel et al., 2013). By considering the different input sources, the cerebellum could be divided into three main parts: the cerebrocerebellum, the spinocerebellum and the vestibulocerebellum. The cerebrocerebellum receives inputs, via pontine nuclei, from various areas of cerebral cortex and it's involved in planning and executing complex spatial and temporal sequences of movement. The spinocerebellum receives inputs from the spinal cord. Its most lateral part is concerned with the movement of distal muscles, while its medial part, the vermis, is concerned with movement of proximal muscles, including oculomotor muscles. The vestibulocerebellum receives input from vestibular nuclei in the brainstem and it's enrolled in the control of movements underlying posture and balance (Eccles et al., 1967; Ito, 1984).

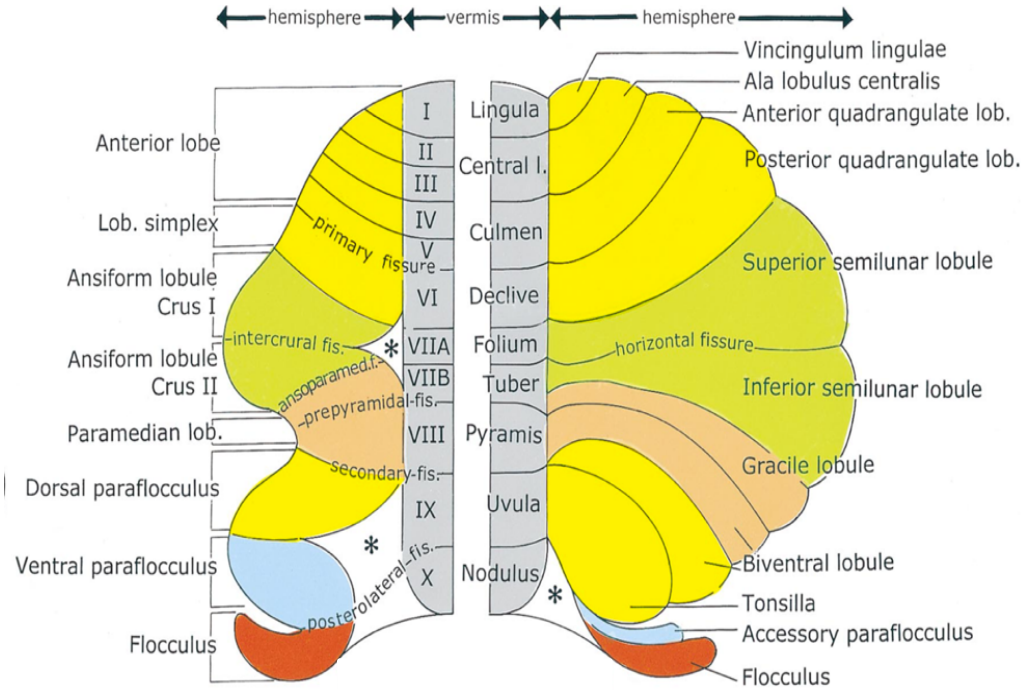

Figure 1. **Mammalian and human cerebellum.** Comparative anatomical nomenclature for the mammalian cerebellum is shown on the left, the nomenclature for the human cerebellum on the right. Homologue lobules are indicated with same colors *(Modified from Voogd, J. & Glickstein, M., 1998).*

1.1.2 Cytoarchitecture of the cerebellum

The cerebellum has a highly regular structure with repeating functional units (Kandel et al., 2013). The cerebellar cortex can be divided into three layers: the granule cell layer, the Purkinje cell layer and the molecular layer **(Fig. 2A-C)**. In these layers seven types of neurons can be observed, with specific spatial arrangements and functions: Purkinje cells (PCs), granule cells, Golgi cells, Lugaro cells, basket cells, stellate cells and unipolar brush cells (Cerminara et al., 2015) **(Fig. 2D)**. The granular layer, the deepest section of cerebellar cortex, is composed of Golgi, Lugaro and granule cells mainly. Golgi cells, the largest interneuron of the granular layer, present two or three apical dendrites and a widely ramified axon (D'Angelo et al., 2013). Differently from basket and stellate cells, which are GABAergic interneurons, Golgi cells present a mixed GABA/glycine transmission (D'Angelo and Casali, 2013). Lugaro cells are located at the upper border of the granular layer and their axon arises from the proximal portion of a dendrite dividing then into two branches. Lugaro cells have a GABAergic transmission and the postsynaptic targets of their axon in the molecular layer are stellate and basket interneurons (Lainé and Axelrad, 1998). Granule cells are small, glutamatergic neurons, considered as the

most numerous elements in the cerebellar cortex. Their axons ascend towards the molecular layer, then bifurcate and terminate on dendrites of PCs and interneurons (Voogd and Glickstein, 1998). Granule cells are regulated by Golgi cells with feedback and feedforward mechanisms (D'Angelo and Casali, 2013). The PC layer is localized in between the molecular and the granular layer. In the PC layer, PCs are disposed linearly (Cerminara et al., 2015). PCs are very large GABAergic neurons, which provide the only source of output from the cerebellar cortex (Voogd and Glickstein, 1998). They have a complex dendritic tree extending into the molecular layer and a very long axon, which forms inhibitory synapses with cells of deep nuclei in white matter (D'Angelo and Casali, 2013). The molecular layer is the superficial portion of the cortex and it mainly contains two types of GABAergic interneurons, the stellate and basket cells, which regulate PC activity. Bergmann glia can be found in this area as well (Voogd and Glickstein, 1998). The Bergmann glia is composed of unipolar astrocytes which locate their cell bodies around PCs and extend radial enwrapping processes on PC dendrites (Yamaba and Watanabe, 2002). The molecular layer is built up mainly by PC dendritic arborizations and by the densely packed thin axons arising from granule cells, called parallel fibers (PF), which bifurcate to form T-shaped branches (Eccles et al., 1967). The deep nuclei are subcortical groups of cells laying in the cerebellar white matter. Three groups of deep nuclei can be distinguished: the fastigial, the interposed and the dentate (Eccles et al., 1967; Ito, 1984). They receive inputs from the cerebellar cortex and are the major source of outputs from the cerebellum. Therefore, PCs from the cerebellar cortex send their axons to the deep cerebellar nuclei first, and, from there, the information is further forwarded to other regions of the nervous system.

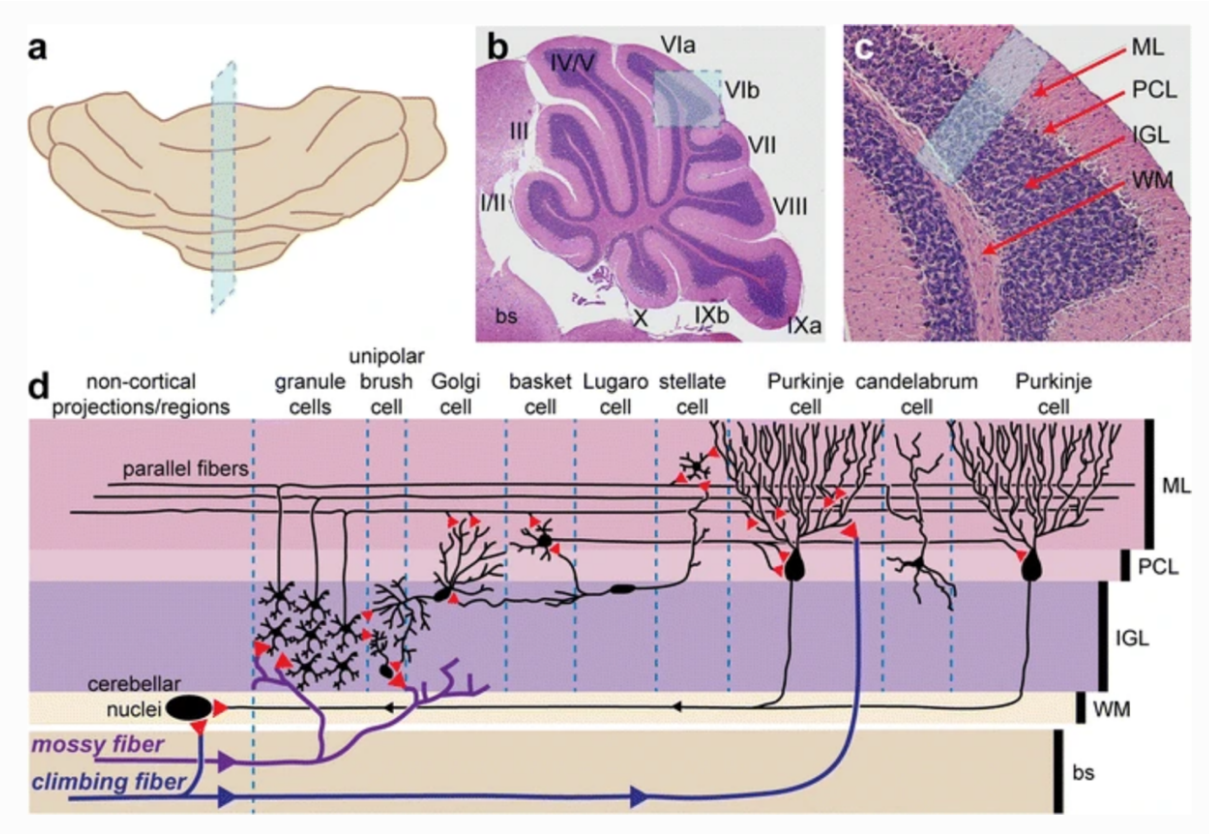

Figure 2. Cerebellar cytoarchitecture. (a) Mature cerebellum. The position of the shaded box indicates a sagittal cross-section illustrated in **(b)** by hematoxylin and eosin staining. The subdivision of the cerebellar vermis into ten major lobules, with each lobule demarcated by a Roman number. **(c)** Further magnification of lobule VIb (blue shaded box in **(b)**) shows the three cortical layers of the cerebellum. The molecular layer (ML), Purkinje cell layer (PCL), and the granular layer (IGL) that reside upon the white matter (WM). **(d)** The schematic representation shows the eight neuronal cell types (labeled on top row with soma contained between blue dotted lines) present in the mature cerebellum and their corresponding locations in the cortex. The two main types of external afferents (mossy and climbing) that project from the brain stem (bs) into the cerebellum have been included on the far left as non-cortical projections/regions. The axons of granule cells bifurcate into a T-shaped structures called parallel fibers. Red triangles denote innervation. *(Constantin, 2017)*

1.1.3 Purkinje cells: the central players in cerebellar circuitry

As sole output of the cerebellar cortex, *PCs* are considered the most functionally important cells in the cerebellum. They have the unique characteristic in the central nervous system (CNS) to produce two different types of action potential: simple and complex spikes. Simple spikes are high-rate firing action potentials (30 to 100 Hz) which are generated spontaneously or result from the excitation of parallel fibers (PFs), via mossy fibers (MFs) stimulation (Eccles et al., 1967; Cerminara et al., 2015; Palmer et al., 2010). The activation of the PFs leads in the PC to small and brief excitatory postsynaptic potential (EPSP), which diffuse passively (Ito, 1984). In contrast complex spikes are low-rate impulses (1-4 Hz) which arise initially like an action potential, which is usually followed by small spikelets (Eccles et al., 1967; Cerminara et al., 2015; Palmer et al., 2010). Differently from simple spikes, complex spikes are generated by big depolarizations induced by the activation of the climbing fibers (CFs) from the inferior olive (Eccles et al., 1967). Despite these basal characteristics, regional differences in PCs have been long known to exist. Therefore, PCs have different soma and axonal diameter, they show different morphology of dendritic arborization from apex to the base of each lobule and they are also different in number, either in different regions of the cerebellum (greater density packaging in anterior than in posterior lobules) and inside the same lobule (fewer PCs in the base of each lobule than at the apex) (Braitenberg et al., 1958; Armstrong et al., 1970; Nedelescu et al., 2013) **(Fig. 3A and B)**. In addition to morphological differences, PCs also show variation in gene expression. The most known one is zebrin II (also known as the enzyme involved in glycolysis, aldolase C) (Brochu et al., 1990; Ahn et al., 1994). The expression of zebrin II is in rostrocaudally oriented stripes (Brochu et al., 1990; Ahn et al., 1994; Fujita et al., 2014). Zebrin II presence is accompanied by the expression of various other molecular markers such as the glutamate transporter EEAAT4, the phospholipase C beta 3 (PLCβ3) for zebrin II-positive PCs, and phospholipase C beta 4 (PLCβ4) and metabotropic glutamate receptor 1 beta (mGluR1β) for zebrin II-negative ones (Sarna et al., 2006) **(Fig. 3C)**. Such a heterogeneity in molecular marker expression is reflected by heterogenous physiology and intrinsic properties of PCs. Zebrin II-negative PCs show higher firing frequencies than the ones belonging to a zebrin II-positive region, which instead present a high irregularity of simple spike firing (Xiao et al., 2014) (**Fig. 3C**). Furthermore, complex spikes of zebrin II-positive PCs display less capacity to activate mGluRs and so to induce plasticity in the PF-PC synapse. EAAT4 expression in these cells leads to a limited duration of glutamate action at CFs and PFs synapses (Wadiche et al., 2005).

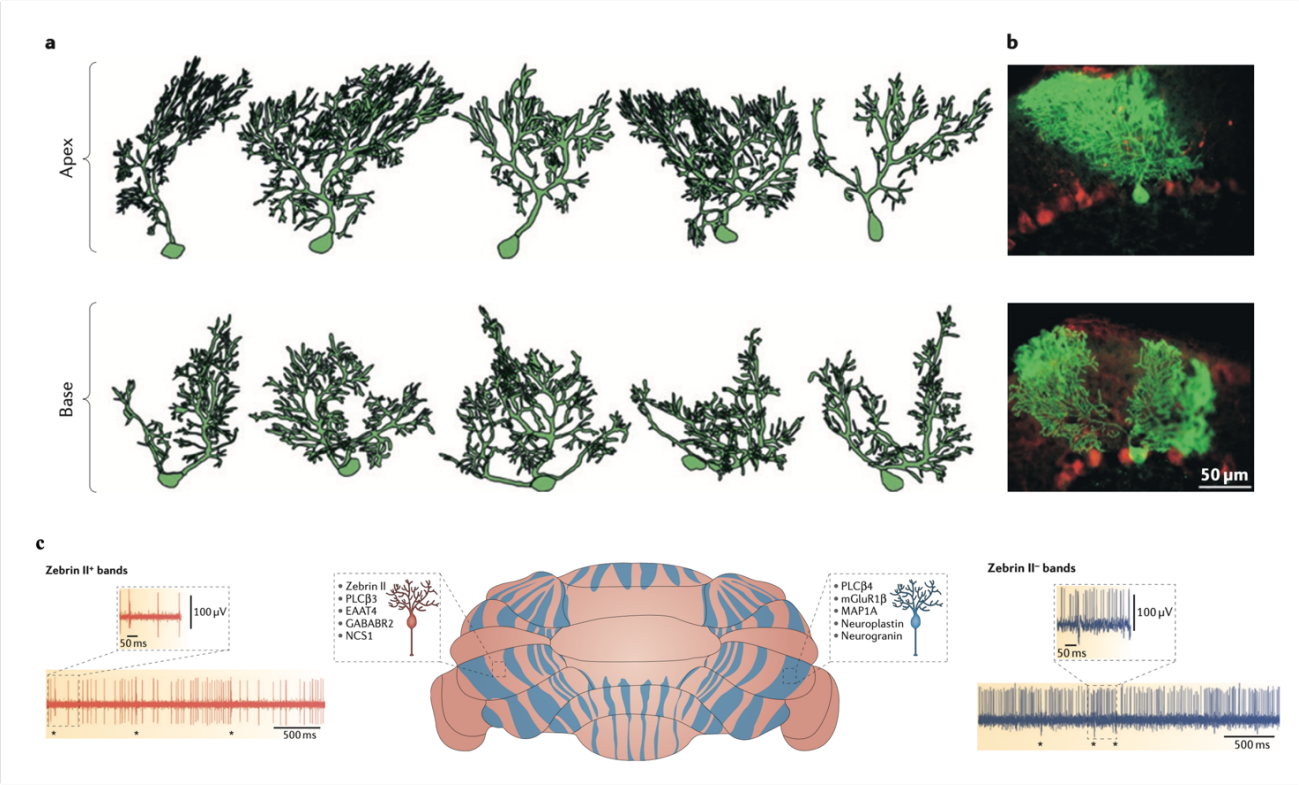

Figure 3. PCs heterogeneity. (a) Drawings representing representative morphologies of Purkinje cells present in the apex (upper panel) and base (lower panel) of cerebellar folia in adult mice. **(b)** GFP-marked PCs (green) among anti-calbindin stained ones (red), showing the complexity of the dendritic tree along the molecular layer. **(c)** Schematic illustration showing alternating bands of zebrin II expression. Colocalization of zebrin II+ Purkinje cells (pink) and zebrin II– Purkinje cells (blue) with various other molecular makers (EAAT4, excitatory amino acid transporter 4; GABABR2, GABA B receptor subtype 2; MAP1A, microtubule-associated protein 1A; mGluR1β, metabotropic glutamate receptor 1β; NCS1, neuronal calcium sensor 1; PLCβ3, phospholipase Cβ3). Laterally there is a schematic representation of their electrophysiological properties obtained through extracellular recordings of Purkinje cells belonging to zebrin II– and zebrin II+ bands. Complex spikes are indicated by asterisks, while insets show expanded spike trains. Zebrin II– Purkinje cells have higher simple spike firing rates. *(Modified from Cerminara et al. 2015)*

1.1.4 Cerebellar circuitry

PCs in the cerebellar cortex receive inputs from two pathways: from MFs, via granule cells and PFs, and from CFs. The MF pathway brings information from many regions of brainstem and spinal cord (in mice, pontine nuclei, vestibular nuclei, lateral reticular nuclei, and external cuneate nucleus). The terminal of each MF axon is anatomically recognizable as rosettes located within the granular layer and contact hundreds of granule cells (Eccles 1967; Konnerth et al., 1990). From these cells, many granule cell axons depart, ascending through the molecular layer, bifurcate and form synapses with PCs, contacting spines on secondary and tertiary branches of the dendritic tree (Strata and Rossi, 1998) **(Fig. 4)**. Every PC receives inputs from more than 100,000 PFs. In PF-PC synapses the release of glutamate, which binds AMPA (α-amino-3-hydroxy-5-methyl-4-isoxazolepropionic acid receptor) and mGluR1 (metabotropic glutamate receptor 1), generates a small and brief excitatory post synaptic potential (EPSP) (Ito, 2006; Hoxha et al., 2016). While a low frequency signal only activates AMPA receptors and generates a fast EPSP, a burst stimulation also activates mGluR1 and generates a slow EPSP resulting in PC depolarization and increase in dendritic calcium concentration (Tempia et al., 1998; Hoxha et al., 2016). Thousands of synapses from PFs can strongly influence action potential generation in PCs, thanks to the temporal and spatial summation of the EPSPs (Eccles et al., 1967). The CF pathways, on the contrary, leads to a one-to-one transmission: every PC receives input from a single CF (Konnerth et al., 1990). CFs originate from the inferior olive in medulla oblongata and contact PCs spines on primary dendrites (Strata and Rossi, 1998) **(Fig. 4)**. This strict correspondence between CF and PC gives rise to an all-or-none EPSP because the only CF fires an action potential only if the strength of the stimulus reaches a specific threshold so that either it occurs fully or it does not occur at all (Eccles et al., 1966; Ito, 1984). CFs make synapses along the entire dendritic tree of PCs and their activation results in a widespread depolarization of PC dendrites, reaching the threshold for the activation of voltage gated calcium channels and generating the complex spike (Konnerth et al., 1992; Miyakawa et al., 1992). PC activity is modulated also by interneurons. Basket cells form inhibitory synapses with PCs by contacting their soma, while stellate cells receive input from PFs and directly inhibit PCs by forming synapses at dendric level (Purves et al., 2004). Finally, Golgi cells receive signals from PFs and act by giving inhibitory feedback to granule cells, so indirectly modulating PCs (Purves et al., 2004).

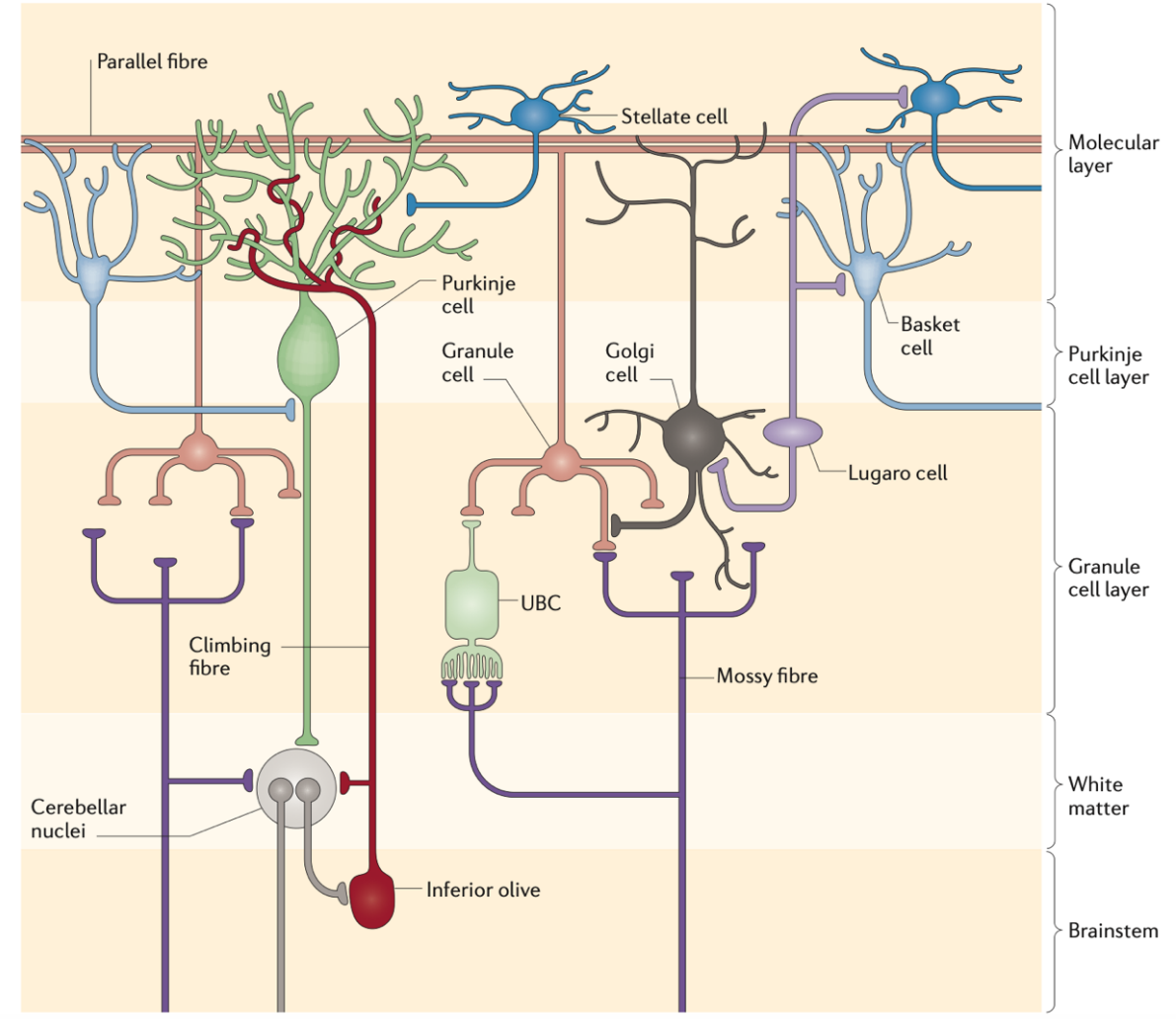

Figure 4. Cerebellar circuitry. The two main types of afferents that project to the cerebellum are the climbing fibers, which synapse directly with Purkinje cells, and the mossy fibers, which synapse with granule cells. The axons of the granule cells ascend up to the molecular layer, where they bifurcate in a T-type manner to form parallel fibres, which extend for several millimetres along the folia of cerebellar lobules. *(Adapted from Cerminara et al. 2015)*

1.1.5 Synaptic plasticity in the cerebellum

Synaptic plasticity is a process consisting of changes in the strength of the contacts occurring among neurons, in response to increase or decrease of the activity of their synapses. There are two main forms of synaptic plasticity: short-term plasticity and long-term plasticity. Short-term plasticity lasts a few minutes or less. Synaptic facilitation is an example of short-term plasticity that induces a rapid increase in synaptic strength after two or more action potential stimulations within few milliseconds of each other (Konnerth et al., 1990). This phenomenon is due to the presence of residual calcium in the presynaptic element so that, when the second stimulus is

applied, it causes release of an increased number of vesicles. The opposite form of short-term plasticity that can occur is short-term synaptic depression. This event consists of a reduced release of neurotransmitter during sustained synaptic activity. Depression is caused by progressive depletion of the pool of presynaptic vesicles that are available for release and lasts several seconds (Konnerth et al., 1990). In contrast, the long-term plasticity can induce changes that persist for weeks, months, or years. A long-lasting increase in synaptic strength is known as long-term potentiation (LTP), whereas other patterns of activity produce a long-lasting decrease in synaptic strength, called long-term depression (LTD). In the cerebellum, these are mechanisms with a leading role in motor learning and they occur at multiple cerebellar synapses, including those on Purkinje cells (Ito, 2000). When PFs are stimulated with two sequential stimuli and a short interval (up to 300 milliseconds) between them, facilitation occurs in response to the second PF stimulation. (Konnerth et al., 1990). If we increase the time interval between the two stimuli (greater than 300 milliseconds), no facilitation is observed in response to PF stimulation (Konnerth et al., 1990). Otherwise, when CFs are stimulated with a short interval, the second response in PCs is depressed and this is due to vesicles depletion at the presynaptic terminal (Konnerth et al., 1990). This depression lasts for several seconds (Konnerth et al., 1990). Increasing the time gap between two CF stimuli (few seconds) allows for the recovery of the response to the second stimulation (Konnerth et al., 1990).

1.1.6 The cerebellum and motor learning

Motor learning is the capacity of the brain to acquire new movements and skills to perform them through practice, and it involves many brain areas. The cerebellum is mainly involved in the learning of accurate and fluent movements, and in performing them rapidly even without visual feedbacks (Ito, 2000). During this process, the cerebellum is necessary to maintain muscular tone and strength, rapidly starts movements, optimizes and memorizes them. Neurons respond selectively to various aspects of movement, including relaxation or contraction of specific muscles, the position of the joints, and the direction of the next movement that will occur. From an electrophysiological point of view, when a novel movement needs to be learned or an old one needs to be modified, the CF fires a spike. The PF/PC synapse that are activated at the same time are potentiated or depressed (Marr, 1969; Albus, 1971; Zang and de Schutter, 2019). If actions are not performed correctly, the cerebellum can selectively modify the synapse with the PF that brings the information and change the output from PC. In simple situations such as reflexes, CFs

convey sensory signals, such as those evoked by a sudden loud sound or pain. These sensory signals suggest a harmful consequence of an inadequately executed movement (Ito, 2000). In fact, error signals arising induce the concomitant activation of the CF and the PF synapse and the latter one undergoes LTP or LTD, reshaping the neuronal circuit of the cerebellum in the direction that minimizes errors (Ito and Kano, 1982; Ito, 2000). All this information is encoded by changes in the discharge pattern of PCs, which modulates the activity of the deep cerebellar nuclear cells. Cerebellar lesions and disease tend to disrupt the modulation and coordination of ongoing movements.

1.2 Hereditary ataxias

The word ataxia means ‘absence of order’, and it is commonly used to indicate a group of motor disorders caused by cerebellar dysfunction. The main signs and symptoms of these diseases consist of cerebellar atrophy, slowly but progressive incoordination of gait mainly associated with poor coordination of hands, speech, and eye movements (Jayadev and Bird, 2013). The ataxias can be of genetic or not genetic origin. Among genetic forms, the hereditary ataxias are a highly heterogeneous group of disorders, which can be inherited through four different modalities: autosomal dominant, autosomal recessive, X- linked, due to maternal inheritance of mitochondrial DNA mutations (Jayadev and Bird, 2013).

1.2.1 Autosomal dominant spinocerebellar ataxias

Autosomal dominant spinocerebellar ataxias (SCAs) are heterogeneous autosomal dominantly inherited diseases, distinguished in more than 40 subtypes (Klockgether et al., 2019). The term “spinocerebellar” refers to the involvement of the brainstem and spinal cord in these cerebellar diseases. However, the spinal cord is unaffected in many SCAs, and pathological alterations occur in other regions of the nervous system, including peripheral nerves and the brainstem and basal ganglia (Klockgether et al., 2019). The principal clinical manifestations of all SCAs are a progressive loss of balance and coordination accompanied by slurred speech and swallow difficulties. Commonly, the onset occurs in mid-adulthood, but manifestation in old age and childhood is possible, by impairing the quality of living and leading to premature death (Durr, 2010; Klockgether et al., 2019). SCAs can be distinguished into three types on the base of the genetic mechanism: (a) polyglutamine expansion ataxia, due to an expansion of glutamine-coding CAG repeats; (b) ataxia caused by repeat expansion of a non-coding sequence and (c) ataxia caused by conventional mutation in critical genes (Hekman and Gomez, 2015). Polyglutamine expansion SCAs are the most common ones and are caused by translated CAG repeat expansion mutations that encode stretches of pure glutamine in the disease proteins. These disorders manifest above a threshold of CAG repeats that varies depending on the gene. The longer is the repeat, the greater is the severity and earlier the onset of the disease (Durr, 2010; Klockgether et al., 2019). Expansion repeat length leads to translation of expanded abnormal PolyQ repeat, which leads to protein misfolding. Misfolded proteins then form aggregates that trigger various cellular process dysfunctions, leading to cell toxicity and degeneration (Hekman and Gomez, 2015). Ataxias due to a repeat expansion of a non-coding sequence are caused by

non-coding repeat expansions, that are expanded repeat tracts identified outside of the recognized protein coding regions, such as in introns or 5'. This alteration leads to a gain of function mechanism, triggered by the accumulation of transcripts containing expanded CUG or CCUG repeats (Durr, 2010; Hekman and Gomez, 2015). Lastly, ataxia caused by conventional mutations (missense, deletion, insertion or duplication) in critical genes often impair genes involved in PCs survival, ion channel genes or genes affecting neuronal excitability (Hekman and Gomez, 2015) **(Fig.5)**.

SCA[a]	Gene (type of mutation)	Protein (wild-type protein function)	Neuropathology	Clinical phenotype
SCAs due to repeat mutations				
SCA1	*ATXN1* (translated CAG repeat)	ATXN1 (gene transcription)	Cerebellum, brainstem and spinal cord	Ataxia, spasticity, ophthalmoplegia, bulbar symptoms and sensory symptoms
SCA2	*ATXN2* (translated CAG repeat)	ATXN2 (RNA repair, ribosomal translation)	Cerebellum, brainstem, substantia nigra, spinal cord and polyneuropathy	Ataxia, slow saccades and sensory symptoms
SCA3/MJD[b]	*ATXN3* (translated CAG repeat)	ATXN3 (deubiquitinase)	Dentate nucleus, basal ganglia, substantia nigra, spinal cord and polyneuropathy	Ataxia, ophthalmoplegia, spasticity, basal ganglia symptoms, sensory symptoms, amyotrophy including facial atrophy and fasciculations
SCA6	*CACNA1A* (translated CAG repeat, missense)	α_{1A}-Subunit of voltage-dependent calcium channel of P/Q-type (neuronal excitability)	Cerebellum	Pure cerebellar ataxia and downbeat nystagmus
SCA7	*ATXN7* (translated CAG repeat)	ATXN7 (subunit of histone acetyltransferase complexes)	Cerebellum, brainstem, basal ganglia and retina	Ataxia, visual loss, ophthalmoplegia and spasticity
SCA8[c]	*ATXN8* (CTG repeat in 3′ untranslated region)	ATXN8, also antisense strand ATXN8OS (unknown)	Cerebellum	Ataxia, spasticity, sensory symptoms, cognitive and mood changes
SCA10	*ATXN10* (intronic ATTCT repeat)	ATXN10 (unknown)	Cerebellum	Ataxia and epilepsy
SCA12	*PPP2R2B* (CAG repeat in 5′ untranslated region)	Brain-specific regulatory subunit of protein phosphatase 2A (serine/threonine phosphatase involved in cell cycle and transcription)	Cerebellum and polyneuropathy	Ataxia and tremor
SCA17	*TBP* (translated CAG repeat)	TATA-box-1-binding protein (gene transcription)	Cerebellum	Ataxia, spasticity, basal ganglia symptoms, psychiatric disorders and dementia
SCA31	*BEAN1* (intronic TGGAA repeat insertion)	Brain-expressed protein associating with NEDD4 homologue (binding partner of NEDD4)	Cerebellum	Pure cerebellar ataxia
SCA36	*NOP56* (intronic GGCCTG repeat)	Nucleolar protein 56 (RNA maturation)	Cerebellum	Ataxia, amyotrophy and hearing loss
SCA37	*DAB1* (intronic ATTTC repeat)	Disabled homologue 1′ (intracellular adaptor in reelin signalling pathway)	Cerebellum	Ataxia and abnormal vertical eye movements
SCAs due to conventional mutations				
SCA5[d]	*SPTBN2* (deletion, missense)	βIII-Spectrin (cytoskeletal protein that stabilizes membrane proteins, including glutamate receptors)	Cerebellum	Pure cerebellar ataxia
SCA13	*KCNC3* (missense)	Subunit K_v3.3 (neuronal excitability)	Cerebellum and brainstem	Ataxia and intellectual disability
SCA14	*PRKCG* (missense)	Protein kinase Cγ (serine/threonine kinase)	Cerebellum	Ataxia and myoclonus
SCA15/SCA16[b]	*ITPR1* (large deletion, missense)	Inositol 1,4,5-triphosphate receptor type 1 (intracellular inositol-triphosphate-gated calcium channel)	Cerebellum	Pure cerebellar ataxia
SCA19/SCA22[b]	*KCND3* (missense, deletion)	Subunit K_v1.3′ (neuronal excitability)	Cerebellum	• SCA19: ataxia, cognitive impairment and myoclonus • SCA22: pure cerebellar ataxia
SCA28	*AFG3L2* (missense)	AFG3-like protein 2 (part of m-AAA protease complexes in the inner mitochondrial membrane)	Cerebellum	Ataxia, spasticity, ophthalmoplegia and ptosis

Figure 5. Genetic cause and phenotype of selected SCAs. ATXN, ataxin; DRPLA, dentatorubral-pallidoluysian atrophy; MJD, Machado–Joseph disease; SCA, spinocerebellar ataxia. The table shows all

known SCAs caused by repeat mutations and the most prevalent SCAs caused by conventional mutations. *(Klockgether et al. 2019)*

1.2.2 Spinocerebellar ataxia 38

Spinocerebellar ataxia 38 (SCA38) is a rare subtype of SCA caused by conventional mutations, which affects in average 5-7 individuals out of 100,000 (Di Gregorio et al., 2014). Besides the ataxic gait, SCA38 is characterized by nystagmus, hyposmia, pes cavus syndrome, peripheral neuropathy and hearing loss. All these symptoms are associated with cerebellar atrophy, especially in the vermis, but without cerebral and brainstem involvement (Di Gregorio et al., 2014; Borroni et al., 2016) **(Fig. 6B)**. SCA38 is a slowly and progressive pathology that has a mean age of onset of 39.1 years old. It is associated neither with parkinsonism nor with cognitive impairment, but in the last decades of patient's life it causes serious difficulties in independent basic activities in daily living (Borroni et al., 2016) **(Fig. 6A)**. The genetic cause of spinocerebellar ataxia 38 is a missense mutation in the very long chain fatty acid elongase-5 gene (*ELOVL5*) (Di Gregorio et al., 2014). *ELOVL5* encodes an enzyme that belongs to the elongase-of-very-long-chain-fatty acids (ELOVL) family, involved in the biosynthesis of long chain fatty acids, like arachidonic acid (ARA) and docosahexaenoic acid (DHA). So far, two missense mutations in sites conserved among vertebrates have been identified: c.214C>G (p.Leu72Val) on exon 3 and c.689G>T (p.Gly230Val) on exon 7 of *ELOVL5*. The pathological mechanisms underlying this neurological disorder are not clear nowadays. It is possible that that the mutated ELOVL5 protein is not degraded, but up regulated and delocalized (Borroni et al., 2016). Indeed, ELOVL5 is a protein physiologically localized in the endoplasmic reticulum (ER), but the mutations occurring in SCA38 leads to mislocalization to the Golgi apparatus and triggers an unfolded protein response (UPR) (Di Gregorio et al., 2014). However, it is not clear whether the genetic alteration induces loss of function of the mutated enzyme, or a toxic gain of function of the unfolded protein. Currently, a mixed model seems to be the most valuable explanation. However, it is known that, as a result of this mutation, the biosynthesis of downstream products of ELOVL5 is impaired, since the dosage of both ARA and DHA in patients serum show decreased levels of these two PUFAs, relative to healthy controls (Di Gregorio et al., 2014). This decrease causes an increase in *ELOVL5* gene expression and protein level in cultured lymphoblasts derived from SCA38 affected subjects. A possible explanation is that ARA and DHA also act at transcriptional level as feedback regulators. Their deficiency might induce an increase in the nuclear form of the transcription factor sterol regulatory element

binding protein 1c (SREBP-1c), responsible for *ELOVL5* expression (Moon et al., 2009; Di Gregorio et al., 2014).

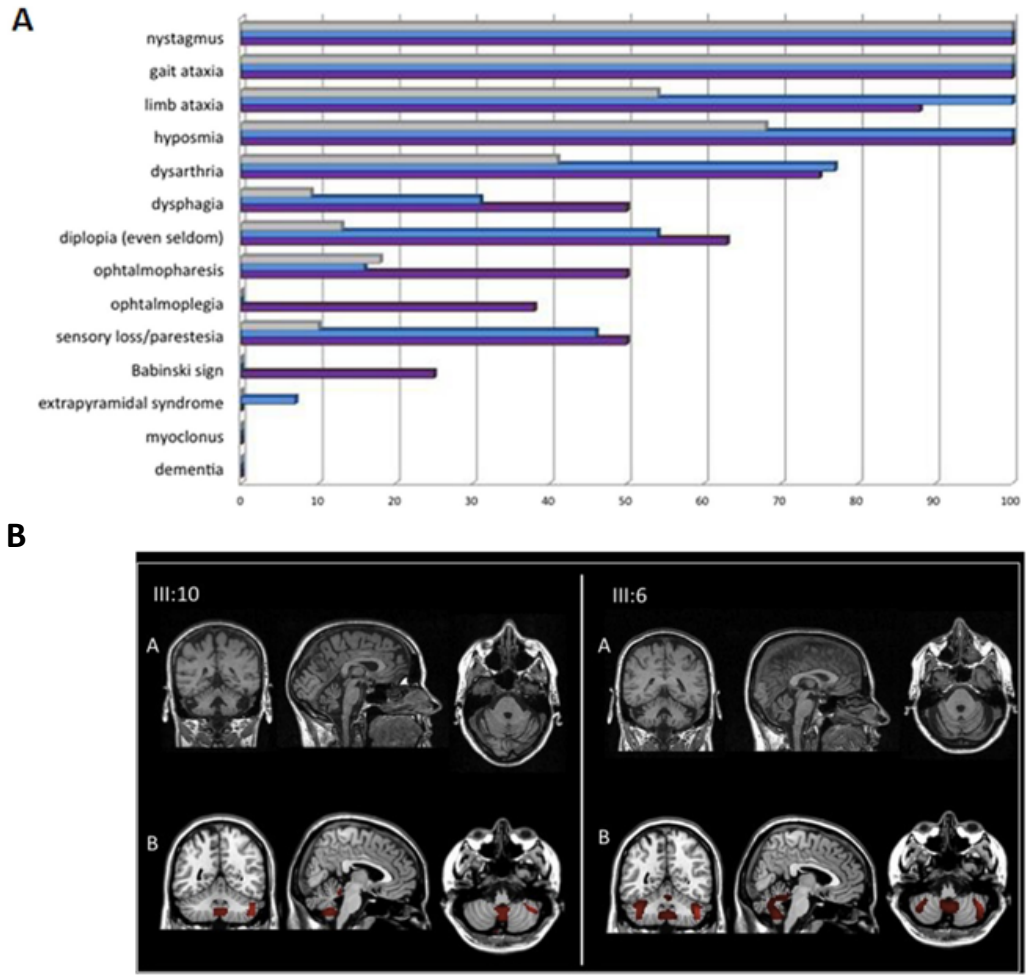

Figure 6. Pathological features of SCA38. **(A)** Signs and symptoms of SCA38 according to decades from disease onset. In grey, symptoms reported in the first 10 years of the disease, in blue those reported from 10 to 20 years of the disease, in violet those reported over 20 years from the onset of symptoms. **(B)** Structural and functional neuroimaging findings in two patients with SCA38. Subpanels A. Coronal, sagittal and axial magnetic resonance imaging sections (MRI), to demonstrate cerebellar atrophy. Subpanels B. FDG-PET images from a single-subject analysis using a group of 19 healthy individuals, showing regions of cerebellar hypometabolism *(Modified from Borroni et al., 2016)*.

1.2.3 SCA38 therapeutic approach

The majority of hereditary ataxias, including SCA38, lacks specific and effective treatments. However, the low serum levels of ARA and DHA in patients affected by SCA38 have driven recent research in the investigation of the effect of dietary PUFA supplementation as possible treatment of the disease. Indeed, DHA supplementation (dosage 600 mg/day) for 56 weeks produces clinical efficacy and amelioration in the cerebellar metabolism: significant improvements were detected in posture and gait and cerebellar hypometabolism (Manes et al., 2017). This short-term treatment after 40 weeks also reduces mutant ELOVL5 cellular levels and slightly reduces its expression in blood (Manes et al., 2017). Further studies have shown that clinical and cerebellar metabolism amelioration were maintained among time and without any side effect, when administration of DHA was extended for almost 2 years, and no worsening in motor symptoms and sensory conduction velocity was observed (Manes et al., 2019). Despite these positive effects, the long-term administration of DHA seems not to affect the DHA decreased level in serum nor the increased *ELOVL5* expression in blood (Manes et al., 2019). Further studies are necessary in order to understand the biological basis of the response to this treatment and to identify the age of turning from presymptomatic to symptomatic stage of the disease. Moreover, no other PUFAs have been tried yet and a set clinical trial for SCA38 patients is not available, because of the lack of studies on preclinical models.

1.2.4 Elovl5$^{-/-}$ mice as a model for the study of SCA38

In 2017 our laboratory showed that a mouse model with the total body deletion of the *Elovl5* gene (*Elovl5*$^{-/-}$) can be used for the study of the SCA38 (Hoxha et al., 2017). These mice, generated in Professor Horton's lab (Moon et al., 2009), well represent all the pathological features and symptoms also presented by patients, so suggesting that the main mechanism which leads to SCA38 development is a loss of function mutation in *ELOVL5* gene. Therefore, *Elovl5*$^{-/-}$ mice showed impairment in motor coordination and balance skills at the balance beam test, denoting a cerebellar phenotype, which worsened with age (Hoxha et al., 2017) **(Fig. 7)**. They also presented hyposmia at 12 months of age, showing an increased latency in finding the olfactory stimulus at the olfactory test (Hoxha et al., 2017) **(Fig. 7)**. Ablation of the *Elovl5* gene has also massive histological consequences on the brain of affected mice. In fact, the total perimeter length of the PC layer and the cerebellar white matter area are markedly reduced at all stages of the disease (Hoxha et al., 2017) **(Fig. 7)**. Furthermore, some of the lobules of the

cerebellum undergo a thinning of the molecular layer, caused by the reduction in the extension of the PC dendrites tree. Interestingly, this dendritic alteration is not accompanied by alteration of the dendritic spines, suggesting that *Elovl5* is not necessary for spine formation but is needed to keep the PC dendritic branches correctly distributed in the molecular layer (Hoxha et al., 2017) **(Fig. 7)**. Taken together, these lines of evidence show that *Elovl5*$^{-/-}$ mice are a good model for the study of SCA38. However, pathophysiological mechanisms leading to SCA38 are not clear yet, and further investigations on *Elovl5*$^{-/-}$ mice are needed, in order also to elucidate the physiological role of *Elovl5* and why its mutations could lead to cerebellar ataxia.

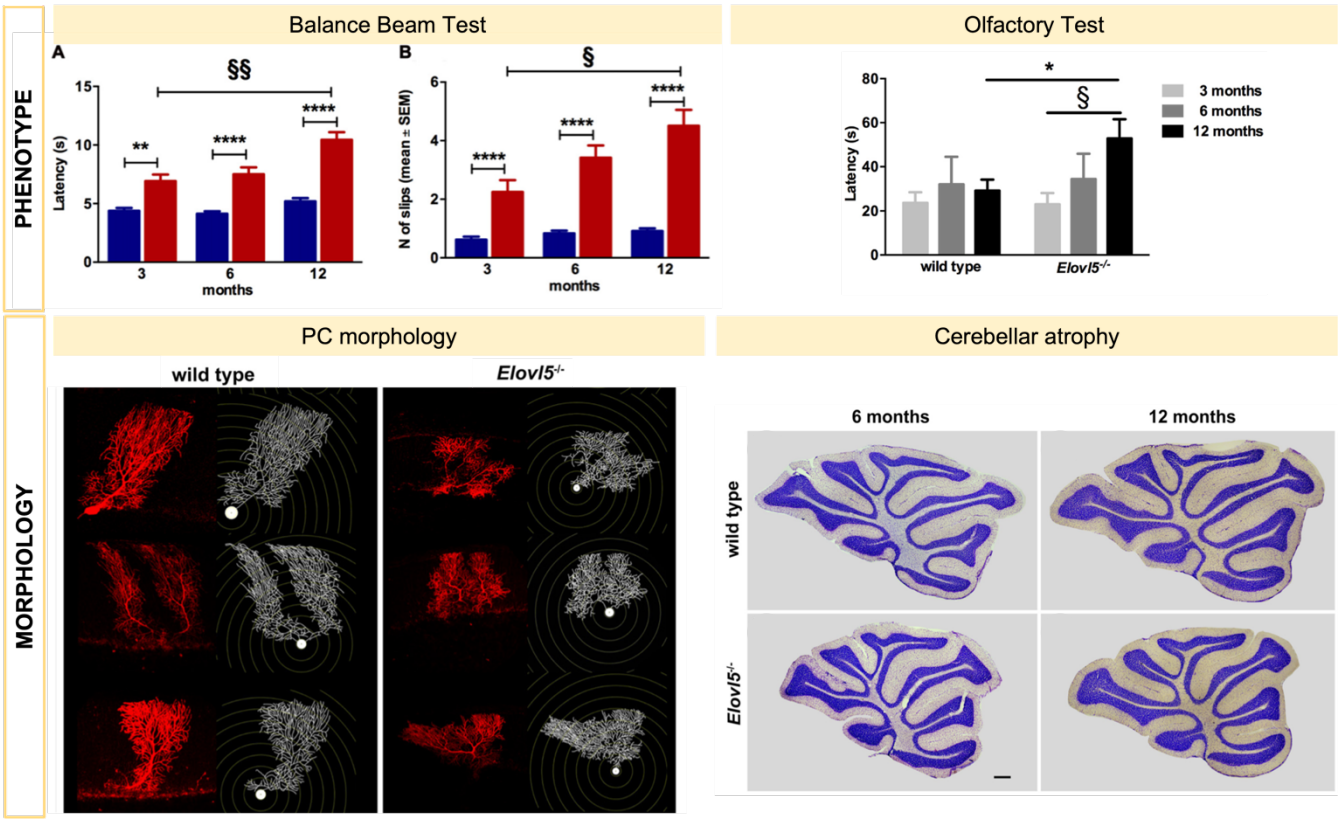

Figure 7. *Elovl5*$^{-/-}$ mice symptoms and pathological features. Top left panel: Increased latency to cross the beam **(A)** and increased mean number of foot-slips for *Elovl5*$^{-/-}$ compared to wild type mice **(B)**; the performance of *Elovl5*$^{-/-}$ mice worsened across months. Top right panel: *Elovl5*$^{-/-}$ mice show hyposmia. The latency to find the buried cookie is significantly longer for *Elovl5*$^{-/-}$ mice compared to wild type animals at 12 months. At younger ages, no significant difference between genotypes was present. Bottom left panel: biocytin filled PCs and reconstructed dendritic structures for wild type and *Elovl5*$^{-/-}$ mice. *Elovl5*$^{-/-}$ mice showed a

reduced extension the dendrites relative to their wild type littermates. Scale bar 40 μm. Bottom right panel: Nissl-stained sagittal sections of the cerebellum from wild type and *Elovl5*$^{-/-}$ mice of 6 and 12 months of age. *Elovl5*$^{-/-}$ mice showed a reduced thickness of the molecular layer of each cerebellar lobule, accompanied by a reduced total perimeter length of the PC layer and white matter area in the cerebellum compared to wild type littermates *(Adapted from Hoxha et al., 2017).*

1.3 ELOVL gene family

The ELOVL family of enzymes in mammals is composed by seven members (ELOVL1-7) that are all located in the ER and are thought to act together like a multimeric complex (Okuda et a., 2010). ELOVLs are elongase enzymes responsible for the initial condensation reaction necessary to elongate saturated and unsaturated fatty acids (Leonard et al., 2004; Jakobsson et al., 2006; Sassa and Kihara, 2014) **(Fig. 8)**. They are rate-limiting and even if each member of the family shows a particular substrate preference, they show a homologue structure (Leonard et al., 2000). Therefore, these enzymes are multi-pass transmembrane proteins containing a large ELO domain, an N-linked glycosylation near the N-terminus, a catalytic histidine motif (HXXHH), essential for the elongase function, and a di-lysine ER- retention motif (KXKXX) in the C-terminus domain that is required for proper localization to the ER (Deák et al., 2019). Recently, interest in these enzymes has grown because mutations in ELOVL genes have been linked to various nervous system diseases.

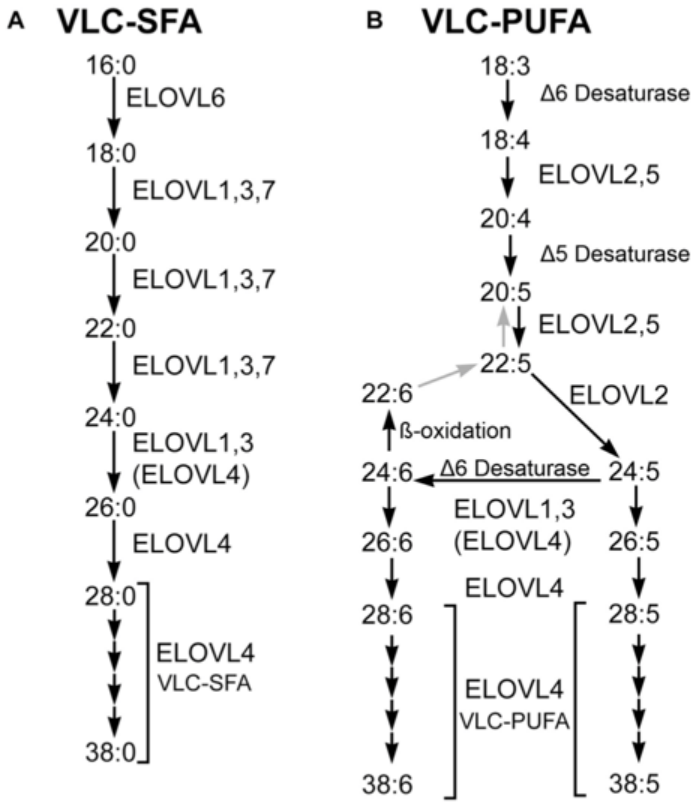

Figure 8. ELOVL family members and their role in the synthesis of very long chain saturated fatty acids (VLC-SFA) and VLC-PUFAs. (A) VLC-SFA biosynthesis pathway. Elongation steps are performed by ELOVL1-7. **(B)** Very long chain PUFA (VLC-PUFA) biosynthesis pathway. Desaturation

and elongation steps are performed by ELOVL1-5, Δ5 Desaturase (fatty acid desaturase-1, FADS1), and Δ6 desaturase (fatty acid desaturase-2, FADS2). Although some ELOVL family members catalyze specific steps in VLC-PUFA synthesis, others are multifunctional and may catalyze multiple steps *(Adapted from Deák et al., 2019)*.

1.3.1 ELOVL5

ELOVL5 has the unique property to condense a wide selection of PUFAs from 18 to 20 carbon atoms, including linoleic (LA) acid to produce ARA, α-linolenic (ALNA), and stearidonic to produce eicosapentaenoic acid (EPA) and DHA (Leonard et al., 2000; Moon et al., 2009; Shikama et al., 2015). It is an essential player for the lipidic metabolisms, therefore its loss induces a depression of a sterol regulatory element-binding protein (SREBP-1c), which led to the transcriptional activation of lipogenic genes, increased lipogenesis, and hepatic steatosis (Moon et al., 2009). Moreover, as already illustrated (see chapter 1.2.2), alteration in ELOVL5 have been identified as the genetic cause of the SCA38 (Di Gregorio et al., 2014; Borroni et al., 2016). *ELOVL5* presents a particular high expression in lung and adult brain, where it shows its higher levels in the cerebellum, in soma and dendrites of PCs (Di Gregorio et al., 2014) **(Fig. 9A-E)**. Up to date no other information about its localization in brain was available. This thesis work was also aimed at filling this gap (see chapter 3.1, Balbo et al., 2021).

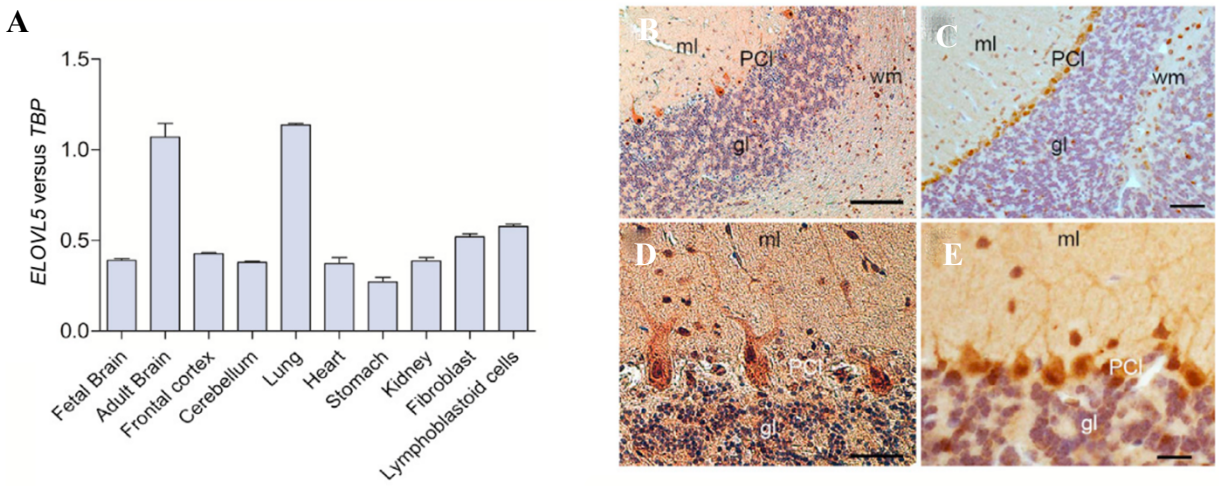

Figure 9. ELOVL5 expression and localization. (A) The normal expression pattern of ELOVL5 in five human tissues, lymphoblastoid cells, and four brain areas. ELOVL5 showed prominent expression in brain and lung. **(B - E)** Sections of healthy human (B and D) and murine (C and E) cerebellar cortex immunostained with ELOVL5 antibody and counterstained with hematoxylin. Higher magnifications of

sections of human and mouse cerebellar cortex are shown in **(D)** and **(E)**, respectively. Note the similar labeling pattern of human and mouse Purkinje cells and the presence of numerous labeled cells in the white matter. ml, molecular layer; PCl, Purkinje cell layer; gl, granular layer; and wm, white matter. Scale bars: 200 μm **(B)**, 80 μm **(C)**, 50 μm **(D)**, and 20 μm **(E)** *(Modified from Di Gregorio et al., 2014).*

1.3.2 Other ELOVL family genes and their associations with human diseases

ELOVL1 elongates saturated or monosaturated fatty acids, in particular ones with chain lengths of 18–24 carbons and it has an overlapping function with ELOVL3 and ELOVL7 (Guillou et al., 2010; Kihara, 2012). *ELOVL1* is expressed at moderate levels in CNS, especially in the corpus callosum and the spinal cord (Tvrdik et al., 2000). An autosomal dominant mutation in human *ELOVL1* leads to ichthyosis, hypomyelination, spastic paraplegia, partial deafness, and optic atrophy (Kutkowska- Kaźmierczak et al., 2018; Mueller et al., 2019). ELOVL2 is selective for very long chain fatty acids (VLCF) and polyunsaturated fatty acids (PUFA), therefore it elongates VLCF with 18–20 carbon chains and PUFA with 20–22 carbon (Guillou et al., 2010; Kihara, 2012). It is essential for the lipid homeostasis, as shown by studies on knockout mice, but its expression in brain is very low (Tvrdik et al., 2000; Pauter et la., 2014). At present, no ELOVL2 mutation has been identified as cause of any human disease, although some polymorphisms have been linked to increase the susceptibility to autism spectrum disorders recently (Sun et al., 2018). Functionally corresponding to ELOVL1, ELOVL3 elongates saturated or monosaturated fatty acids, in particular the ones with chain lengths of 18–24 carbons (Guillou et al., 2010; Kihara, 2012). *ELOVL3* is mainly expressed in the skin and poorly in CNS (Tvrdik et al., 2000). To date, no human brain disease has been found correlated to its mutations. ELOVL4 elongates long-chain PUFA and long-chain VLCF of 24 carbon length up to 38 carbons (Guillou et al., 2010; Kihara, 2012). Its expression in CNS is very abundant and it is one of the best characterized (Sherry et al., 2017). In mouse brain, expression of ELOVL4 is especially prominent in the olfactory bulb, hippocampus, cerebral cortex, thalamus, and cerebellum. An exception to this pattern are the basal ganglia, which show very little ELOVL4 expression (Sherry et al., 2017). This enzyme is mainly expressed by neurons, although small ELOVL4-positive cells have been observed in brain white matter suggesting potential expression in oligodendrocytes too (Sherry et al., 2017). *ELOVL4* mutations cause autosomal dominant spinocerebellar ataxia type 34 (SCA34), erythrokeratodermia variabilis (EKV) (Cadieux-Dion et al., 2014; Bourassa et al., 2015; Ozaki et al., 2015) and autosomal dominant Stargardt-like macular dystrophy (STGD3) (Bernstein et al., 2001; Edwards et al., 2001; Zhang et al., 2001).

ELOVL6 mediates the first, rate-controlling step in fatty acid elongation of saturated and unsaturated/polyunsaturated fatty acids with chain length of 16 carbons (Moon et al., 2001; Guillou et al., 2010; Kihara, 2012; Moon et al., 2014). It is expressed at high levels in liver, adipose tissue, and brain (Tvrdik et al., 2000). Studies on knockout mice, show ELOVL6 essential role in metabolism regulation and in regulating thermogenic activity in brown fat adipocytes (Matsuzaka et al., 2007; Tan et al., 2015). No direct causal linkage of *ELOVL6* mutations to human disease has been established. Being functionally identical to ELOVL1 and ELOVL3, ELOVL7 elongates saturated or monosaturated fatty acids, in particular the ones with chain lengths of 18–24 carbons (Guillou et al., 2010; Kihara, 2012). It is highly expressed in CNS, particularly in spinal cord, basal ganglia and midbrain (Tvrdik et al., 2000). *ELOVL7* polymorphisms have been associated with early onset Parkinson's disease and multiple system atrophy (Sailer et al., 2016; Li et al., 2018; Keo et al., 2020).

1.4 Polyunsaturated fatty acids (PUFAs)

Polyunsaturated fatty acids (PUFAs) are a group of fatty acids characterized by at least two double bonds. By considering the last double bond position, called omega, it is possible to divide them into two families: omega-3 (n-3) and omega-6 (n-6), respectively. (Nelson and Cox, 2017). PUFAs cannot be synthesized *de novo* in human tissues, but their precursors (linoleic acid and alpha-linolenic acid) must be obtained from diet, through the assumption of fish, seeds or oil. Such precursors are then processed to more complex PUFAs by the liver and then transported to other districts with bloodstream or they can be processed directly in the target tissue. Despite this fact, this process is not efficient, with less than 1% of precursors which are converted into more complex compounds (Plourde and Cunnane, 2007). In addition to long chain PUFA synthesized in the liver, shorter chains precursors are provided by plasma, to allow local synthesis in brain. Besides the crucial structural role in membranes, various PUFA metabolites also possess signaling functions, with roles in neurogenesis, neuronal survival, synaptic activity and regulation of brain inflammation (Guillou et al., 2010; Bazinet and Layé, 2014; Serhan et al., 2014).

1.4.1 PUFAs synthesis

In mammals, PUFAs synthesis results from an alternation of desaturation and elongation from the dietary fatty acids. In fact, the essential fatty acids 18:2n6 (LA) and 18:3n3 (ALNA) are required to start the series of desaturation and elongation reactions in the ER which generate long-chain PUFAs. The Δ6 desaturase uses 18:2n6 and 18:3n3 as substrates and inserts a double bond to produce 18:3n6 (gamma-linolenic acid) and 18:4n3 (stearidonic acid). PUFAs with a double bond at Δ6 are then elongated by ELOVL-family enzymes, which use malonyl-CoA to add two carbons to the C-terminal end of the fatty acids, producing 20:3n6 (dihomogamma-linolenic acid) and 20:4n3 (eicosatetraenoic acid). These fatty acids are substrates for a Δ5 desaturase, originating 20:4n6 (ARA) and 20:5n3 (EPA) (Wallis et al., 2002). These C20 products then undergo two succeeding elongation cycles followed by a Δ6 desaturation, occurring in the ER. After transfer of the fatty acid to peroxisomes, there is a specific β-oxidation which leads to 22:5n6 (docosapentaenoic acid, DPA) and 22:6n3 (DHA) (Wallis et al, 2002) **(Fig. 10)**.

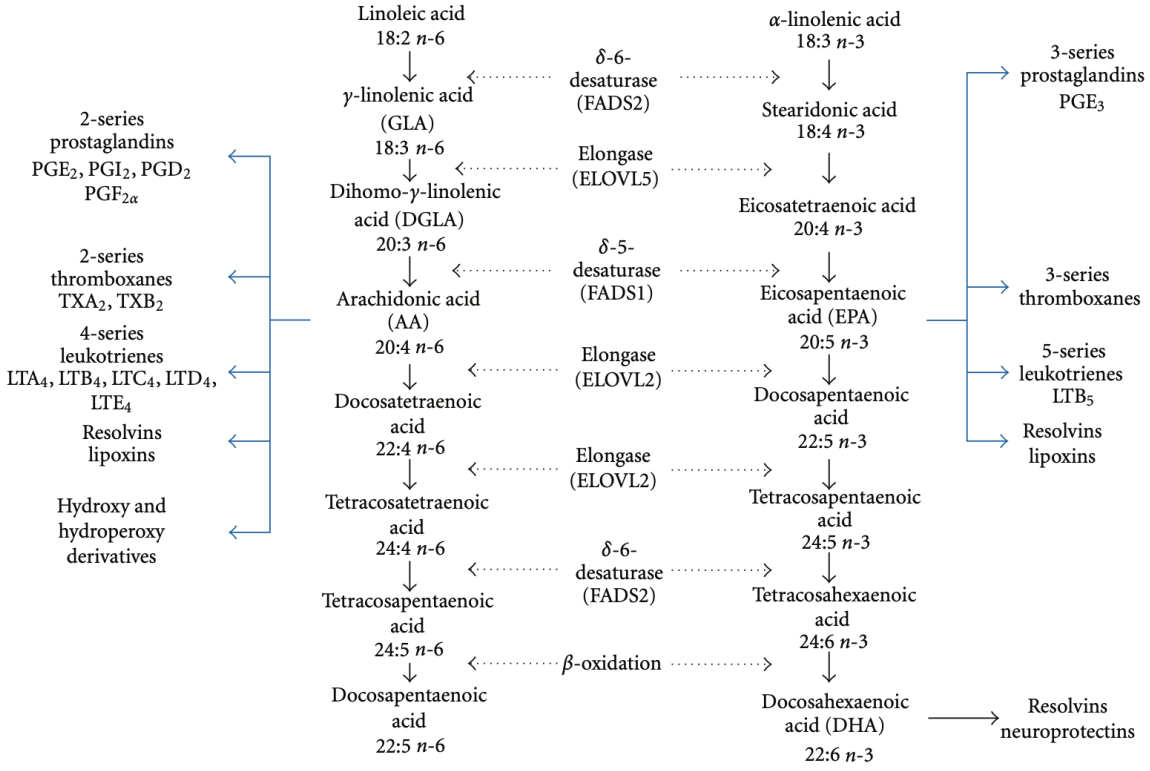

Figure 10. PUFAs omega-3 and omega-6 biosynthesis. All the steps necessary for the biosynthesis of PUFAs omega-3 and omega-6. The most common mediators produced from ARA, EPA and DHA are indicated *(Patterson et al., 2012).*

1.4.2 PUFA transport into brain

PUFAs enter the brain as unesterified *(*free fatty acid) or esterified to lipids by forming lysophospholipids and lipoproteins, generally. In particular, they can cross the blood-brain barrier (BBB) in three different ways: via passive diffusion through the membranes of endothelial cells, through the transcytosis pathway or by lipoprotein receptor, when they are esterified to a glycerol (Pifferi et al., 2021). Transfer via passive diffusion through the membranes of endothelial cells requires the dissociation of the non-esterified fatty acid from albumin. This process depends upon the affinity of the fatty acid with albumin and its frequency of dissociation, and the usage of this fatty acid by endothelial and neuronal cells (Pifferi et al., 2021). Interesting evidence shows that DHA is able to cross the BBB via simple diffusion, as EPA, thanks to a high liposolubility and a molecular weight under 400 Da (Ouellet et al., 2009). Transcytosis can be mediated by vesicles coated with clathrin or by caveolae. Both these ways involve low-density lipoprotein (LDL) receptors which recognize adapter proteins and, following vesicles internalization, directs LDL to lysosomes that degrade them to release

cholesterol and fatty acids, or transfer LDLs across the plasma membrane, preventing their degradation (Kirchhausen et al., 2005; Robinet et al., 2006; Yang et al., 2020). The most efficient mechanism of BBB passage begins with the esterification of the fatty acid to a glycerol into lysophosphatidylcholine (lysoPC) (Lacombe et al., 2018). When lysoPCs bind lipoprotein receptors, they are internalized into endothelial cells and then lipids of the lipoproteins are split. PUFAs are released and finally selectively transferred to their specific transporters at the abluminal membrane of the endothelial cells (Pifferi et al., 2021). Among the transporters involved in this mechanism there are different fatty acid transport proteins (FATPs), each one selective for a wide range of PUFAs (Edmond, 2001). DHA is mainly transported by the major facilitator superfamily, Mfsd2a, involved in the regulation of brain endothelial cell lipid composition (Nguyen et al., 2014; Andreone et al., 2017). Once entered, most PUFAs (like ARA and DHA) are esterified to phospholipid membranes, while others (such as LNA, ALA and EPA) are oxidized (Bazinet and Layé, 2014).

1.4.3 PUFAs physiological functions in brain

PUFAs are essential players in brain correct functioning. They influence neuronal functions through direct effects on membrane biophysical properties, and via neurotransmission, by providing a precursor pool for signaling molecules and lipid-derived mediators. From a structural point of view, PUFAs are fundamental components of both glial and neuronal cell membranes, but also of myelin sheaths and their presence influences their integrity and proper physiological functions. It is widely known that a good balance of unsaturated relative to saturated fatty acids impacts on membrane fluidity, thickness and rigidity (Fernstrom, 1999; Yehuda et al., 2002; Dyall and Michael-Titus, 2008; Harayama and Shimizu, 2020). This is incredibly important in brain and can affect synaptic regulation by altering the membrane curvature and disrupting phospholipid packing of the lipid bilayer of synaptic membranes (Antonny et al., 2015; Lauwers et al., 2016). Furthermore, recent evidence suggests a possible role of PUFA and long-chain saturated fatty acids in synaptic vesicle fusion with the presynaptic terminal and the consequent neurotransmitter release (Hopiavuori et al., 2018; Hopiavuori et al., 2019). Nevertheless, this involvement in neurotransmitters release is not the only way PUFAs can influence neurotransmission. Indeed, they can generate many bioactive derivates, so called mediators, originating from the de-esterification of membrane phospholipids by phospholipase A2 (PLA2), which is coupled to many receptors in the brain, such as dopaminergic, cholinergic,

serotoninergic and NMDA (Bazinet and Layné, 2014). Once de-esterified, enzymes like lipoxygenase (LOX), cyclooxygenase (COX) and cytochrome P450 mediate the conversion of PUFAs in bioactive lipidic products. These mediators produced can act as agonists for many receptors, so activating cell signaling pathways. One of the best characterized family of derivates are the endocannabinoids (eCBs). The eCBs most produced in brain are 2-arachidonoylglycerol (2-AG) and anandamide (AEA), which derive both from ARA and act on neurons and glial cells (Castillo et al., 2012). They bind cannabinoid receptor type 1 (CB1) and type 2 (CB2) and modulate synaptic transmission by acting like retrograde messengers in many brain regions, including the cerebellum (Castillo at al., 2012; Lu and Meckie, 2016). In the cerebellum, CB1 is expressed by PC dendrites, CFs, PFs and basket cells (Lu and Meckie, 2016). The release of eCBs influences GABAergic synapses and follows the depolarization of the postsynaptic terminal and the consequent rise in of intradendritic calcium concentration. Such an augmented concentration induces the synthesis and the release of eCBs in the synaptic cleft, which bind the receptors localized at presynaptic terminal, resulting in a transient suppression of neurotransmitter release (Castillo et al., 2012; Lu and Meckie, 2016). This retrograde signaling mediates several forms of short and long term synaptic plasticity: i) depolarization-induced suppression of excitation (DSE), a postsynaptic calcium-dependent process that modulates glutamatergic transmission (Kreitzer and Regehr, 2001; Diana and Marty, 2004); ii) LTD, which requires mGluR1 activation (Safo and Regher, 2005; Kano et al., 2008); iii) synaptically evoked suppression of excitation (SSE), a physiological process aimed at circumscribing stimulation to interested dendrites preventing a spread to others on the same or on neighboring PCs (Brown et al. 2003). Besides the eCBs, the elovanoids are well characterized PUFAs mediators deriving from oxygenation of very long-chain omega-3 PUFAs (Jun et al., 2017). Elovanoids have been found to provide a neuroprotective feedback signal to enhance expression of pro-survival proteins by the photoreceptors in the retina to compensate for high levels of oxidative stress (Jun et al., 2017). Moreover, they showed a protective effect in neurons subjected to oxygen and glucose deprivation in an animal model of ischemic stroke (Bhattacharjee et al., 2017). Similar effects are shown by DHA and its mediator synaptamide, which provide not only neuroprotection and survival, but also neuronal differentiation and synaptogenesis (Kim et al., 2011 and 2013). Finally, PUFAs play a role in regulation of inflammation, which is an essential process in order to maintain the correct homeostasis of the brain in response to infections and lesions. This response is carried out by microglial cells, through the production of pro and anti-

inflammatory cytokines. However, when this production is sustained for too long, these molecules become neurotoxic and rapidly commit the brain to neuronal damage (Layè et al., 2010). PUFAs act at both sides of this process. Therefore, firstly, they serve as precursors of several pro-inflammatory mediators such as eicosanoids, prostaglandins, thromboxane and leukotrienes. Then, they act down-regulating cytokine gene expression, while inducing lipid mediators involved in the resolution of inflammation (Layè, 2010). They have also been shown to directly modulate microglial function, phenotype and migration (Layè, 2010). ARA-produced metabolites, eicosanoids, have general proinflammatory effects, while EPA-derived ones play the opposite function (Tapiero et al., 2002). DHA and its mediators have shown to have a potent anti-inflammatory and pro-resolving properties in peripheral tissues and brain, by reducing the risk of onset of neurological diseases that have an inflammatory component, like Alzheimer's disease, Parkinson's disease and major depression (Laye, 2010).

AIM OF THE THESIS

As showed in this bibliographic examination, in the recent years interest has risen in *ELOVL* family genes and related human diseases (see chapter 1.3). Especially in the brain, mutations in some of these genes induce functional and structural impairments, which in most cases lead to neurological and neuropsychiatric disorders. However, the knowledge about the role of these biosynthesis enzymes is incomplete and contradictory, maybe also due to the variety of biological process their products are involved in. Among the others, Elovl5 has the unique characteristic to condense a wide selection of PUFAs from 18 to 20 carbon atoms to produce compounds like ARA, EPA and DHA, essential for many physiological functions in nervous system (Leonard et al., 2000; Moon et al., 2009; Shikama et al., 2015). A loss of function of this enzyme leads to the pathological condition of SCA38, that, within three decades from the onset, severely impairs life quality of patients (Borroni et al., 2016). The range of symptoms showed by patients indicates that functional alterations occur not only in the cerebellum, but also in other brain regions. Despite this fact, there is a poor knowledge about the physiological role of Elovl5 in brain. This thesis is aimed at filling this gap, by studying the consequences of this enzyme loss in the mouse model of SCA38, *Elovl5*$^{-/-}$ mice. The first important information to clarify is where exactly this enzyme is localized and by which cell types it is produced. In fact, understanding the expression pattern could be an important hint for the study of the functional aspects. Thus, we started by investigating the protein localization in different brain areas and cell types. Following the identification of the regions and of the cellular subpopulations expressing Elovl5, we wanted to know its role in the central and peripheral nervous system. To this aim, we decided to start from the observation of the symptoms showed by *Elovl5*$^{-/-}$ mice and delved deeper to have a better comprehension of the pathological mechanisms induced by Elovl5 loss. Finally, we attempted to obtain a reversal of the phenotype observed in *Elovl5*$^{-/-}$ mice, by imposing them a PUFA-rich diet. As told in the previous chapters (see chapter 1.2.3), the administration of DHA has been already tried on SCA38 patients and this therapeutic approach proved to be safe and well tolerated, relatively inexpensive and easy to administer as a dietary intervention (Manes et al., 2017; Manes et al., 2019). However, even if the patients showed beneficial effects, the previous studies do not provide evidence for maintenance of the improvement over time, and they did not find a biological explanation for the ameliorations observed. Most importantly, these works supply data for the administration of only one PUFA downstream Elovl5. So, we tried the administration of the complete product range to *Elovl5*$^{-/-}$ mice and we observed

symptoms progression over time. Our study can lead to a better understanding of the molecular correlates of presymptomatic and symptomatic stages of this pathology, and potentially be a guide for better clinical trials.

CHAPTER 2 – MATERIALS AND METHODS

2.1 Animals

Elovl5$^{-/-}$ mice (C57BL/6 background) have been kindly provided by Dr. Moon and Dr. Horton of the UT Southwestern Medical Center (Moon et al., 2009) and bred in our Animal Facility at NICO (Orbassano, Italy). Experimental animals and wild type controls were obtained by mating heterozygous *Elovl5*$^{+/-}$ mice, with the expected Mendelian frequency of 1/4 *Elovl5*$^{-/-}$ and 1/4 *Elovl5*$^{+/+}$, heterozygous *Elovl5*$^{+/-}$ offspring were discarded.

Both males and females were used for all the experimental paradigms since no difference in motor deficit between sexes has been found. During the whole experimental period *Elovl5*$^{-/-}$ and wild type littermates from 1 month to 20 moths were used.

All experimental procedures have been approved by the Ethical Committee of the University of Torino and authorized by the Italian Ministry of Health (authorization number: 161/2016-PR).

2.1.1 Mice feeding

Both *Elovl5*$^{-/-}$ mice and their wild type littermates were kept from birth on an omega-3 and omega-6 free diet (Teklad Global 18% Protein Rodent Diet, Harlan Laboratories), to allow just the endogenous synthesis of downstream products of Elovl5 enzyme.

To assess the effect of a PUFA rich diet in our pathological model, a control group composed by both *Elovl5*$^{-/-}$ and wild type mice was kept in standard rodent diet (4RF25, Mucedola Srl). While another group was imposed this PUFA rich diet after weaning (1 month old).

In order to assure this difference in diet administration, we quantified the amount of free fatty acids both downstream and substrates of Elovl5 in both foods (**Table 1**).

Fatty acid	**PUFA precursors diet (Teklad Global 18% Protein Rodent Diet, Harlan Laboratories)**	**Complete PUFA diet (4RF25, Mucedola Srl)**
Linoleic acid C18:2n-6	2227.234 ± 48.492	1542.747 ± 183.529
gamma-Linolenic acid C18:3n-6	325.807 ± 11.766	302.807 ± 25.603
Arachidonic acid C20:4n-6	0.254 ± 0.031	9.901 ± 0.365
Eicosapentaenoic acid C20:5n-3	0.190 ± 0.034	28.677 ± 1.564
Docosahexaenoic acid C22:6n-3	0.096 ± 0.027	125.449 ± 1.686
Oleic acid (C18:1)	1920.966 ± 68.373	1847.310 ± 174.768

Erucic acid (C22:1)	15.155 ± 0.361	12.909 ± 0.392
Nervonic acid (C24:1)	2.081 ± 0.170	2.203 ± 0.024
Palmitic acid (C16:0)	1243.140 ± 50.405	875.832 ± 70.505
Margaric acid (C17:0)	10.233 ± 0.180	11.495 ± 0.606
Stearic acid (C18:0)	256.665 ± 4.021	241.530 ± 11.131
Arachidic acid (C20:0)	17.404 ± 0.034	18.555 ± 1.564
Behenic acid (C22:0)	16.268 ± 0.732	14.383 ± 0.236

Table 1. Fatty acids content of PUFA only and complete diets. Data are expressed as ng/mg (mean ± standard error)

2.1.2 Genotyping mice

The genotype of both *Elovl5*$^{-/-}$ and wild type mice was confirmed by means of PCR using the following primers:

ELOVL5

ELOVL5 FW: (5') ACC ACT AGT CAT ATG ACG GC (3')

ELOVL5 RV: (5') TAC AAA GCG TAC AAA GGC TG (3')

ELOVL5 MUT: (5') ATA CAG TCC TCT TCA CAT CC (3')

Samples were studied by using following PCR protocol: 94°C for 2 minutes, 30 cycles of 94°C for 30 seconds, 60°C for 1 minute, 72°C for 1 minute and by a last step of extension at 72°C for 10 minutes.

2.2 Immunohistochemistry, immunofluorescence and electron microscopy

2.2.1 Tissue preparation

To assess Elovl5 expression in brain slices adult *Elovl5*$^{-/-}$ and wild type mice (6 to 12 months old mice) were anesthetized using a cocktail of ketamine (100 mg/kg body weight) and xylazine (10 mg/kg body weight) via intraperitoneal injection. The mice were intracardially perfused initially with a physiological solution (NaCl 0.9%) and then with 4% paraformaldehyde in 0.12 M phosphate buffer, pH = 7.2–7.4. Following perfusion, the brain and the spinal cord were removed and stored at 4◦C for 24 h immersed in the same fixative and later transferred to a solution made of 30% sucrose in 0.12 M phosphate buffer for few days. Perfused brains and spinal cords were embedded in paraffin, cut into 5 μm-thick sagittal slices and mounted on

superfrost glass slides (Fisher Scientific, Göteborg, Sweden) with Tris-glycerol supplemented with 10% Mowiol (Calbiochem, LaJolla, CA, United States).
To assess Elovl5 expression in glial cells in vitro, postnatal day 2 (P2) pups were cryoanesthetized in melting ice. The experimental plan was designed according to the guidelines of the NIH, the European Communities Council (2010/63/EU) and the Italian Law for Care and Use of Experimental Animals (DL26/2014). The study was conducted according to the ARRIVE guidelines.

To check cerebellar architecture and to analyze correct circuitry functioning, following perfusion,12 months old mouse brains were removed and stored at 4◦C for 24 h immersed in the same fixative. The brains were then transferred to a cryoprotectant solution made of 30% sucrose in 0.12 M phosphate buffer for few days. For each mouse, the cerebellum was separated and embedded in optimal cutting temperature compound, frozen in ice-cold isopentane. Samples were stored at −80◦C until sectioning. Cerebella were serially cut by a cryostat in 30 µm-thick sagittal slices and collected in phosphate buffered saline (PBS).

To study possible alteration of the nodal-paranodal structure in peripheral nervous system, 12 months old *Elovl5*$^{-/-}$ (n = 3) and wild type (n = 3) littermates were anesthetized with isoflurane (Isoflurane-Vet, Merial, Milan, Italy) and decapitated. Sciatic nerves were then exposed, separated from the surrounding muscular tissue and dissected. Samples were fixed in cold 4% paraformaldehyde for 30 min subsequently transferred in cold 0.1 M phosphate buffered saline (1x PBS) pH 7.2–7.4, and stored overnight at 4°C. The following day, nerves were embedded in optimal cutting temperature compound (OCT), serially cut by a cryostat (Leica CM1900, Leica Microsystem, Milan, Italy) in 50 µm-thick longitudinal slices and stored at 4°C until usage. Floating slices were incubated with blocking solution (0.5% Triton X100, 5% Normal Goat Serum [NGS], in 1x PBS) for 1 h at room temperature.

2.2.2 Immunofluorescence reactions

To study Elovl5 expression in brain slices adult *Elovl5*$^{-/-}$ and wild type mice, slides were washed with PBS for three times and then incubated with a cocktail containing: monoclonal primary anti-Elovl5 antibody made in rabbit (1:300 NBP2-33500, Novus biologicals, Centennial, United States) and anti-GFAP made in rabbit (1:1000, Dakopatts, Z334) **(Table 2)**, 1.5% NGS and

PBS+ overnight at room temperature (RT) in a humid dark chamber. The following morning the tissues was washed three times with PBS (5 min each) and incubated with biotinylated secondary antibody anti rabbit (1:200, Vector Labs, Burlingame, United States) for 2 h. Slides were then washed three times with PBS (5 min each) and incubated with streptavidin-HRP (1:100, PerkinElmer, Milano, IT), and PBS+ for 1 h at RT. Following the incubation, sections were washed three time in PBS (5 min each) and incubated with Tyramide-FITC (1:100 PerkinElmer, Milano, IT) for 5 min at RT in the humid dark chamber. After a 5-min incubation with DAPI (1:1,000, Fluka, Saint Louis, United States), when dry, glass coverslip was applied using Mowiol (Calbiochem, LaJolla, CA, United States). For immunocytochemistry on cell cultures, after 7 days in vitro cells were fixed for 20 min at RT with 4% PFA in 0.1M PB and labeled with anti-AN2 (rat homologue of NG2, 1:100; kind gift of Miltenyi Biotech GmbH, Bergisch Gladbach, DE, and Prof. J. Trotter, Johannes Gutemberg University of Mainz, DE), -MBP (Smi-99 clone, 1:1,000 Sternberger), -Iba1 (1:1,000; Wako Chemicals, Richmond, VA), -Elovl5 (1:300; NBP2-33500, Novus biologicals, Centennial, United States) antibodies overnight at 4◦C in PBS with 0.25% Triton-X **(Table 2)**. Then, coverslips were incubated with Alexa488- and Alexa555-conjugated secondary antibody (Molecular Probes, Eugene, Oregon) for 1-h RT. After a 5-min incubation with DAPI (1:1,000, Fluka, Saint Louis, United States), coverslips were mounted with Tris- glycerol supplemented with 10% Mowiol (Calbiochem, LaJolla, CA, United States). In order to check ELOVL5 expression in peripheral glial cells , immortalized rat Schwann cells RT4-D6P2T (ATCC, Manassas, VA, USA) were cultured in Dulbecco's Modified Eagle Medium (DMEM) (D5796, Sigma Aldrich, MI, USA) supplemented with 10% (v/v) heat-inactivated fetal bovine serum (FBS) (F2442, Sigma Aldrich, MI, USA), 100 U/mL of penicillin, and 100 μg/mL of streptomycin (P4333, Sigma Aldrich, MI, USA). For immunofluorescence staining RT4-D6P2T were cultured on glass cover slides in 12-well cell culture dishes. Cells were fixed with 4% paraformaldehyde in 0.12 M phosphate buffer, pH 7.2–7.4 for 10 min, washed three times with PBS and then incubated with the primary antibody anti-Elovl5 (1:300, Novus Biologicals) overnight at room temperature. The next day after washing with PBS three times, the cells were incubated 1 h at room temperature with secondary antibody donkey anti-rabbit Alexa Fluor 555 (1:500, Invitrogen). After processing, sections were mounted on microscope slides with Pro Long Gold Antifade Reagent with DAPI (P36935, Molecular Probes, Thermo Fisher Scientific, MA, USA).

To analyze the nodal-paranodal structure in sciatic nerve of 12 months old *Elovl5*$^{-/-}$ and wild type mice, immunofluorescence was performed incubating slices with primary antibody mouse monoclonal anti-Caspr (1:500, kindly gifted by Professor Elior Peles) diluted in a 0.1% triton X-100 solution and 5% NGS one night at 4C **(Table 2)**. The following day, sections were washed three times in 1x PBS (15 min) and then incubated with goat anti-mouse IgG1 secondary antibody Cy5 (1:300, kindly gifted by Professor Elior Peles) and DAPI (1:1000, Fluka, Saint Louis, United States) diluted in a 0.1% triton X-100 solution and 5% NGS, 45 min at room temperature. Finally, slices were washed three times (15 min) in 1x PBS, mounted and, when dry, glass coverslip was applied using Mowiol (Calbiochem, 308 LaJolla, CA, United States).

To study cerebellar connectivity alterations, free-floating slices from 12-16 months old *Elovl5*$^{-/-}$ and wild type mice cerebella were washed for two hours in phosphate buffered saline (PBS) and then incubated with a permeabilization buffer (PBS 1%, Triton 0.5 % and Tween20 0.5%) for 5 minutes with gentle agitation. Then, floating slices were washed with PBS for three times 5 minutes each. Slices were then incubated with 5% Normal Donkey Serum (NDS) diluted with PBS for 30 minutes and then incubated overnight at 4°C with agitation with the following primary antibodies: rabbit anti-metabotropic glutamate receptor (mGluR1 1:800, Euroclone), guinea pig anti-vescicular GABA transporter (VGAT, 1:700, Synaptic Systems), rabbit anti-Caspr (1:1000, Abcam), mouse anti-Calbindin (1:1500, SWANT 300) and rabbit anti-vescicular glutamate transporter 1 and 2 (VGLUT1, 1:1500, 135 303, Synaptic System and VGLUT2, 1:300 AB2251-I, Sigma Aldrich) dissolved in PBS-T buffer containing 1.5% NDS **(Table 2)**. The morning after each series was washed in PBS for three times and then incubated with secondary antibody (Alexa 488 or 555, 1:500, anti-rabbit Ig-G, Invitrogen), 0.6% NDS and PBS-T for 1 hour and 30 minutes with agitation. Then series were washed for three times with PBS and incubated with DAPI (4',6-diamino-2-phenylindole) 1:500 and PBS+ for 1 minute and 30 seconds. Then slices were washed again for three times (5 minutes each) and mounted on a slide.

Antibody	**Host**	**Concentration**
Anti-ELOVL5 (NBP2-33500, Novus biologicals)	Rabbit	1:300
Anti-AN2 (kind gift of Miltenyi Biotech GmbH and Prof. J. Trotter)	Rat	1:100

Anti-MBP (Sternberger)	Mouse	1:1000
Anti-Iba1 (Wako Chemicals, Richmond)	Mouse	1:1000
Anti-GFAP (Dakopatts, Z334)	Rabbit	1:1000
Anti- CASPR (gifted by Professor Elior Peles)	Mouse	1:500
Anti-Calbindin (SWANT 300)	Mouse	1:1500
Anti-CASPR (ab34151, Abcam)	Rabbit	1:1000
Anti-VGLUT1 (135 303, Synaptic System)	Rabbit	1:1500
Anti-VGLUT2 (AB2251-I, Sigma Aldrich)	Guinea Pig	1:300
Anti-VGAT (131 308, Synaptic System)	Guinea Pig	1:700
Anti-mGluR1 (BK12551S, Euroclone)	Rabbit	1:800

Table 2. Primary antibody used for this study. Table indicating the primary antibodies, the manufacturers, the specificity and the concentrations used for this thesis.

2.2.3 Immunohistochemistry

To assess Elovl5 expression we first mapped β-galactosidase activity in homozygous and heterozygous Elovl5 knock-out mouse line where lacZ was included as a reporter under the control of Elovl5 promoter (for the model generation see Moon et al., 2009). Floating slices (30 μm-thick brain sagittal slices) were incubated overnight at 37◦C with a solution containing 1 mg/ml X-gal, 0.02% Nonidet P-40, 0.01% sodium deoxycholate, 2 mM MgCl2, 5 mM potassium ferricyanide, and 5 mM potassium ferrocyanide (pH = 7.5). Subsequently, the sections were mounted on gelatin-coated slides and let air dry overnight. The next day the sections were counter- stained with Nuclear Fast Red: mounted series were washed for 2 min in distilled water and then stained in 0.1% NFR (nuclear fast red) solution for 2 min. Sections were then rinsed

again in distilled water for 2 min, and subsequently dehydrated using a series of alcohols: 50% (2 min), 75% (2 min), 90% (2 min), and 100% (2 min). Afterward, the gelatin- coated slides were immersed in xylene for 5 min and finally a clear glass coverslip was applied using a permanent mounting medium.

Cresyl Violet Staining (Nissl Staining) was performed on one series for each *Elovl5*$^{-/-}$ and wild type mouse at 12 months of age. Free-floating sections were washed twice in PBS (15 min each). The series were mounted on gelatin coated slides and let air dry overnight. The staining was performed as follows: mounted series were washed for 2 min in distilled water to remove any residual salts and then stained in 0.1% Cresyl violet solution for 15 min. Following, sections were rinsed again in distilled water for 2 min, and then dehydrated using a series of alcohols: 50% (2 min), 70% (2 min), 95% (I) (2 min), 95% (II) (few seconds) and 100% (2 min). Next, the gelatin-coated slides were immersed in xylene for 5 min and finally a clear glass coverslip was applied using a permanent mounting medium. It should be noted that quantitative measurements might be not comparable to others reports, in which the tissues didn't undergo shrinkage due to the dehydrating and drying steps.

2.2.4 Images Acquisition and Processing

For the expression study, slides were scanned with Slide-Scanner Axiscan Z1 (ZEISS, Oberkochen, DE) both at low and high magnification (5x and 20x). Images obtained were then modified and adapted in color, contrast and brightness with Zen Software 2.1 (ZEISS, Oberkochen, DE). All the structures were analyzed and recognized by using the Interactive Atlas Viewer [IAV; Allen Human Brain Atlas–Allen Institute for Brain Science. Mouse Brain Atlas].
Whereas cell coverslipped cultures were examined using an E-800 Nikon microscope (Nikon, Melville, NY) connected to a color CCD Camera and a Leica TCS SP5 (Leica Microsystems, Wetzlar, DE) confocal microscope. Adobe Photoshop 6.0 (Adobe Systems, San Jose, CA, United States) was used to assemble the final plate.

Analysis of the slices for axon termina functionality was performed by acquiring images with Leica TCS SP5 confocal with a 63x objective and 1 um steps for the z-stack (Leica Microsystems, Wetzlar, Germany). The images were analyzed with Fiji software. For VGLUT1, 2 and mGluR1 three slices per mouse (wild type = 3; *Elovl5*$^{-/-}$ = 3) were used. Three stacks per

slice, both for the anterior and the posterior lobes, was analyzed; in each stack the intensity of four areas was measured. To analyze the axon terminals a count of the overlapping signals of Calbindin and VGAT in the white matter was made in three slices per mouse in all the stacks.

The nodal gap and paranode length analysis were performed on confocal images acquired using 63X oil objectives with a Leica TCS SP5 (Leica Microsystems, Milan, Italy) confocal microscope. Images (1024 x 1024 pixel, 0.50 μm thick optical sections) were analyzed using ImageJ software (1.52 t version). At least three slices/animal were analyzed. For cerebellar analysis, three random field for anterior lobules and posterior ones per each slice.

To evaluate possible amelioration on cerebellar atrophy of *Elovl5*$^{-/-}$ and wild type littermates belonging to the three groups at 12 months of age, we evaluated for each slice the white matter area/total area of the slice ratio. At least three vermal slices/animal and three animals were analyzed. The ratio was determined on the whole extent of each lobule, on Nissl-stained slices by using Neurolucida software (MBF bioscience, Williston, USA) connected to an E-800 Nikon microscope (Nikon, Melville, NY) with a 10× objective. All measurements were done blind relative to the mouse genotype.

2.2.5 High resolution light microscopy and transmission electron microscopy

High resolution light and transmission electron microscopy were carried out as reported in (Mancini et al., 2019). 12 months old *Elovl5*$^{-/-}$ and control mice were anesthetized by intraperitoneal injection with ketamine (100 mg/kg body weight) and xylazine (10 mg/kg body weight). For each animal the sciatic nerve was exposed, and a nerve segment was removed. Samples were first fixed in 2.5% glutaraldehyde in 0.1 M phosphate buffer (pH 7.4) for at least 4 h at 4°C and then were postfixed with 2% osmium tetroxide for 2 h and dehydrated in ethanol from 30% to 100% (5 min each passage). After two passages of 7 min in propylene oxide and 1 h in a 1:1 mixture of propylene oxide and Glauerts' mixture of resins, samples were embedded in Glauerts' mixture of resins (made of equal parts of Araldite M and the Araldite Harter, HY 964, Sigma Aldrich). In the resin mixture, 0.5% of the plasticizer dibutyl phthalate (Sigma Aldrich) was added. For the final step, 2% of accelerator 964 was added to the resin in order to promote the polymerization of the embedding mixture, at 60C. Transverse semithin sections (2.5 μm thick) were obtained using an ultramicrotome (Ultracut UCT, Leica, Wetzlar, Germany), and

stained with 1% toluidine blue and 2% borate in distilled water for high resolution light microscopic examination and design-based stereology. A DM4000B microscope equipped with a DFC320 digital camera was used for section analysis. Quantification of total number of myelinated nerve fibers was performed on toluidine blue- stained semi-thin sections. At this purpose, the two-dimensional dissector method (Geuna et al., 2000) together with a systematic random sampling scheme was applied: 12–16 sampling fields were randomly selected and, in each field, the two-dimensional dissector procedure was carried out. The total cross-sectional area of the whole nerve was also measured and used to calculate the total number of myelinated fibers (Geuna et al., 2000; Mancini et al., 2019). The G-ratio (inner perimeter/outer perimeter), the axon diameter (as frequency distribution), the myelin sheath thickness and myelin periodicity were analyzed in ultrathin (70– 100 nm) sections using a transmission electron microscope (JEOL, JEM- 1010, Tokyo, Japan) equipped with a Mega-View-III digital camera and a Soft-Imaging-System (SIS, Münster, Germany) for computerized acquisition of the images. The analysis was performed using ImageJ software (https://imagej.net/Fiji, RRID: SCR_003070). The quantifications of G-ratio, axon diameter and myelin sheath thickness were performed on at least 125 axons/animal and on 3–5 mice per genotype.

2.3 RNA and protein quantification

2.3.1 Magnetic-Activated Cell Sorting (MACS) Isolation of Oligodendrocytes and Cell Culture Procedures

To assess Elovl5 expression in glial cells in vitro, oligodendrocyte progenitor cells (OPCs) were isolated from P2 mouse brain (C57/BL6J background) by Magnetic-Activated Cell Sorting (MACS; Miltenyi Biotech GmbH, Bergisch Gladbach, DE) as in Boda et al. (2015). After tissue dissociation with the Neural Tissue Dissociation Kit P (Miltenyi Biotech GmbH, Bergisch Gladbach, DE), mouse OPCs were enriched by positive selection using an anti-PDGFRα antibody conjugated to magnetic beads, according to the manufacturer's instructions (Miltenyi Biotech GmbH). MAC-sorted OPCs were then plated onto poly-D- lysine (1 μg/ml, Sigma-Aldrich, Saint Louis, MS, United States) coated glass coverslips in a proliferative medium including Neurobasal, 1X B27 (Invitrogen, Milan, Italy), 2 mM L-glutamine (Sigma-Aldrich, Saint Louis, MS, United States), 10 ng/ml PDGF-BB, and 10 ng/ml human bFGF (Miltenyi Biotech GmbH, Bergisch Gladbach, DE), or in differentiative medium including Neurobasal, 1X

B27 (Invitrogen, Milan, Italy), 2 mM L-glutamine (Sigma-Aldrich, Saint Louis, MS, United States), 0.5 nM triiodothyronine (T3; Sigma-Aldrich). In all cases, purity of the MACS-selected OPCs was verified by immunocytochemistry (more than 95% of the cells were NG2+ at 6 h post-plating). Microglial cells have been obtained by orbital shaking method from mixed glial cell cultures and polarized toward either a proinflammatory (M1) or pro-regenerative (M2) phenotype by incubating with TNF-α (20 ng/ml) or IL-4 (20 ng/ml) (R&D, Milan, Italy) for 48 h, as described in Lombardi et al. (2019).

2.3.2 Quantitative RT–PCR

Total RNA from cell cultures was extracted with the Directzol RNA Miniprep kit (Zymo Research, Irvine, United States), and reverse transcribed to cDNA with the High-Capacity cDNA Archive kit (Thermo Fisher Scientific, Waltham, United States). Quantitative Real Time RT-PCR was performed as described in Sacco et al. (2010), with the pre-developed Taqman assay #Rn01446631_m1 (Thermo Fisher Scientific, Waltham, United States). A relative quantification approach was used, according to the 2-ddCT method. β-actin and glyceraldehyde-3-phosphate dehydrogenase (GAPDH) (Taqman assay #Rn00667869_m1; Thermo Fisher Scientific, Waltham, United States) was used to normalize expression levels.

2.3.3 Western blot assay

Sciatic nerves from wild type (n = 8) and *Elovl5*$^{-/-}$ (n = 4) mice were resuspended in 20% (w/v) RIPA buffer (25mM Tris–HCl pH 7.4, 150 mM NaCl, 1 mM EGTA, 1 mM EDTA, 1 mM dithiothreitol, 0.5 mM PMSF, 10 μg/ml Aprotinine, 10 μg/ml Leupeptine, 2mM sodium orthovanadate), and homogenized with a tissue lyser (Russo et al., 2018). The lysates were centrifuged at 10,000 g for 20 min at 4°C and the supernatant was collected and stored at -80°C until use. Twenty micrograms of proteins were separated by using a 4–12% Bis-Tris precast gel (Life Technologies) and transferred onto nitrocellulose membrane (GE- Healthcare). Membranes were than blocked with 50 g/L (5%) nonfat dry milk (Bio-Rad) in 50 mM Tris–HCl pH 7.4, containing 200 mM NaCl and 0.5 mM Tween-20 and then incubated overnight at 4C with primary antibodies. The following primary antibodies were used: MBP (1:1000, Covance, Cat# SMI-99P-500, RRID: AB_10120130), CNP-ase (1:500, Millipore, Cat# MAB326R, RRID: AB_94780), MPZ (1:3000, GeneTex Cat# GTX134070, RRID: AB_2876362), β-Actin (1:16000, Abcam, Cat# ab8226, RRID: AB_306371). HRP-conjugated goat anti-mouse (1:5000,

Bio-Rad, Cat# 170–6516, RRID: AB_11125547) and goat anti-rabbit (1:5000, Bio-Rad, 170–6515, RRID: AB_11125142) immunoglobulins, in Tris-buffered saline Tween containing 20 g/L non-fat dry milk, was used for detection with Luminata Forte Western substrate (WBLUF0100, Millipore). Densitometric values were normalized to β-Actin. Images were acquired by Chemidoc (Bio-Rad) and quantified by ImageLab software (RRID: SCR_014210, Bio-Rad).

2.4 Electrophysiological recordings

12-14 months old *Elovl5*$^{-/-}$ mice and wild type controls of both genders were used for all electrophysiological recordings.

Cerebellar slices were prepared as previously described (Hoxha et al, 2012). The animals were anesthetized with isoflurane (Isoflurane-Vet, Merial, Milan, Italy) and decapitated. The cerebellar vermis was removed and transferred to an ice-cold artificial cerebrospinal fluid (ACSF) containing (in mM): 125 NaCl, 2.5 KCl, 2 $CaCl_2$, 1 $MgCl_2$, 1.25 NaH_2PO_4, 26 NaHCO3, 20 glucose, which was bubbled with 95% O_2/5% CO_2 (pH 7.4). Parasagittal cerebellar slices (200 µm thickness) were obtained using a vibratome (Leica Microsystems GmbH, Wetzlar, Germany) and kept for 1 h at 35°C. Single slices were placed in the recording chamber, which was perfused at a rate of 2–3 ml/min with ACSF bubbled with the 95% O_2/5% CO_2.

2.4.1 Current clamp recordings

Whole-cell patch-clamp recordings were done at room temperature (20-24°C) from PCs using an EPC-10 patch-clamp amplifier (HEKA Elektronik, Lambrecht/Pfalz, Germany). The soma of PCs was visually identified using a 40× water-immersion objective of an upright microscope (E600FN, Eclipse, Nikon, Japan), and its upper surface was cleaned by a glass pipette, pulled from sodalime glass to a tip diameter of 10–15 µm, filled with ACSF. Pipettes of borosilicate glass with resistances between 2.5 and 3.0 MΩ were used for patch-clamp recording. For all the experiments, digitized data were stored on a Macintosh computer (G5, Apple computer) using the Patch Master software (HEKA Elektronik) and analyzed off-line. Patch pipettes were filled with a K-gluconate-based internal solution containing (in mM): 140 K-gluconate, 10 HEPES, 0.5 EGTA, 4 $MgCl_2$, 4 Na_2ATP, 0.4 Na_3GTP and the pH was adjusted to 7.3 with KOH and filtered at 0.2 µm. Gabazine (SR 95531, 20 µM) was added to the recording chamber to inhibit the GABA A receptors.

2.4.2 PC intrinsic membrane excitability

Recordings were performed after manually adjusting the holding current at a value, which kept the membrane voltage close to -70 mV (±1 mV). When holding current was greater than 400 pA neurons were discarded. Data were filtered at 9.1 kHz and sampled at 20 kHz. A series of current steps, each lasting 1000 ms, was delivered to the PC. Such current steps ranged from +100 to

+500 pA, in increments of 100 pA, spaced by 10 s. Data were analyzed using Axograph software (AxoGraph Scientific, Sydney, Australia) and afterwards the data were collected in a Microsoft Excel (Microsoft Corporation, Bellevue, WA, USA) spreadsheet. The results are expressed as a relation between the amplitude current and the frequency of evoked action potentials.

2.4.3 Responses of PCs to PF stimulation

To evoke excitatory postsynaptic potentials (EPSPs), derived from PF (PF-EPSPs) inputs onto PCs, square pulses (100 μs) were applied through a stimulating electrode (glass pipette, diameter 10-15 μm). PF-EPSPs were evoked by stimulating the PFs in the molecular layer and recorded at a holding potential of -90 mV. Negative current pulses were applied until the threshold to evoke an action potential was reached. The stimulus pulses were chosen 30% under the threshold current. Paired pulse facilitation was elicited by twin pulses at different time intervals (50, 100, 200, 300, 400, 500, 1000ms), and the ratio of the amplitude of the second PF-EPSP over the first one was calculated. All PF recordings were performed in the presence of gabazine (SR 95531, 20 μM) in the saline solution. PCs were current clamped at -90 mV.

2.4.4 mGlu1-mediated slow EPSC

PC was current clamped at 70 mV using EPC-9 patch-clamp amplifier (HEKA Elektronik, Lambrecht/Pfalz, Germany). Slow-EPSCs mediated by the mGluR1 receptor were recorded in the presence of a cocktail of (2,3-dihydroxy-6-nitro-7-sulfamoyl-benzo[f]quinoxaline-2, 3-dione) (NBQX 20 μM) and DL-2-Amino-5-phosphonovaleric acid (D-AP5, 10 μM) to block ionotropic glutamate receptors. PFs were stimulated with 4, 8, 12 and 16 stimuli at constant stimulation intensity.

2.4.6 Synaptically induced suppression of excitation (SSE)

Parallel fibers were stimulated with the following protocol: a train of ten stimuli at 200 Hz preceded and followed by a low stimulation frequency at 0.5 Hz. PC was current clamped at 70 mV. The magnitude of SSE (%) was calculated as follows: 100 x [(mean amplitude of 2 EPSCs after tetanic stimulation/mean amplitude of 5 EPSCs before the tetanic stimulation)]. Values of two to three trials were averaged for each neuron. For this recording, Gabazine was purchased from Abcam and applied via the chamber perfusion line.

2.4.7 Long-term depression (LTD)

For LTD experiment, the internals solution consisted of (mM): 130 potassium gluconate, 2 NaCl, 4 MgCl2, 4Na2ATP, 0.4 NaGTP, 20 HEPES, 0.25 EGTA. For LTP experiments, the internal solution was (in mM): 120 potassium gluconate, 9 KCl, 3.5 MgCl2, 10 Hepes, 4 NaCl, 17.5 sucrose, 4 Na2ATP 0.4 Na3GTP. Only the recoding with the series resistance less than 10 MΩ were accepted. The holding potential was set at −60 mV. Data were filtered at 3 kHz, digitized at 10 kHz, and stored using the Pulse software (HEKA Elektronik). A sodalime glass pipette (tip diameter 10–15 μm, filled with extracellular saline solution) was placed in the molecular layer to stimulate PFs with double pulses (using an interpulse interval of 100 ms) delivered every 20 s by an isolated stimulator (A/M Systems, Carlsborg, WA, USA). For each cell, the EPSC amplitude was normalized to the mean EPSC amplitude during 10-min baseline recording (immediately before treatment). Drugs were bath applied by switching perfusion lines without altering the perfusion rate. To reach the recording chamber the measured delay was 90 s. In all analyses, time 0 of drug application indicates the time at which the drug reached the chamber. During recording the extracellular saline solution always contained Bicuculline (20 μM) to block GABAA receptors. Slices were treated with vehicle as sham treatment for control. The PKA blocker PKI6-22 amide was dialyzed intracellularly via the patch pipette for at least 30 min before drug application. CL 316243 and SR 59230A were purchased from Tocris Bioscience (Bristol, UK). Bicuculline was purchased from HelloBio (Bristol, UK). Wortmannin was purchased from Sigma-Aldrich (Milan, Italy). PKI6- 22; was purchased from Enzo Life Sciences, Inc.

2.4.8 Responses of PCs to CF stimulation

To study the CF-PC synapse EPSCs were evoked by sending inputs onto PCs, square pulses (100 μs) were applied through a stimulating electrode placed in the granular layer. A holding potential of +40mV was used to record CF-EPSCs and avoid the problems related to the large size of CF-evoked synaptic currents at negative potentials. CF-EPSCs were identified by their all-or-none fashion and the presence of paired-pulse depression. The paired-pulse depression was elicited by twin pulses at different time intervals (50, 100, 150, 200, 400, 800, 1600, 3200 ms) when the threshold was detected. All CF recordings were performed in the presence of the GABAA antagonist gabazine (SR 95531, 20 μM) in the saline solution.

2.4.9 Antidromic action potential conduction

Antidromic action potential propagation on PC was evaluated in cell-attached configuration helding the cell at -70 mV. The stimulating electrode was placed in the granular layer at a distance of 100 μm from the PC soma. The conduction velocity of the action potential was analyzed. All drugs were purchased from Hello Bio (Bristol, UK) and applied via the chamber perfusion line.

2.4.10 Caudal nerve conduction velocity

Mice were anesthetized via intraperitoneal injection with ketamine (100 mg/kg body weight) and xylazine (10 mg/kg body weight). Stain- less steel subdermal needle electrodes (Technomed, medical accessories) were used to deliver supramaximal stimulation with 0.05 ms impulses using an isolated stimulator (A-M System 2100, Sequim, WA, USA). Low frequency filters were set to 300 Hz and high frequency filters were set to 10 kHz.

The nerve conduction velocity (NCV) in the tail nerve was assessed by placing needle electrodes in the tail, with the positive recording electrode at a few centimeters from the base of the tail. In proximal to distal direction the distances from the first electrode were: negative recording electrode 0.5 cm, ground 1.5, negative stimulation electrode 4 cm, positive stimulation electrode 4.5 cm. The latency of the potentials recorded after nerve stimulation was measured and the NCV was calculated accordingly. All neurophysiological determinations were performed under standard conditions and external body temperature was maintained at 34°C with a heating lamp.

2.5 Lipidic analysis

2.5.1 Liquid chromatography–tandem mass spectrometry analysis

The levels of total phospholipids were evaluated by means Liquid Chromatography–tandem mass spectrometry (LC)-MS/MS according to published protocol (Cermenati et al., 2015) with some modifications described below. Briefly, internal standards (13C-all labeled linoleic acid and 13C-all labeled palmitic acid) were added to samples (10 mg for tissues), and lipid extraction was performed using 1 ml of methanol (MeOH)/Acetonitrile (1/1; v/v). Phospholipids analysis: methanolic extracts were analyzed by liquid chromatography tandem mass spectrometry (LC–MS/MS) using XTerra Reverse Phase C18 column (3.5 μm 4.6 x 100 mm, Waters) and as isocratic mobile phase MeOH with 0.1% formic acid with 274 multiples reaction

monitoring (MRM) transitions for positive ion mode in 5 min total run for each sample. LC-ESI-MS/MS for negative ion mode was conducted with a cyano-phase LUNA column (50 mm x 4.6 mm, 5 μm; Phenomenex) and as isocratic mobile phase 5 mM ammonium acetate pH 7 in MeOH with 50 MRM transitions in 5 min total run for each sample. The identity of the different phospholipid families was confirmed using pure standards, namely one for each family. An ESI source connected with an API 4000 triple quadrupole instrument (AB Sciex, USA) was used. MultiQuantTM software version was used for data analysis and peak review of chromatograms. Changes between detected phospholipid families were calculated as percent of single phospholipid species normalized to total phospholipid analyzed. Data points have been graphically displayed by the "ggplot2" package of "R" programming language.

2.6 Behavioral study

2.6.1 Balance beam test

To analyze balance and motor coordination, we performed the balance beam test on *Elovl5*$^{-/-}$ and wild type mice. The beam test was performed as previously described (Hoxha et al., 2012). Briefly, we used a metal beam 1 cm wide and 100 cm long suspended 12 cm above the bench. The mice had to cross the beam to reach a cage enriched with toys. To allow the mice to familiarize with the experimental apparatus, thus reducing the stress due to an unknown procedure, the experiment was preceded by 3 days of habituation. On the day of the test, the animals were placed to acclimate in the behavioral room at least 15 min before the experiment. Both *Elovl5*$^{-/-}$ and wild type mice were tested individually, and each animal was encouraged to traverse the beam at least three times. The test was repeated for three consecutive days. The test was recorded using a video camera and analyzed offline by an operator blind to the genotype. The performance was assessed by measuring the number of slips committed while traversing the beam. The third day mice were also measured in weight to exclude weight involvement in data found. The test was recorded using a video camera and analyzed offline by an operator blind to the genotype.

2.7 Statistical Analysis

Statistical analyses were carried out with GraphPad Prism 7 (GraphPad sofware, Inc). The Shapiro–Wilk or Kolmogorov–Smirnov test were first applied to test for a normal distribution of the data. For data not normally distributed, Mann-Whitney U-test (to compare two groups) and Kruskal-Wallis test (for multiple group comparisons) were used. In all instances, $P < 0.05$ was considered as statistically significant. Histograms represent mean ± standard error (SE).

CHAPTER 3 – RESULTS

3.1 Elovl5 Expression in the Central Nervous System of the Adult Mouse (Balbo et al., 2021)

Mutations of specific *ELOVL*-family genes have a different impact on nervous system leading to distinct pathological conditions in humans. This might be explained by the tissue-specific expression and role of *ELOVL*-family genes. While *ELOVL2*, *ELOVL7*, and *ELOVL1* have a restricted CNS distribution (Tvrdik et al., 2000; Lein et al., 2007), Elovl4 expression is abundant and well characterized in both adult and perinatal mouse brain (Sherry et al., 2017). In contrast, the Elovl5 expression pattern remains largely uninvestigated so far. So, to counteract to this lack of information, one of the main goals of this thesis is to map Elovl5 expression in the adult mouse CNS and to provide relevant insights to understand its role in specific CNS areas and cell types.

3.1.1 Elovl5 Gene Expression in the Central Nervous System

In the lacZ reporter mouse, XGal staining revealed a widespread expression with some region-specific differences **(Fig. 11** and **Table 3)**. It is important to note that the XGal staining observed in Elovl5 lacZ reporter mouse reflected the *in-situ* hybridization published in Allen Mouse Brain Atlas. Specifically, in the telencephalon, a prominent labeling was found in the olfactory bulb (mitral cell layer, **Fig. 11A**), in the neocortex, in the hippocampus (**Fig. 11A**) and in the midbrain (**Fig. 11B**). The thalamus showed a less pronounced, moderate XGal labeling, except for a strong expression in the reticular nucleus (**Fig. 11A**). As previously shown (Hoxha et al., 2017), in the cerebellum PCs and deep cerebellar nuclei were the most expressing cell types (**Fig. 11B**). Interestingly, we also found several labeled cells in the cerebellar white matter, in the granular layer and in the deeper part of the molecular layer. In the spinal cord, we observed a pronounced labeling in the gray matter, in neurons of different cell body size (**Fig. 11C**).

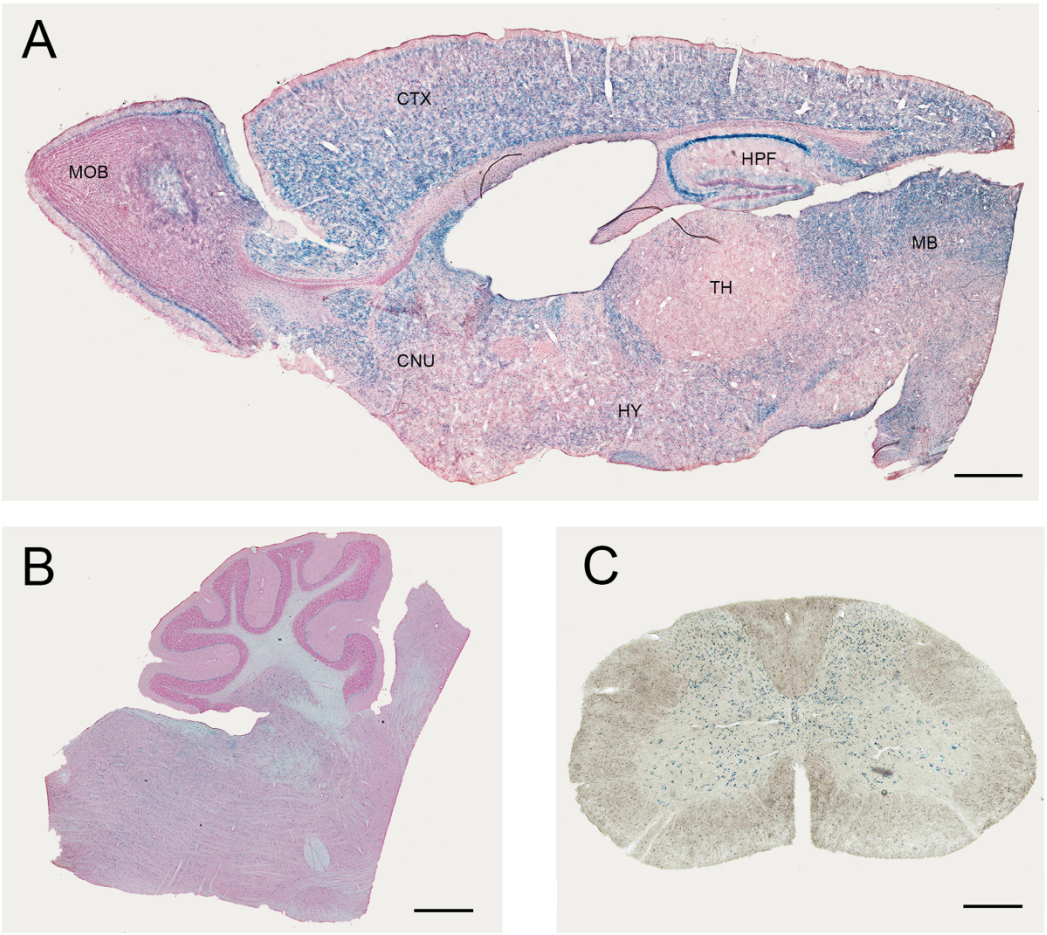

Figure 11. Expression of Elovl5 in the central nervous system. XGal staining (blue) indicates an ubiquitary expression of Elovl5 gene in forebrain **(A)**, cerebellum and brainstem **(B)**, spinal cord **(C).** MOB, Main Olfactory Bulb; CTX, Cortex; HPF, Hippocampus; MB, midbrain; TH, thalamus; HY, Hypothalamus; CNU, cerebral nuclei. Scalebars: **(A, B)** 500 µm and **(C)** 50 µm.*(Balbo et al., 2021)*

3.1.2 Elovl5 Protein Distribution in Brain Regions

Protein localization was analyzed in wild-type mice by immunofluorescence labeling throughout different brain regions in order to define the expression pattern in diverse cell populations (**Table 3**). The intensity of immunoreactivity varied in different regions and neuronal populations.

3.1.2.1 Elovl5 distribution in the telencephalon

The olfactory regions presented a very peculiar labeling (**Fig. 12**). In the main olfactory bulb, mitral cells were found strongly positive for Elovl5 staining. In the superficial part of the outer plexiform layer small cells, likely tufted cells, showed moderate Elovl5 labeling, whereas no positive cells were observed in the granular layer (**Fig. 12A**). The accessory olfactory bulb presented a similar expression pattern with a strong staining in the mitral cells (**Fig. 12D**). In anterior olfactory nucleus positive cells for Elovl5 were found mainly in layer II (**Fig. 12C**), whereas in the olfactory tuberculus in layers II and III (**Fig. 12D**).

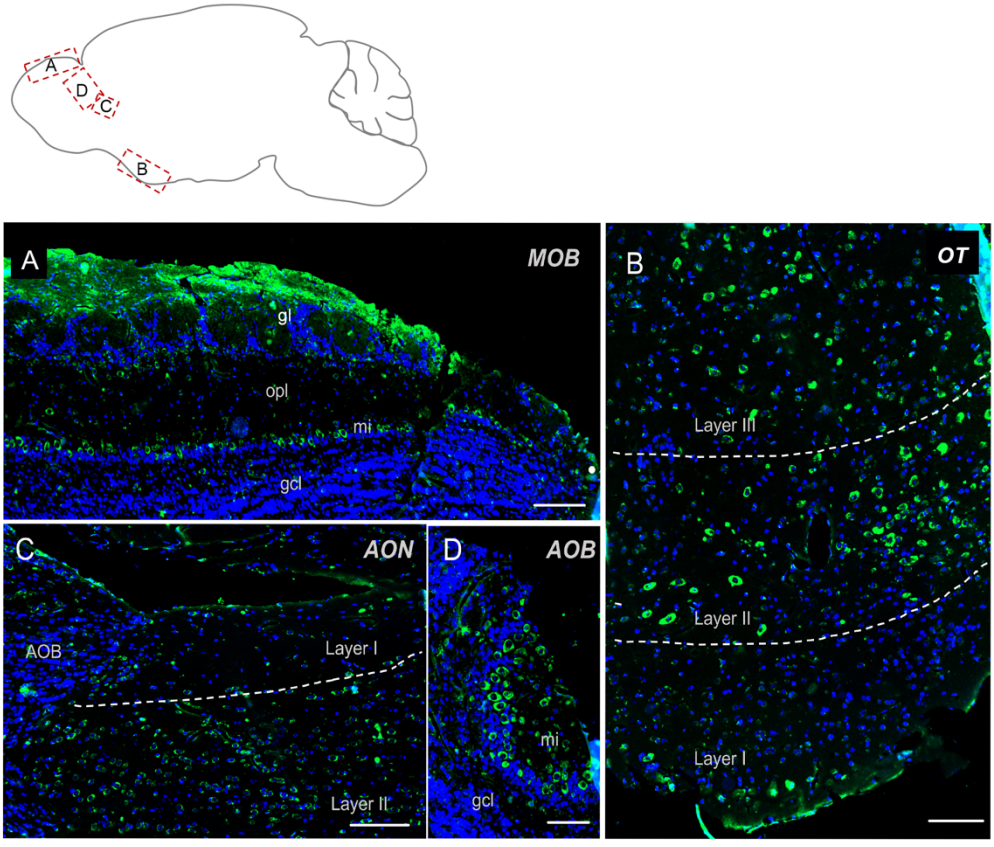

Figure 12. Elovl5 distribution in olfactory regions. (A) In the olfactory bulb, immunohistochemical labeling for Elovl5 (green) and DAPI (blue), shows a strong signal in mitral cells (mi) and in the glomerular layer (gl), while cells belonging to the granule cell layer (gcl) are negative. **(B)** The olfactory

tubercle (OT) (shown at high magnification) shows a predominant expression of Elovl5 (green) in layer II and layer III neurons. **(C)** In layer II neurons of the accessory olfactory nucleus (AON) a moderate presence of the enzyme is detected. **(D**) The accessory olfactory bulb shows a similar signal as the one detected in the main bulb, with a high intensity in mitral cells (mi) and no signal in the granule cell layer (gcl). MOB, Main Olfactory Bulb; mi, mitral cells; gl, glomerular layer; opl, outer plexiform layer; gcl, granular cell layer; OT, Olfactory Tubercle; AON, Anterior Olfatory Nucleus; AOB, Accessory Olfactory Bulb. Scalebars: **(A, C)** 200 μm, **(B)** 100 μm, and **(D)** 50 μm. *(Balbo et al., 2021)*

Elovl5 immunolabeling was expected to be extremely strong in the hippocampus, because of the high signal obtained with the XGal staining (**Fig. 11A**). Immunofluorescence analysis confirmed a relatively strong labeling of pyramidal neurons, but with regional differences (**Fig. 13A**). In fact, in all hippocampal fields Elovl5 labeling was clearly present in pyramidal neurons, with a gradient of intensity: the signal was stronger in CA2 and CA3 than in CA1 and subiculum, where it was just moderately intense. Hilar neurons and several neurons of the strata oriens and radiatum were strongly labeled. On the other hand, neurons of the dentate gyrus were negative, except for a few strongly labeled cells in the subgranular zone.

The cerebral neocortex showed a layer-specific expression pattern (**Fig. 13B**). Cells showing moderately strong Elovl5 labeling were found in layer II/III, IV and V, while in layer VI neurons displayed a weak intensity staining. The piriform and endopiriform cortex showed a strong Elovl5 labeling (**Fig. 13C**), whereas claustrum displayed a moderate intensity labeling (**Fig. 13C**). In the corpus callosum, sparse positive cells were found. In the amygdala, neurons showed a moderate reactivity for Elovl5 in general: more prominent in the cortical regions than in medial ones (**Fig. 13D**).

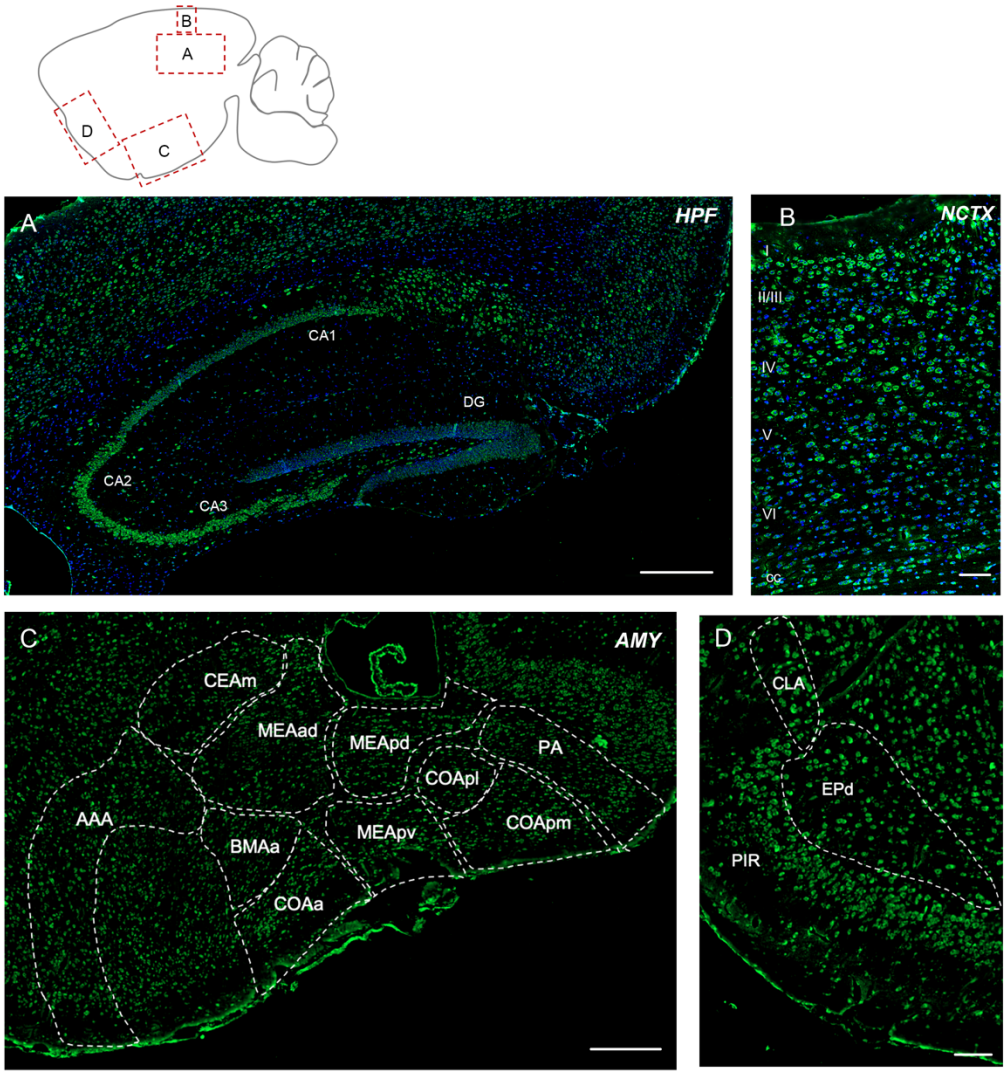

Figure 13. Elovl5 expression in cortical and subcortical regions. (A) In the hippocampus, Elovl5 (green) is strongly expressed by CA2 and CA3, in a moderate way by CA1, while it is not present in dentate gyrus. Oriens, radiatum, and hilar interneurons are strongly labeled. Cell nuclei are counterstained by DAPI (blue). **(B)** In the neocortex Elovl5 labeling is present in a moderately strong way in layers II/III, IV and V. In layer VI, neurons display a weak intensity staining. **(C)** In the amygdala Elovl5 expression is more prominent in the cortical areas than in medial ones. **(D)** The claustrum is moderately positive for Elovl5 staining, while piriform and endopiriform cortex show a strong signal. HPF, hippocampal formation; CA, Cornu Ammonis; DG, dentate gyrus; NCTX, neocortex; AMY, Amygdala; AAA, Anterior amygdalar area; CEAm, Central amygdalar area, medial part; MEAad, Medial amygdalar area, anterodorsal part; MEApd, Medial amygdalar area, posterodorsal part; MEApv, Medial amygdalar area, posteroventral part; COApl, Cortical amygdalar area, posterior part; COApm, Cortical amygdalar area, posterior part, medial zone; PA, posterior amygdalar nucleus; BMAa; Basomedial amygdalar nucleus,

anterior part; PIR, piriform cortex; CLA, claustrum; EPd, endopiriform nucleus, dorsal part. Scalebars: **(A)** 500 µm, **(B, D)** 100 µm, and **(C)** 250 µm. *(Balbo et al., 2021)*

In the basal ganglia, caudate, putamen and nucleus accumbens just few sparse cells were strongly labeled. The subthalamic nucleus, the substantia nigra pars compacta and the ventral tegmental area showed a strong labeling. A strong staining was observed also in the globus pallidus, in both internal and external parts (**Table 3**).

3.1.2.2 Elovl5 presence in diencephalon

In the thalamus, the reticular nucleus showed the most prominent labeling for Elovl5, compared to the other nuclei (**Fig. 14**). The peripeduncular nucleus also showed a strong labeling. The parvicellular part of subparafascicular nucleus, geniculate complex and ventral posteromedial andposterolateral nuclei of the thalamus presented instead moderate immunoreactivity to Elovl5 staining (**Fig. 14** and **Table 2**). In the zona incerta there was a strong labeling (**Fig. 14** and **Table 3**).

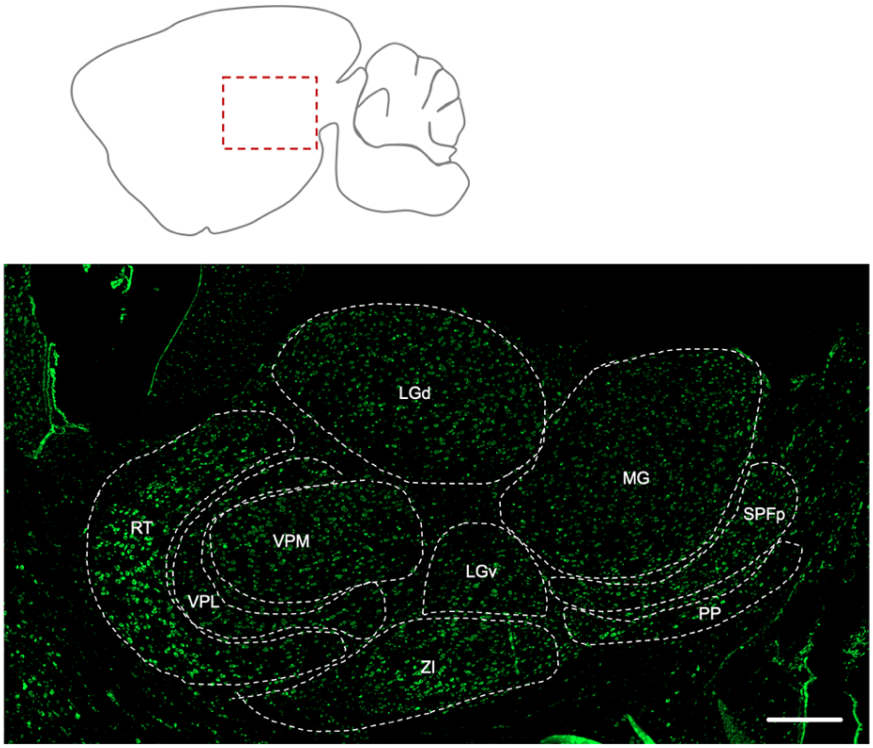

Figura 14. Distribution of Elovl5 in thalamus. Elovl5 (green) expression in the thalamus has a region-specific intensity. The most intense labeling is shown by the reticular nucleus. LGd, dorsal part of lateral geniculate complex; LGv, ventral part of lateral geniculate complex; MG, medial geniculate complex;

SPFp, subparafasciular nucleus, parvicellular part; PP, peripeduncular nucleus; ZI, zona incerta; VPM, Ventral posteromedial nucleus of thalamus; VPL, Ventral posterolateral nucleus of thalamus; RT, Reticular nucleus of thalamus. Scale bar: 200 μm. *(Balbo et al., 2021)*

In the hypothalamus, the tuberal nucleus, retrochiasmatic area and anterior hypothalamic nucleus displayed the most prominent labeling for Elovl5 compared to the other structures belonging to this region. The lateral hypothalamic area showed a heterogenous expression pattern: the immunofluorescence signal was stronger in the rostral part of the nucleus while it had a weaker intensity in the caudal part (**Table 3**). Supramammillary and lateral mammillary nuclei, as well as lateral preoptic area presented a moderate immunoreactivity to Elovl5 antibody.

3.1.2.3 The expression of Elovl5 in brainstem

The Elovl5 expression pattern was very complex in the brainstem. The brainstem together with the cerebellum showed the highest intensely labeled cells (**Table 3**).

In midbrain, the inferior colliculus displayed weak or no labeling for Elovl5, whereas the superior colliculus showed a moderate signal. The most prominent labeling in this region was in the red nucleus. The periaqueductal gray and the midbrain reticular nucleus displayed moderate labeling (**Table 3**).

In the pons, tegmental nuclei showed the most prominent labeling for Elovl5 (**Fig. 15A**). Pontine nuclei, tegmental reticular nucleus and superior olivary complex displayed a strong presence of positive cells too (**Fig. 15A**). The pontine reticular nuclei were found to be moderately and non-homogeneously positive for Elovl5 labeling (**Fig. 15A** and **Table 3**).

In the medulla, the medial vestibular nucleus and spinal vestibular nucleus presented a very strong labeling for Elovl5 (**Fig. 15B**). The nucleus of the solitary tract, intermediate reticular nucleus and gigantocellular reticular nucleus showed moderate to weak reactivity to Elovl5 antibody. The paragigantocellular reticular nucleus and medullary reticular nucleus, instead, displayed a peculiar pattern of expression: in both areas, the Elovl5 signal was not homogeneous (**Fig. 15B**). In the paragigantocellular reticular nucleus, the parvicellular part showed a more prominent expression compared to the magnocellular one (**Fig. 15B**). In the medullary reticular nucleus, the most intense signal was presented by neurons with bigger cell body compared to smaller ones, except for the fiber tract, in which small cells, probably oligodendrocytes, displayed an incredible high signal for Elovl5 labeling. The inferior olivary complex showed strong staining for Elovl5 (**Table 3**).

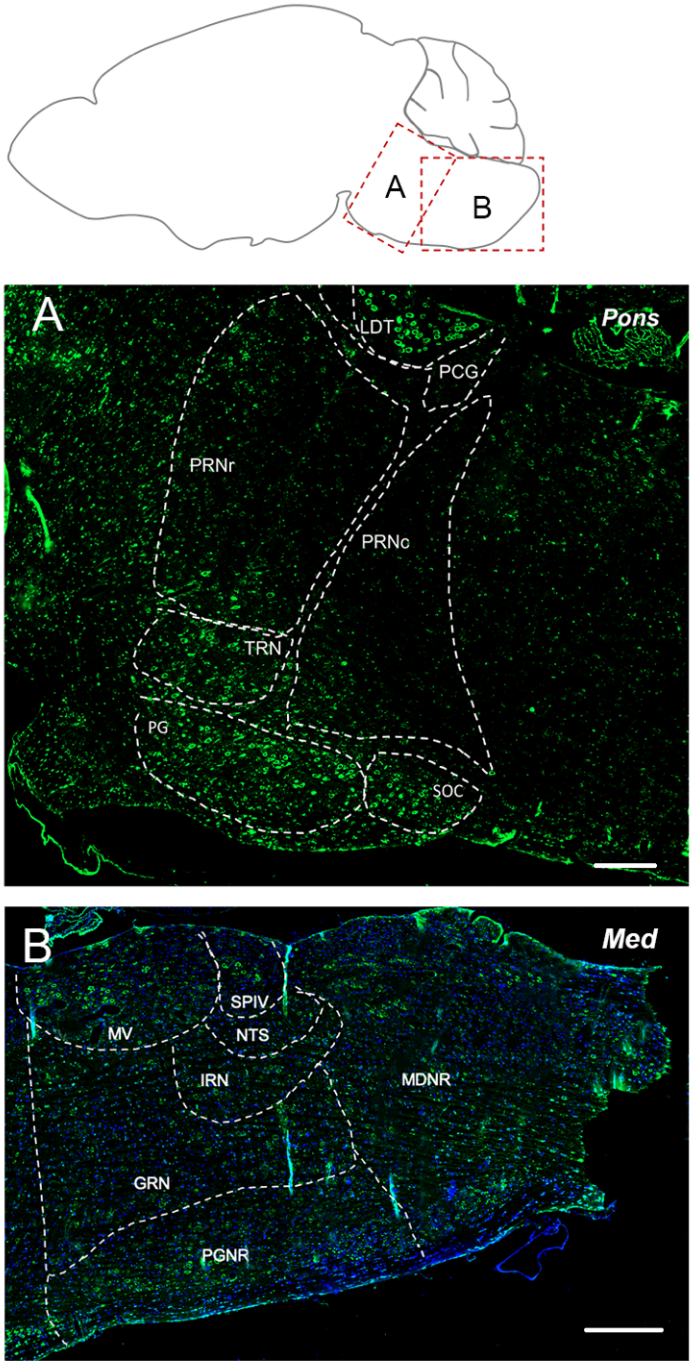

Figure 15. Elovl5 expression in pons and medulla. (A) In the pons, the most prominent labeling for Elovl5 is shown by tegmental nuclei, while pontine nuclei, tegmental reticular nucleus and superior olivary complex displayed a moderately strong signal. Medium-low intensity is shown by pontine reticular nuclei. **(B)** In the medulla, very strong labeling for Elovl5 is shown by medial vestibular nucleus and spinal vestibular nucleus. A moderate to weak signal is detected in the nucleus of the solitary tract, intermediate reticular nucleus and gigantocellular reticular nucleus. A non-homogeneous pattern of expression is present in the paragigantocellular reticular nucleus and medullary reticular nucleus. **(A)** LDT, Laterodorsal Tegmentel Nucleus; PCN, Pontine Central Nuclei; PRNc, Pontine Reticular Nucleus, caudal part; PRNr, Pontine Reticular Nucleus, rostral part; TRN, Tegmental Reticular Nucleus; PN, Pontine Nuclei; SOC, Superior olivary Complex. **(B)** MV, Medial Vestibular Nucleus; SPIV, Spinal

Vestibular Nucleus; NTS, Nucleus of Solitary Tract; IRN, Intermediate reticular Nucleus; GNR, Gigantocellular Reticular nucleus; PGNR, Paragigantocellular Reticular nucleus; MDRN, Medullary Reticular nucleus. Scale bars: **(A)** 200 µm and **(B)** 250 µm. *(Balbo et al., 2021)*

3.1.2.5 Elovl5 in the cerebellum

In adult cerebellum the immunofluorescence labeling for Elovl5 reflected faithfully the XGal staining (**Fig. 11B**). PCs showed a strong positivity in cell bodies (**Fig. 16A**) with no differences in the expression pattern between anterior and posterior lobules (Hoxha et al., 2017). The labeling was present also in some sparse neurons in the granular layer, in the deeper part of the molecular layer and cerebellar white matter (**Fig. 16A**). Interestingly, the cells of the deep cerebellar nuclei displayed the most intense labeling (**Fig. 16B**).

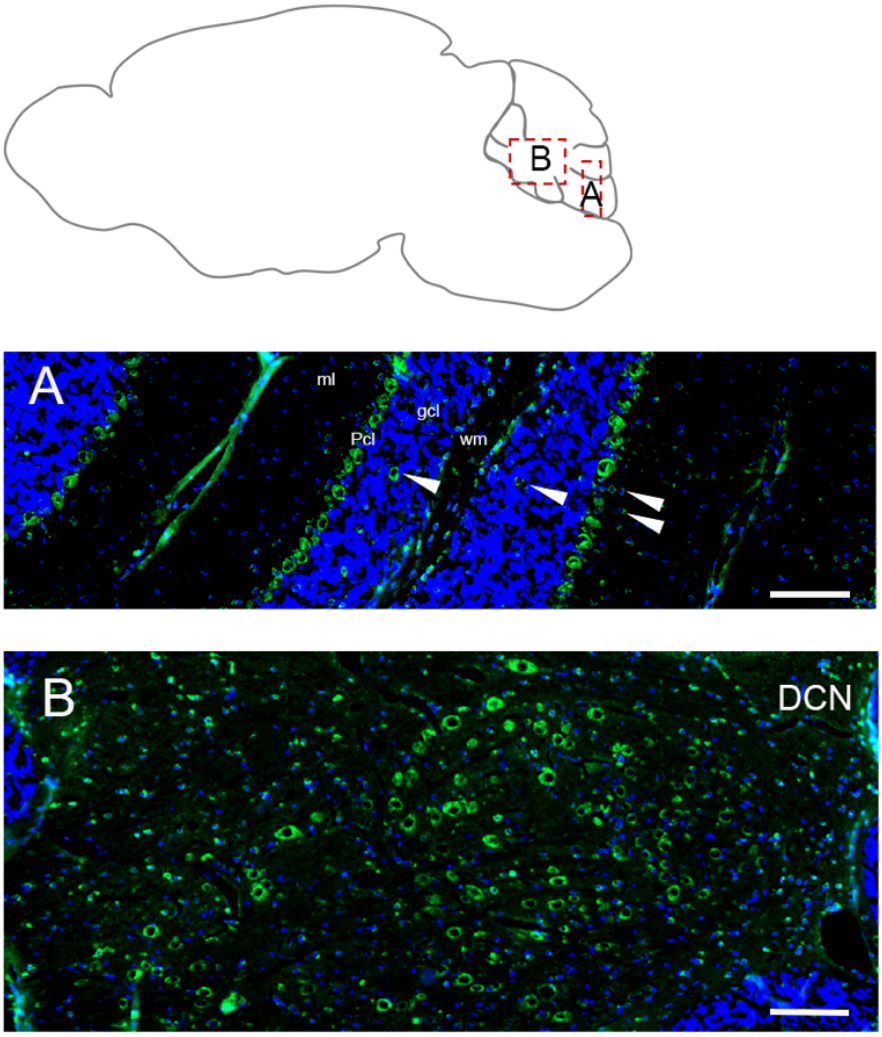

Figure 16. Distribution of Elovl5 in the cerebellum. (A) High magnification of the cerebellar cortex. Purkinje cells (Pcl) strongly express Elovl5; a moderate signal is present in sparse positive cells in white

matter (wm), deeper part of the molecular layer (ml) and granular layer (gcl) (white arrow). **(B)** Prominent expression of Elovl5 (green) (DAPI in blue) by deep cerebellar nuclei (DCN). Scale bars: **(A, B)** 100 µm. *(Balbo et al., 2021)*

3.1.2.6 Elovl5 localization in spinal cord

In the spinal cord, Elovl5 showed a well distinguishable cell-type expression pattern (**Fig. 17A-D**). In fact, by analyzing the gray matter, motor neurons belonging to laminae VIII and IX presented a moderate intensity signal for Elovl5 staining (**Fig. 17B**). From laminae I to VII, instead, cells displayed very weak labeling. The most prominent expression seemed to belong to glial cells in the white matter (**Fig. 17C, D**).

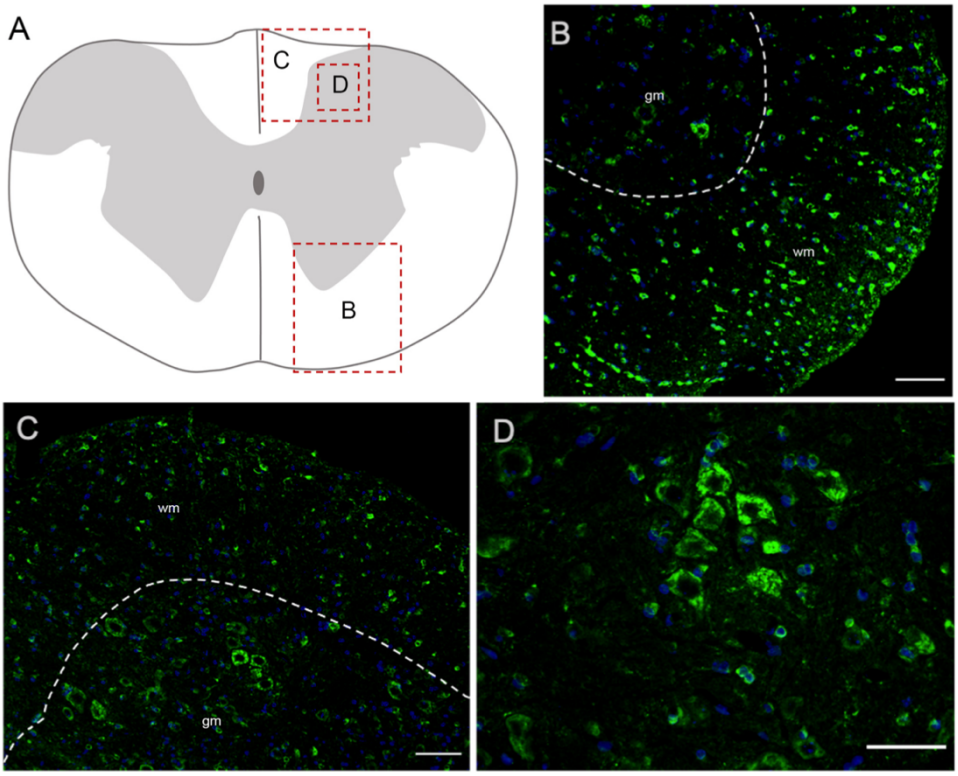

Figure 17. Elovl5 in the spinal cord. (A) Schematic representation of a spinal cord coronal section and areas magnified showed in panels **(B–D)**. **(B, C)** Elovl5 (green) is strongly expressed by small cells in the spinal cord white matter and in a moderate way by motor neurons in the gray matter. **(D)** High magnification of large neurons of the dorsal horn, positive for Elovl5 staining (green). **(B, C)** wm, white matter; gm, gray matter. Scale bars: **(B, C)** 100 µm and **(D)** 50 µm. *(Balbo et al., 2021)*

3.1.3 Elovl5 Expression in Glial Cells

In each analyzed region of the CNS Elovl5 immunoreactivity was not restricted to neurons, but rather comprises glial cells, whose immunophenotyping was in most cases hampered by the slice treatments required for anti-Elovl5 immunostaining (see section "Materials and Methods"). Thus, in order to identify Elovl5 positive glial cell types, double immunofluorescence staining was performed on primary cell cultures and on sagittal mouse brain sections. Elovl5 was expressed by virtually all immature oligodendrocyte precursor cells (identified by the expression of the chondroitin sulfate proteoglycan AN2; Boda et al., 2011) and by oligodendrocytes (expressing the myelin basic protein, MBP) in vitro (**Fig. 18A-C**).

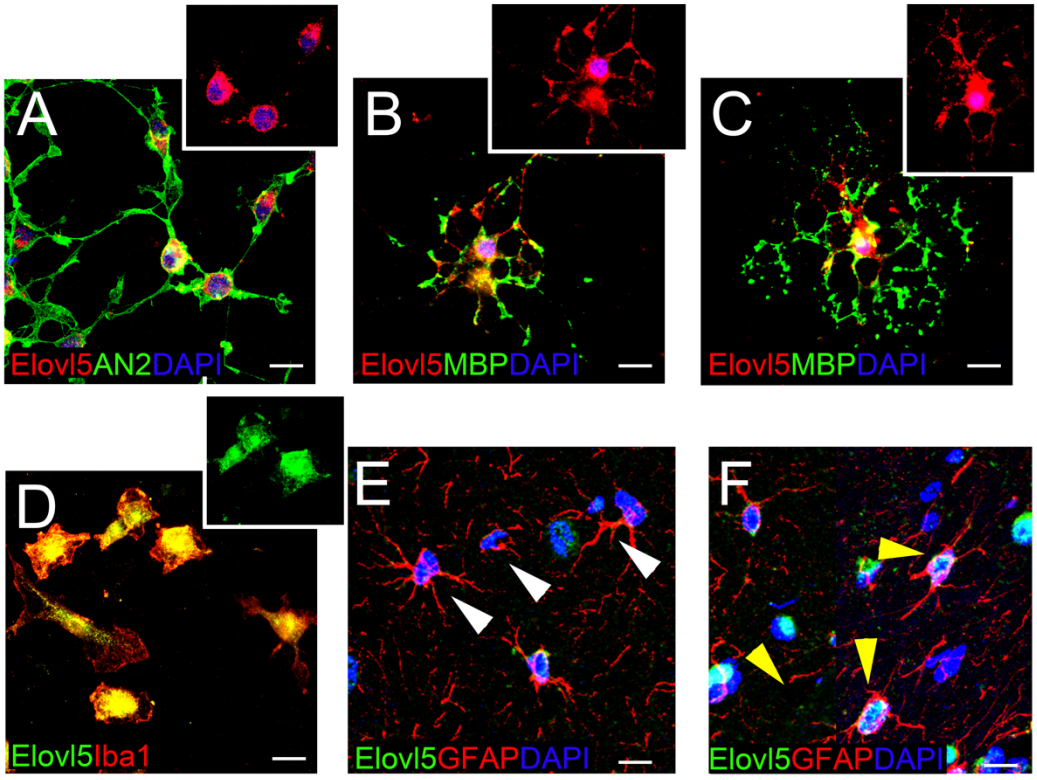

Figure18. Elovl5 expression in glial cells. (A–C) Widespread distribution of Elovl5 (red) in cultured AN2+ (green) oligodendrocyte precursor cells **(A)** and in maturing **(B)** and differentiated ramified **(C)** MBP+ (green in B-C) oligodendrocytes. **(D)** Elovl5 (green) expression in cultured Iba1+ (red) microglia. **(E, F)** Sagittal brain slices showing low and heterogeneous expression of Elovl5 (green) in GFAP+ (red) astrocytes. White arrowheads in **(E)** point to negative cells. Yellow arrowheads in **(F)** point to Elovl5+ cells. Scale bars: 10 µm. *(Balbo et al., 2021)*

Notably, Elovl5 mRNA level appeared remarkably increased in oligodendrocytes compared to immature OPCs (**Fig. 19A**, $P < 0.05$ Mann-Whitney U-test), suggesting Elovl5 participation in

oligodendroglia maturation. Elovl5 immunolabeling was also found in microglial cells, identified by expression of ionized calcium-binding adapter molecule 1 (Iba1) (**Fig. 18D**). In these cells, Elovl5 mRNA expression showed a non-significant tendency to increase when microglia were polarized toward a proinflammatory M1 phenotype, compared to resting microglia (**Fig. 19B**). In contrast, microglia polarization toward a proregenerative M2 phenotype was not associated to changes in Elovl5 transcript levels (**Fig. 19B**). Finally, while most astrocytes showed no or little immunolabeling for Elovl5, a subpopulation of glial fibrillary acidic protein (GFAP) positive astrocytes was found positively marked (**Fig. 18E, F**).

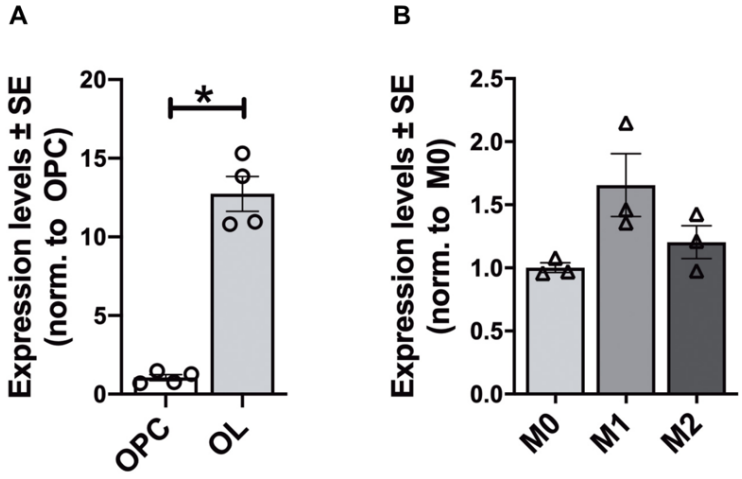

Figure 19. Gene expression analysis of Elovl5 in glial cells. (A) Elovl5 expression in oligodendrocytes (OL, n = 4) compared to immature oligodendrocyte precursor cells (OPC, n = 4) ($P < 0.05$ Mann-Whitney U-test). **(B)** Elovl5 levels in microglial cells in resting (M0, n = 3), proinflammatory M1 phenotype (n = 3) and proregenerative M2 phenotype (n = 3). The expression levels were compared to the microglial cells in resting state. *$P < 0.05$. *(Balbo et al., 2021)*

		XGAL	Immunofluorescence
Olfactory Bulb	Glomerular layer	-	-
	Outer plexiform layer	-	SP
	Mitral cell layer	+++	+++
	Internal plexiform layer	-	-
	Granular layer	-	-
Anterior Olfactory nucleus		++	++
Pyriform cortex		+++	+++
Olfactory Tubercle		+	++
Islands of Calleja		+++	+++
Amygdala	Cortical amygdaloid nuclei	+	+++
	Medial amigdaloid nuclei	++	++
Lateral Septum		++	+
Hippocampus	Pyramidal layer	+++	++
	Stratum oriens interneurons	++	++
	Dentate gyrus	- *	-
	Hylar neurons	++	++
	Subiculum	+	+
Neocortex	Layer I	++	++
	Layer II/III	++	++
	Layer IV	++	++
	Layer V	++	++
	Layer VI	+	+
Basal Ganglia	Nucleus Accumbens Core	+	+
	Nucleus Accumbens Shell	-	+
	Caudate/Putamen	++	+
	Globus pallidus	-	++
	Subthalamic nuclus	+++	++
	Substantia Nigra Reticulata	-	+
	Substantia Nigra Compacta/VTA	+++	++
Thalamus	Reticular nuclei	+	+++
	Pedipeduncular nucleus	+	++
	Subparafasciular nucleus	+	++
	Geniculate complex	+	++
	Medial geniculate complex	+	+
	Ventral posteromedial nuclei	+	++
	Ventral posterolateral nuclei	+	++

* positive cells in the subgranular region

		XGal	Immunofluorescence
Hypothalamus	Tuberal nucleus	++	++
	Retrochiasmatic area	++	++
	Anterior hypothalamic nucleus	++	++
	Lateral hypothalamic area	++	++/+
	Supramammillary nucleus	++	++
	Mammillary nucleus	++	++
	Preoptic area	++	++
	Zona incerta	++	+
Midbrain	Inferior colliculus	+	+
	Superior colliculus	++	++
	Red nucleus	+++	+++
	Ventral tegmental area	++	++
	Periaqueductal grey	++	++
	Midbrain reticular nucleus	++	++
Pons	Tegmental nuclei	++	++++
	Pontine grey	++	+++
	Tegmental reticular nucleus	++	+++
	Supraolivary complex	+++	+++
	Pontine reticular nuclei	++	++
Medulla	Vestibular nuclei	++++	++++
	Lateral reticular nucleus	+++	+++/++
	Medullary reticular nucleus	+++	++
	Nucleus of solitary tract	++	++
	Inferior olivary complex	++++	+++
Cerebellum	Purkinje cells	+++	+++
	Molecular Layer	SP	SP
	Granular Layer	SP	SP
	Deep cerebellar nuclei	++++	++++
Spinal cord	Motorneurons – laminae I to VII	+	+
	Motorneurons – lamina VIII	+++	+++
	Motorneurons – lamina X	+++	+++

Table 3. Summary of brain regions expressing Elovl5. Signals were rated as ++++, very high to intense; +++, intense; ++, moderate; +, low; -, not detectable; SP, labeling restricted to sparse cells. *(Balbo et al., 2021)*

3.2 Elovl5 is required for proper action potential conduction along peripheral myelinated fibers (Hoxha et al., 2021)

Myelin sheaths wrapped around axons enable saltatory propagation of action potentials, thereby increasing their velocity (Suminaite et al., 2019). Myelin, constituted by multiple layers of lipid-rich membranes, provides electrical insulation preventing leakage of current by increasing the resistance between the axonal cytoplasm and the interstitial fluid (Bakiri et al., 2011). This effect increases the space constant, promoting faster transfer of action potentials from one node of Ranvier to the next. At the same time, myelin reduces membrane capacitance at the internode, thereby reducing the time constant, so that electrical charging becomes faster, speeding up action potential conduction. These properties are strictly dependent on the compactness of myelin layers, which assures that internodes are almost entirely formed by lipid membranes with minimal cytoplasmic content (Simons, 2016). Lipids are the main component of myelin, constituting about 80% of its dry mass (O'Brien & Sampson, 1965; Quarles et al., 2005). In myelin, the main lipid classes are phospholipids (glycerophosphatides), sphingolipids and cholesterol (Norton & Poduslo, 1973; O'Brien & Sampson, 1965). The structural integrity of myelin depends on the interaction between lipids and membrane proteins (Bradl, 1999; Min et al., 2009; Ohler et al., 2004). Even subtle alterations in lipid or protein composition can disrupt the normal myelin structure and function (Maganti et al., 2019). So, since Elovl5 is essential for the biosynthesis of such lipidic compound (see chapter 1.4.1) and, as demonstrated in the previous section (chapter 3.1.3), it is highly expressed in oligodendrocytes, we investigated the physiological involvement of Elovl5 in myelin formation and composition in peripheral nervous system, exploiting the murine model lacking the Elovl5 gene (*Elovl5*$^{-/-}$ mice).

3.2.1 ELOVL5 expression in peripheral myelin

The expression of Elovl5 at peripheral level was checked with immunofluorescence staining on immortalized Schwann cell culture RT4-D6P2T (**Fig. 20A**) and confirmed with gene expression analysis of *Elovl5* in sciatic nerves of wild-type mice (**Fig. 20B**). These data showed a moderate presence of this enzyme in peripheral glial cells.

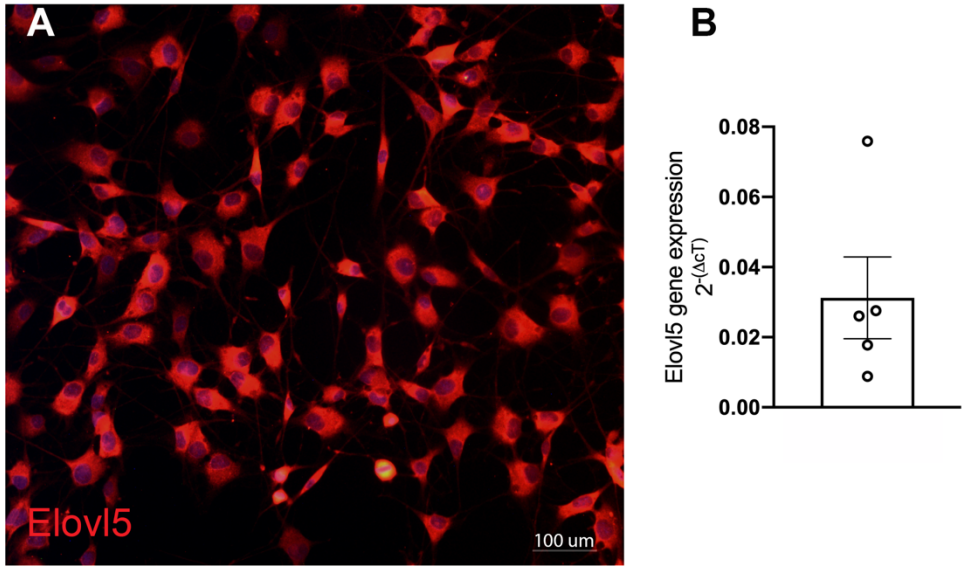

Figure 20. Elovl5 expression by RT4-D6P2T cell line and gene expression of Elovl5 in sciatic nerves. **(A)** Representative images showing RT4-D6P2T cells stained with Elovl5 antibody (red) and DAPI (blue). **(B)** Gene expression analysis of Elovl5 in sciatic nerves of wild type mice. Relative gene expression was calculated by the normalized comparative cycle threshold (Ct) method $2^{-\Delta Ct}$ *(Hoxha et al., 2021)*

3.2.2 Structural alterations of sciatic nerve of Elovl5$^{-/-}$ mice

Stereological analysis of sciatic nerve fibers showed no significant difference between wild type (n = 4) and *Elovl5*$^{-/-}$ mice (n = 5) in the total number of myelinated fibers (wild type: 3441 ± 213.1; *Elovl5*$^{-/-}$ mice: 3104 ± 217.4; Unpaired Student's t-test $t_{[7]} = 1.09$, $p > .05$). Myelin ultrastructure analysis revealed that sciatic nerve fibers of *Elovl5*$^{-/-}$ mice displayed a lower G-ratio compared to control littermates (wild type: 0.76 ± 0.01; *Elovl5*$^{-/-}$ mice: 0.69 ± 0.02; Student's t-test $t_{[5]} = 2.60$, $p < .05$, **Fig. 21A, C**). The G-ratio was smaller for fibers of any caliber (**Fig. 21D**), $p < .001$, Mann–Whitney U-test). A smaller G-ratio refers to a higher myelin thickness relative to axon diameter. The mean axonal diameter exhibited no difference between genotypes (wild type: 1.74 ± 0.06 µm; *Elovl5*$^{-/-}$ mice: 1.71 ± 0.22 µm; Student's t-test $t_{[5]} = 0.09$, $p > .05$) and also their frequency distribution (**Fig. 21E**, Mann–Whitney U-test, $p = .20$), while myelin thickness was significantly larger in *Elovl5*$^{-/-}$ mice (wild type: 0.66 ± 0.08 µm; *Elovl5*$^{-/-}$ mice: 0.97 ± 0.09 µm; Unpaired Student's t-test $t_{[7]} = 2.62$, $p < .05$, **Fig. 21F**). To investigate the ultrastructural cause of the increased myelin thickness, the period between myelin layers was analyzed. *Elovl5*$^{-/-}$ sciatic nerves showed expanded myelin periodicity relative to wild type

nerves (wild type: 19.35 ± 0.66 nm; *Elovl5*$^{-/-}$ mice: 21.67 ± 0.26 nm; Student's t-test $t_{[4]} = 3.21$, $p < .05$, **Fig. 21B**).

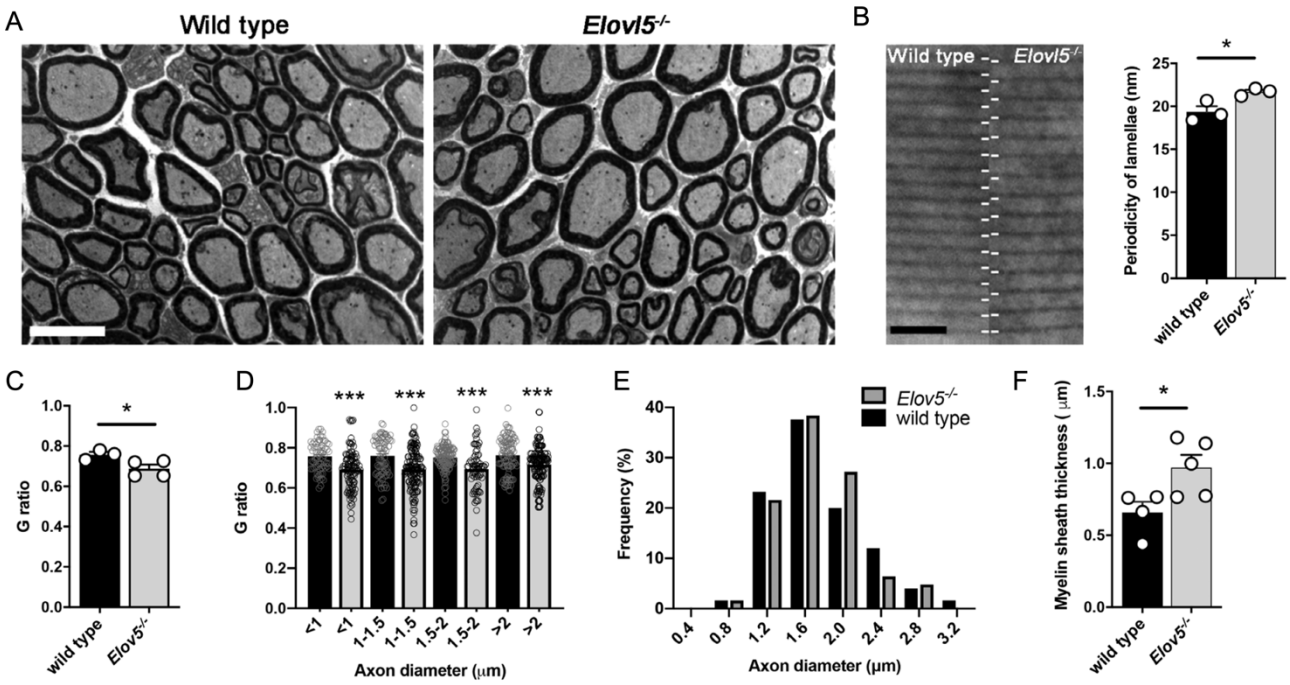

Figure 21. Structural alterations of sciatic nerve of *Elovl5*$^{-/-}$ mice. (A) Representative images of fibers in wild type and in *Elovl5*$^{-/-}$ sciatic nerves (scale Bar = 10 μm). **(B)** Ultra structural representation of myelin periodicity (scale Bar = 40 nm) and of the distance between consecutive major dense lines (*Elovl5*$^{-/-}$ n = 3 mice vs. wild type n = 3 mice). **(C)** bar graph representing the G-ratio (inner perimeter/outer perimeter) of sciatic nerve myelinated fibers (*Elovl5*$^{-/-}$ n = 4 mice vs. wild type n = 3 mice). **(D)** Graph representing the relative frequency of axonal diameters (μm) (*Elovl5*$^{-/-}$ n = 4 vs. wild type n = 3). **(E)** Bar graph representing myelin sheath thickness (mm) of sciatic nerve myelinated fibers (*Elovl5*$^{-/-}$ n = 5 vs wild type n = 4). **(F)** G-ratio quantification of fibers accounting for axon diameter (*Elovl5*$^{-/-}$ n = 4 vs. wild type n = 3). Data are expressed as mean ± SEM and p-values are determined by the appropriate statistical test. *p < .05; ***p < .001 *(Hoxha et al., 2021)*

3.2.3 Increased nodal gap and paranode length in sciatic nerves of Elovl5$^{-/-}$ *mice*

We next addressed the possibility that the decompaction of myelin in nerves of *Elovl5*$^{-/-}$ mice was associated with alterations of axonal domain organization. By means of confocal microscopy performed on teased sciatic nerve fibers, we analyzed the node/paranode complexes (where the nodal gap is the space flanked by two Caspr positive paranodes) in *Elovl5*$^{-/-}$ mice and wild type littermates (**Fig. 22A, B**). Interestingly, we found that the distribution of measurements

of the nodal gap length in *Elovl5*$^{-/-}$ mice was significantly shifted to the right (Kolmogorov–Smirnov test, D = 0.10, p < .001, **Fig. 22C**) with a mean nodal gap length significantly higher (wild type: 0.81 ± 0.01 µm; *Elovl5*$^{-/-}$ mice: 0.87 ± 0.02 µm; Student's t-test $t_{[4]} = 3.43$, p < .05, **Fig. 22D**). The increase in the nodal gap length was also accompanied by an increase of the average Caspr domain length (Kolmogorov–Smirnov test, D = 0.10, p < .001, **Fig. 22E**) with a tendency to higher values of the mean nodal gap (wild type: 1.86 ± 0.02 µm; *Elovl5*$^{-/-}$ mice: 2.02 ± 0.05 µm; Student's t-test $t_{[4]} = 2.69$, p = .055, **Fig. 22F**). The increase of the nodal gap and the mean paranode length is reflected in a stretched structure of the complex node-paranode in *Elovl5*$^{-/-}$ mice (Kolmogorov–Smirnov test, D = 0.14, p < .001, **Fig. 22G**, wild type: 4.78 ± 0.03 µm; *Elovl5*$^{-/-}$ mice: 5.17 ± 0.11 µm; Student's t-test $t_{[4]} = 3.43$, p < .05, **Fig. 22H**) which might affect the action potential conduction along myelinated axons.

3.2.4 Reduced action potential propagation in peripheral axons of Elovl5$^{-/-}$ *mice*

To study the contribution of Elovl5-dependent fatty acids on myelin functioning in the peripheral nervous system we performed action potential recordings on the caudal nerve of *Elovl5*$^{-/-}$ (n = 5) and wild type mice (n = 4, **Fig. 23A**). *Elovl5*$^{-/-}$ mice showed a significant increase in the latency of the action potential (AP) relative to their wild type littermates (wild type: 1.03 ± 0.0001 ms, n = 4; *Elovl5*$^{-/-}$ mice: 1.17 ± 0.00002 ms, n = 5; Unpaired Student's t-test $t_{[7]} = 5.41$, p < .001, **Fig. 23B**) and a significant decrease of conduction velocity (wild type: 33.40 ± 0.43 m/s; *Elovl5*$^{-/-}$ mice: 29.95 ± 0.52 m/s; Unpaired Student's t-test $t_{[7]} = 5.83$, p < .001, **Fig. 23C**). Moreover, the AP duration was significantly longer in *Elovl5*$^{-/-}$ mice (wild type: 1.3 ± 0.06 ms; *Elovl5*$^{-/-}$ mice: 1.53 ± 0.06 ms; Unpaired Student's t-test $t_{[7]} = 2.74$, p < .05, **Fig. 23D**). On the other hand, no difference was observed for AP area (wild type: 86 ± 11.4 V*s; *Elovl5*$^{-/-}$ mice: 88.7 ± 10 V*s; Unpaired Student's t-test $t_{[7]} = 0.18$, p > .05).

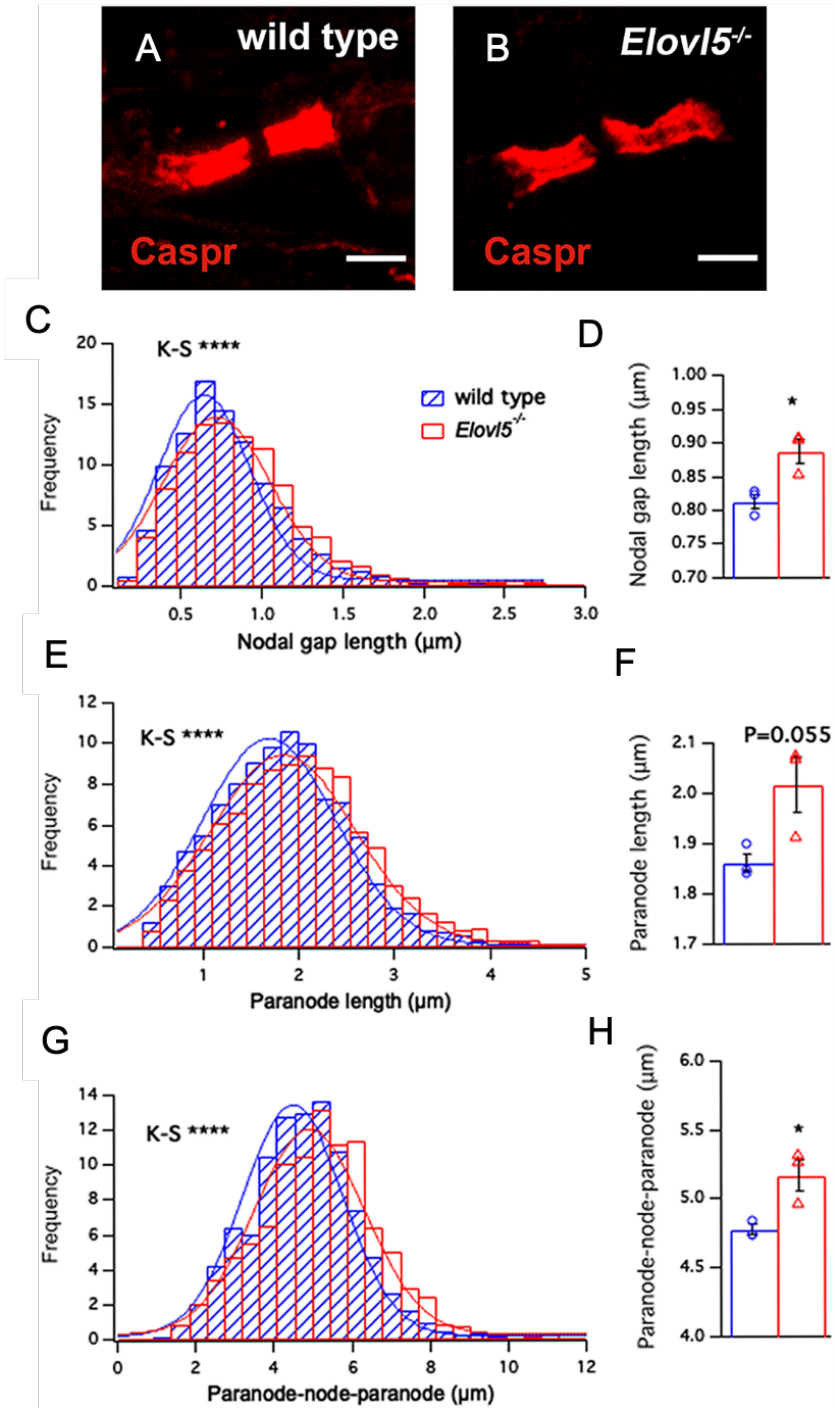

Figure 22. Increased length of the node/paranode complexes of sciatic nerves of *Elovl5*$^{-/-}$ mice. Confocal images of a single teased sciatic nerve from **(A)** wild type (n = 3) and **(B)** *Elovl5*$^{-/-}$ mice (n = 3) showing paranodes labeled for Caspr (red). **(C)** Histogram distribution of nodal gap length ($p < .001$, Kolmogorov–Smirnov test) and **(D)** mean ± SEM of the node lengths for wild type (blue) and *Elovl5*$^{-/-}$ mice (red) (Student's t-test, $p < .05$). **(E)** Histogram distribution of paranodal length ($p < .001$, Kolmogorov–Smirnov test) and **(F)** mean ± SEM of paranodal length (Student's t-test, $p < .05$). **(G)**

Histogram distribution of node/paranode length ($p < .001$, Kolmogorov–Smirnov test) and **(H)** mean ± SEM of node/paranode length (Student's t-test, $p < .05$). *$p < .05$; ***$p < .001$ *(Hoxha et al., 2021)*

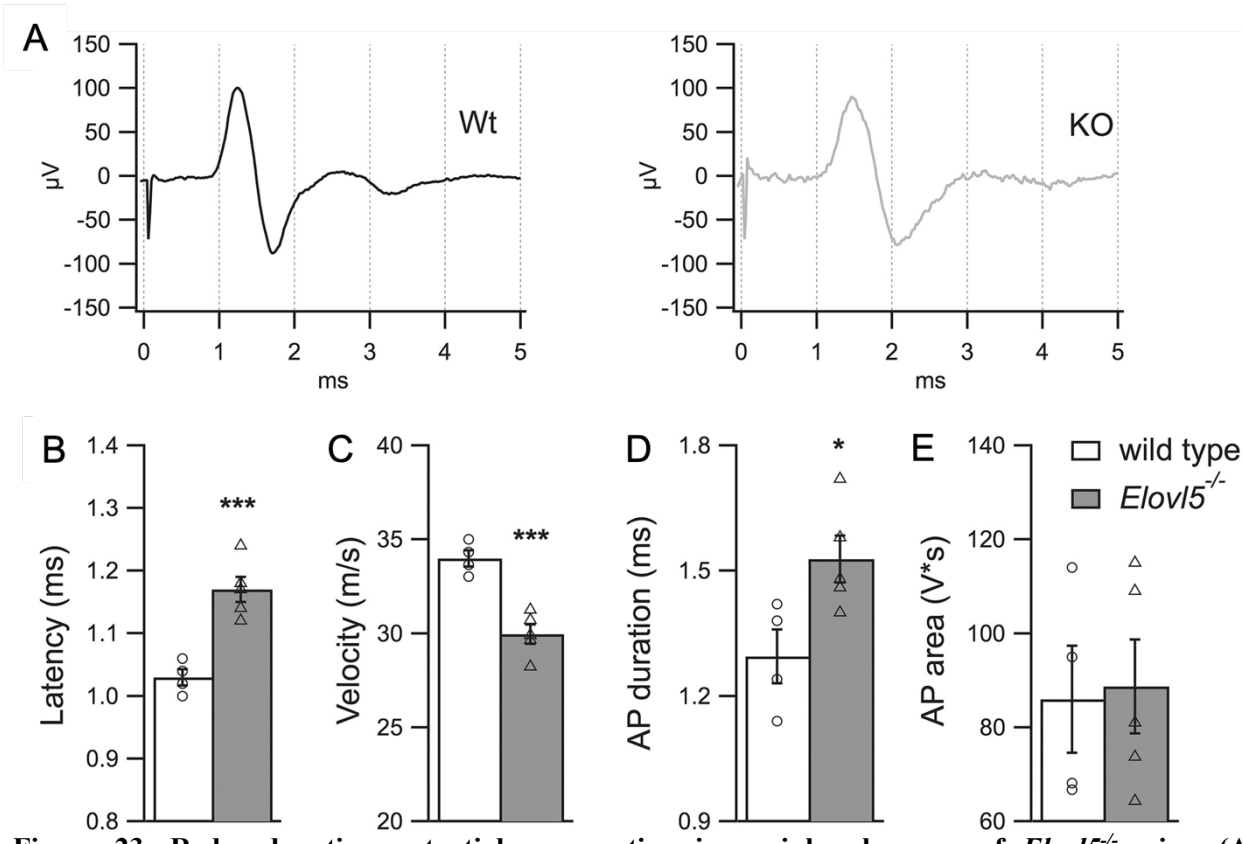

Figure 23. Reduced action potential propagation in peripheral axons of *Elovl5*$^{-/-}$ mice. (A) Representative traces of action potentials evoked by stimulation of the tail nerve for wild type (black) and *Elovl5*$^{-/-}$ mice (light gray). **(B–E)** Bar graphs representing mean values of latency, nerve conduction velocity, action potential duration and action potential area respectively (*Elovl5*$^{-/-}$ n = 5 mice vs. wild type n = 4 mice). Data are expressed as mean ± SEM and p-values are determined by unpaired Student's t-test. *$p < .05$; ***$p < .001$ *(Hoxha et al., 2021)*

3.2.5 Myelin proteins in sciatic nerve of Elovl5$^{-/-}$ *mice*

Myelin possesses a peculiar structure that differs from other membranes for the high lipid to protein ratio. Proteins participate in several mechanisms including stabilization of the structure of myelin sheaths or signaling during myelination (Campagnoni & Skoff, 2006). To verify whether the expanded myelin periodicity, in sciatic nerve of *Elovl5*$^{-/-}$ mice, was accompanied by changes in protein expression we performed western blot analysis. We found unchanged levels

of, MPZ, MBP, and CNPase proteins in *Elovl5*$^{-/-}$ compared to wild type sciatic nerves (Student's t-test, p > .05, **Fig. 24A, B**).

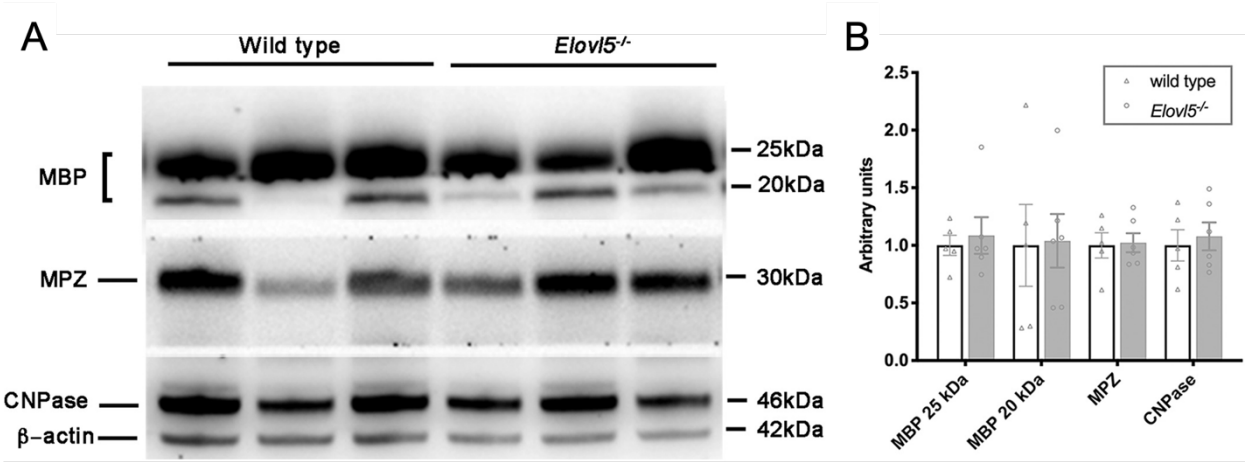

Figure 24. Proteins of myelin. (A) Representative western blots of sciatic nerve extracts from wild type and *Elovl5*$^{-/-}$ mice. **(B)** Densitometric quantification shows comparable levels of MBP, MPZ, and CNPase proteins in the sciatic nerve extracts of *Elovl5*$^{-/-}$ mice compared to their control littermates (wild type n = 5; *Elovl5*$^{-/-}$ n = 6). β Actin served as loading control. *(Hoxha et al., 2021)*

3.2.6 Phospholipid profile of Elovl5$^{-/-}$ *sciatic nerve*

Based on the myelin defects described above and considering that Elovl5 is involved in fatty acid elongation, we next sought to determine the profile of phospholipids. The sciatic nerves were extracted from wild type and *Elovl5*$^{-/-}$ mice (n = 5–6 mice/genotype) and the lipidomic profile was resolved. The composition in terms of phospholipid species detected across the two experimental groups was comparable as well as the total amount of phospholipids detected. However, we detected 46 different phospholipids that were significantly affected by the lack of Elovl5 (**Table 4**). Specifically, 2 lysophosphatidylcholines (lyso PC), a phosphatidylglycerol, a lysophosphatidic acid (LPA), 2 phosphatidic acids (PA), 2 phosphatidylinositols (PI), a phosphatidylserine (PS), a sphingomyelin (SM), 2 ceramides (Cer), 3 sulfatides (Sul), 7 phosphatidylcholines (PCaa) and 13 phosphatidylethanolamines (PEaa) carrying different fatty acids bound to the glycerol moiety by two ester linkages at both sn-1 and sn-2 position (di-acyl form, therefore aa means acyl-acyl), 11 plasmalogens (these molecules are phospholipids characterized by the presence of a vinyl ether linkage at the sn-1 position and an ester linkage at the sn-2 position of the glycerol moiety; (alkyl-acyl form, therefore ae means alkyl- acyl) (Table 3). The most common plasmalogens in mammals carry either ethanolamine

(plasmenylethalomines) or choline (plasmenylcholines) as head group. Among phospholipids with 2 acyl chains, we found that *Elovl5*$^{-/-}$ peripheral nerves showed increased levels of those with 3 or <3 unsaturated bonds and with up to 36 carbon atoms (**Fig. 25**). The only exceptions are PEaa with lower saturation (44:1 and 42:2), PEaa 44:12 and PEae 36:5. On the other hand, significantly decreased phospholipids with 2 acyl chains had >36 carbon atoms and >3 unsaturated bonds. This result agrees with the reduction of lysoPCs (which have a single acyl chain) with 20 carbon atoms and 3 or 4 unsaturated bonds. We detected mainly saturated or monounsaturated sphingomyelins, ceramides and sulfatides, with a few instances of increased expression **Fig. 25**). Together, these data demonstrate that despite a comparable composition in terms of phospholipid families between wild type and *Elovl5*$^{-/-}$ sciatic nerves, the lack of Elovl5 negatively impacts some phospholipids that contribute to myelin compaction.

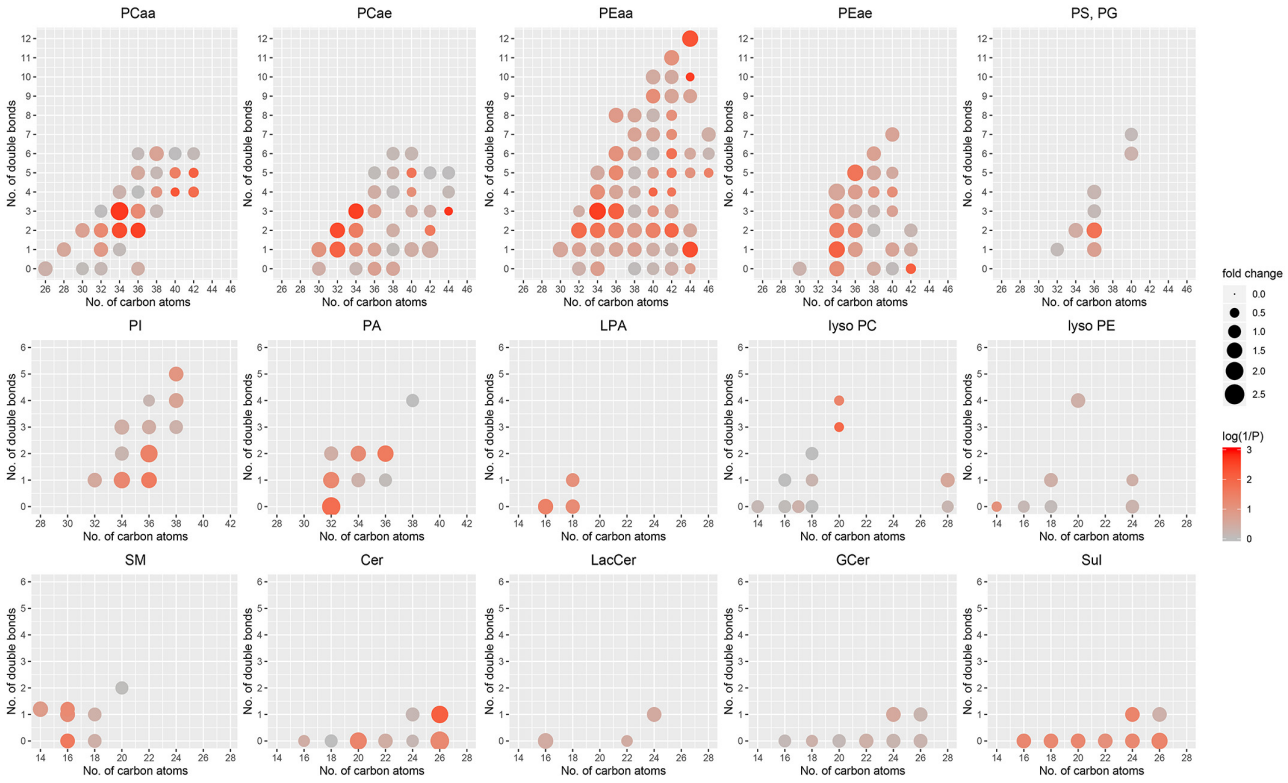

Figure 25. Altered phospholipid profile of *Elovl5*$^{-/-}$ sciatic nerve. Fold change of the main classes of phospholipids in *Elovl5*$^{-/-}$ sciatic nerve relative to wild type. The fold change is represented by the size of the circles (see scale legend on the right). The color (from gray to red) represents the statistical significance level (1/p) with full red corresponding to $p \leq .001$ (see color legend on the right). Note that the significant increases concern phospholipids with 2 acyl chains with 3 or <3 unsaturated bonds and

with up to 36 carbon atoms. The significantly decreased phospholipids with 2 acyl chains have >3 unsaturated bonds and >36 carbon atoms. PCaa, phosphatidylcholines; PCae, plasmenylcholines; PEaa, phosphatidylethanolamines; PEae, plasmenylethalomines; PS, phosphatidylserines; PG, phosphatidylglycerols; PI, phosphatidylinositols; PA, phosphatidic acids; LPA, lysophosphatidic acids; lyso PC, lysophosphatidylcholines; lyso PE, lysophosphatidylethanolamines; SM, sphingomyelins and sphingomyelins (OH) (the latter are plotted slightly upward shifted); Cer, ceramides; LacCer, lactosylceramides; GCer, glucosylceramides; Sul, sulfatides. *(Hoxha et al., 2021)*

Phospholipid name	**wild type (ng/mg)**	***Elovl5*$^{-/-}$ (ng/mg)**	**t, df**	**P value**
lysoPC C20:4	0.269±0.045	0.149±0.013	2.366, 9	0.0422
lysoPC C20:3	0.031±0.005	0.016±0.002	3.073, 10	0.0118
PC aa C34:3	0.168±0.013	0.337±0.039	4.078, 10	0.0022
PC aa C34:2	4.986±0.480	7.232±0.365	3.725, 10	0.0039
PC aa C36:2	3.937±0.322	5.479±0.223	3.933, 10	0.0028
PC aa C40:5	0.160±0.014	0.113±0.013	2.480, 10	0.0325
PC aa C40:4	0.415±0.030	0.180±0.060	3.502, 10	0.0057
PC aa C42:5	0.072±0.005	0.039±0.009	3.231, 10	0.0090
PC aa C42:4	0.195±0.013	0.124±.0.020	2.982, 10	0.0138
PC ae C32:2	0.035±0.004	0.050±0.001	3.754, 10	0.0038
PC ae C32:1	0.076±0.007	0.117±0.010	3.227, 10	0.0091
PC ae C34:3	0.046±0.004	0.067±0.003	3.972, 10	0.0026
PC ae C34:2	0.669±0.041	0.881±0.075	2.580, 9	0.0297
PC ae C40:5	0.048±0.004	0.027±0.006	2.782, 10	0.0194
PC ae C42:2	0.013±0.001	0.008±0.001	2.688, 9	0.0249
PC ae C44:3	0.007±0.001	0.003±0.001	4.125, 10	0.0021
PE aa 32:2	0.058±0.007	0.088±0.007	3.049, 10	0.0123
PE aa 34:3	0.222±0.025	0.389±0.034	3.984, 10	0.0026
PE aa 34:2	1.303±0.138	1.831±0.123	2.862, 10	0.0169

PE aa 36:3	1.626±0.183	2.499±0.192	3.285, 10	0.0082
PE aa 36:2	5.340±0.668	7.875±0.960	2.252, 10	0.0480
PE aa 40:4	0.6457±0.095	0.272±0.073	3.108, 10	0.0111
PE aa 40:2	0.465±0.052	0.648±0.055	2.418, 10	0.0362
PE aa 42:6	0.057±0.006	0.037±0.003	2.850, 10	0.0173
PE aa 42:5	0.113±0.015	0.063±0.012	2.693, 10	0.0226
PE aa 42:4	0.124±0.022	0.054±0.014	2.741, 10	0.0208
PE aa 42:2	0.793±0.043	0.980±0.041	3.141, 10	0.0105
PE aa 44:12	0.141±0.013	0.226±0.020	3.590, 10	0.0049
PE aa 44:10	0.282±0.026	0.110±0.034	3.999, 10	0.0025
PE aa 44:1	0.009±0.001	0.014±0.001	3.661, 10	0.0044
PE aa 46:5	0.005±0.001	0.003±0.001	2.401, 10	0.0373
PE ae 34:2	0.020±0.002	0.028±0.002	2.568, 10	0.0280
PE ae 34:1	0.065±0.009	0.105±0.009	3.230, 10	0.0090
PE ae 36:5	0.015±0.002	0.025±0.003	2.766, 10	0.0199
PE ae 42:0	0.112±0.011	0.065±0.008	3.310, 10	0.0079
SM 16:0	0.092±0.010	0.120±0.004	2.632, 10	0.0251
Cer-d18:1/20:0	0.001±0.0001	0.002±0.0003	2.310, 10	0.0435
Cer-d18:1/26:1	0.020±0.003	0.036±0.004	3.284, 10	0.0082
PG 36:3	0.038±0.003	0.056±0.006	2.828, 10	0.0179
PA 32:0	0.030±0.008	0.064±0.008	2.945, 10	0.0147
PA 36:2	0.031±0.004	0.051±0.006	2.622, 10	0.0255
LPA 16:0	0.082±0.004	0.117±0.007	4.247, 10	0.0017
PI 36:2	0.014±0.002	0.027±0.005	2.382, 10	0.0385
PI 36:1	0.025±0.002	0.038±0.005	2.592, 10	0.0269

Sul-d18:1/24:1	11.350±0.896	14.650±1.114	2.309, 10	0.0436
Sul-d18:1/26:0	0.136±0.030	0.223±0.022	2.332, 10	0.0419

Table 4. Quantification of sciatic nerve phospholipids LysoPC, lyso-phosphatidylcholine; PC, phosphatidylcholine; aa, acyl-acyl; ae, acyl-alkyl; PE, phosphatidylethanolamine; SM, sphingomyelin; Cer, ceramides; PG, phosphatidylglycerol; PA, phosphatidic acid; LPA, lysophosphatidic acid; PI, phosphatidylinositol; Sul, sulfatide. *(Hoxha et al., 2021)*

3.3 The role of Elovl5 in cerebellar circuitry

Since Elovl5 is highly expressed in PCs and it has a crucial role for the synthesis of ARA and DHA, which are known to modulate neuronal excitability (Borjesson et al., 2008; Danthi et al., 2005; Lauritzen et al., 2000; Poling et al., 1996; Seebungkert and Lynch, 2002; Vreugdenhil et al., 1996; Xiao and Li, 1999; Young et al., 2000; Chen and Bazan, 2005), we hypothesized that the lack of Elovl5 might have a negative impact on neuronal function, in particular on cerebellar circuitry signaling. So, we investigated at first the intrinsic properties of PCs, then we addressed the main synapses formed with them and main plasticity mechanisms present in the cerebellum.

3.3.1 Preserved intrinsic properties of PCs in Elovl5$^{-/-}$ mice

To better understand the origins of the motor impairment associated with the ELOVL5 mutation, we searched for alterations of action potential generation in PCs in sagittal cerebellar slices in 12 months old wild type and *Elovl5*$^{-/-}$ mice. We recorded PCs evoked action potential discharge, in current clamp configuration, applying current step protocols of increased intensity in both *Elovl5*$^{-/-}$ and wild type mice (**Fig. 26A).** Current-frequency plots showed no significant difference between genotypes at all stimulus intensities (two-way ANOVA repeated measures $P>0.05$, **Fig. 26B**). Moreover, the duration of the first ten interspike intervals was comparable between genotypes (two-way ANOVA repeated measures $P>0.05$, **Fig. 26C**). However, the action potential frequency adaptation of PCs from *Elovl5*$^{-/-}$ mice was significantly impaired compared to wild type (two-way ANOVA repeated measures $P<0.05$, **Fig. 26C**). These data indicate that the basal properties of PCs are conserved in absence of Elovl5.

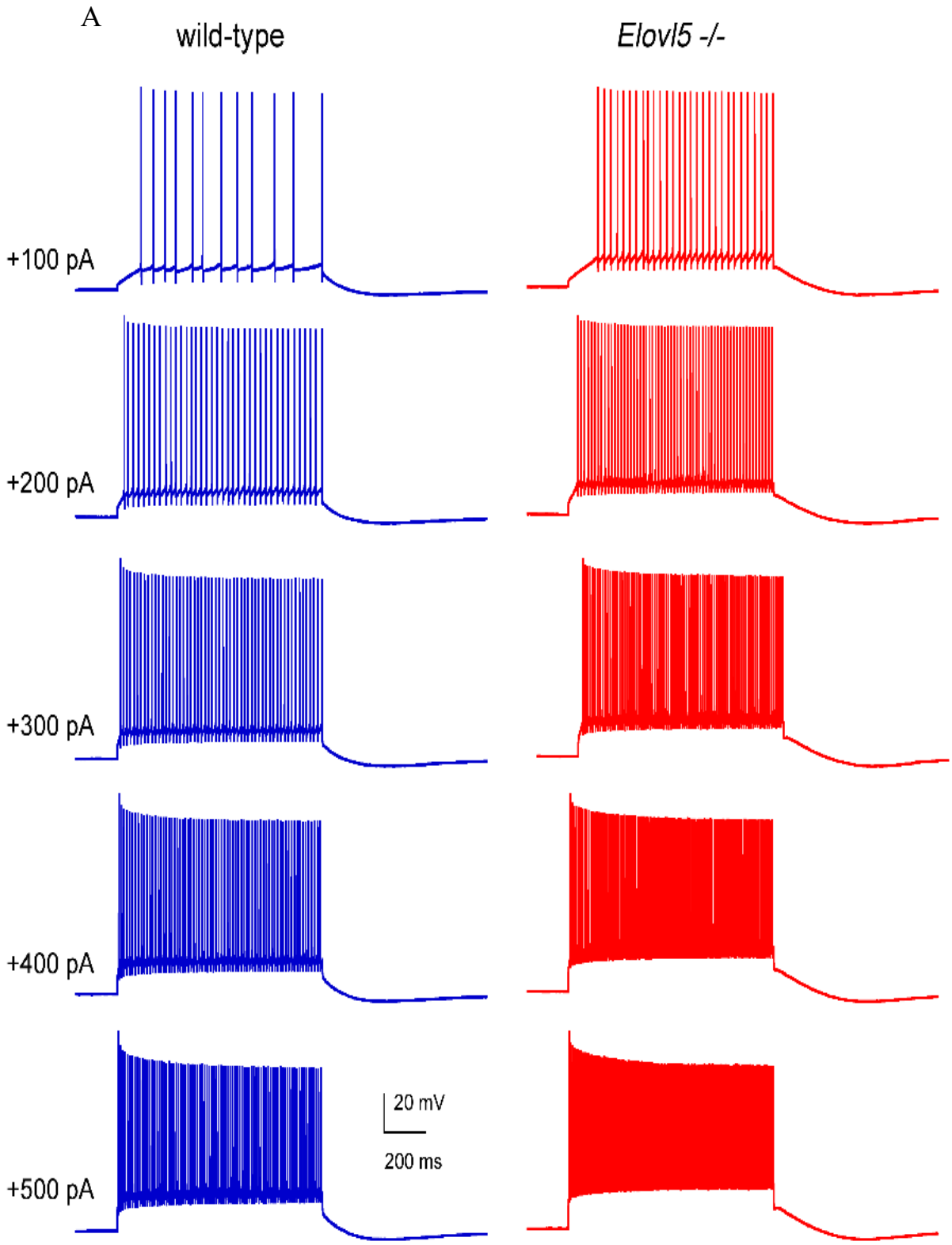
A
wild-type
Elovl5 -/-
+100 pA
+200 pA
+300 pA
+400 pA
+500 pA
20 mV
200 ms

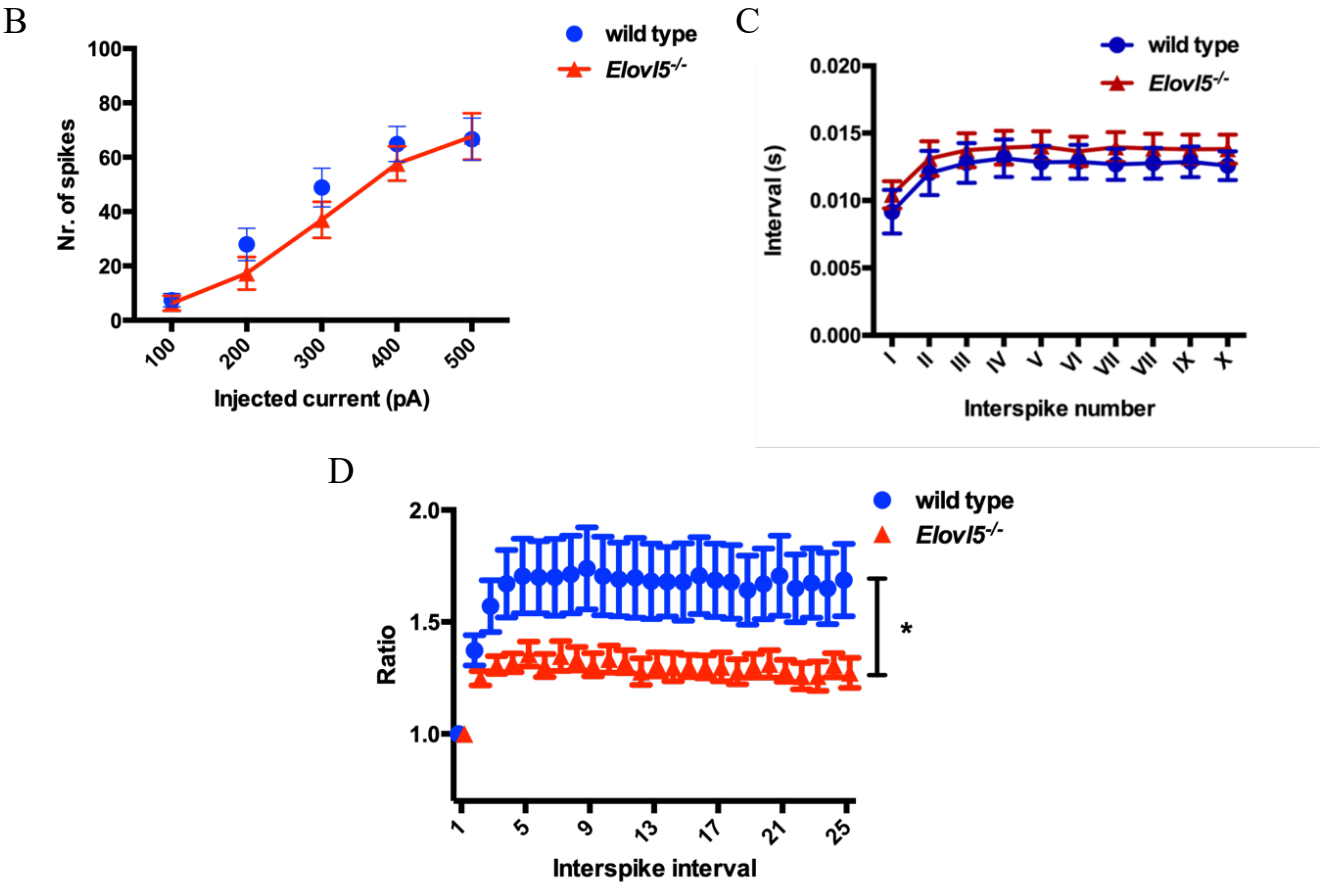

Figure 26. Basal activity of *Elovl5*$^{-/-}$ and wild type mice. (A) Representative traces of evoked discharge for (blue) wild type and (red) *Elovl5*$^{-/-}$ mice. **(B)** Current frequency plot of *Elovl5*$^{-/-}$ (red) and wild type (blue) PCs. **(C)** Interspike number interval graph of *Elovl5*$^{-/-}$ (red) and wild type (blue). **(D)** Action potential frequency adaptation, expressed as the ratio between the frequency of the first evoked spike on the other ones. Results are reported as mean ±SEM.

3.3.2 Conserved excitatory postsynaptic current of PF-PC synapse in Elovl5$^{-/-}$ *mice*

Cerebellar cortical function is essential for motor learning, and it is thought to be the result of a fine coordination between the PF- PC synaptic network and the "error reporting" of CF-PC input (Ito, 2006). We assessed the functionality of PF-PC synapse by stimulating PFs with 10 to 70 µA stimuli and recorded in voltage clamp mode. The PF-EPSC amplitudes in *Elovl5*$^{-/-}$ mice were not significantly different from their wild type littermates at all stimulus intensities (wild-type = 7; *Elovl5*$^{-/-}$ = 7; two-way ANOVA repeated measures P>0.05; **Fig. 27 A, B**). This result indicates that the basal synaptic transmission at the PF-PC synapse is preserved in *Elovl5*$^{-/-}$ mice. To verify the presynaptic functionality, we performed paired-pulse stimulation with variable inter-

stimulus interval. The time course of paired-pulse facilitation was similar in wild type and *Elovl5*$^{-/-}$PCs at all inter-stimulus intervals (from 50 to 200 ms; two-way ANOVA repeated measures P>0.05; **Fig. 27 C, D**). Furthermore, we examined the presynaptic function by performing the analysis of the expression levels of the presynaptic marker VGLUT1 (vesicular glutamate transporter), which is selectively expressed at parallel fiber synaptic varicosities. We performed immunohistochemical staining on cerebellar sagittal sections in *Elovl5*$^{-/-}$ mice and control littermates and limited our analysis to the molecular layer where all PF-PC synapses are located. We found that the expression of VGLUT1 in the molecular layer of the cerebellum of *Elovl5*$^{-/-}$ mice was indistinguishable from that of wild type mice (Unpaired Student's t-test P>0.05; **Fig. 28 A, B**).

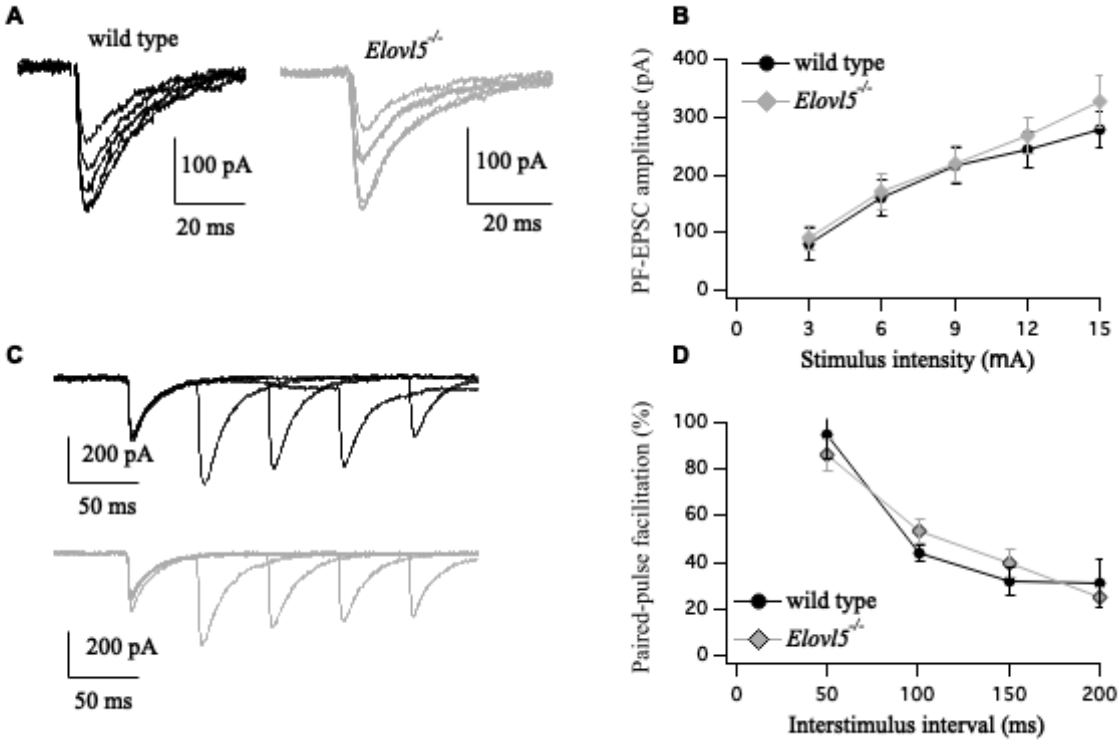

Figure 27. Normal PF-EPSC in *Elovl5*$^{-/-}$ mice. (A) Representative traces showing wild type (left black) and *Elovl5*$^{-/-}$ (right gray) EPSC. **(B)** No significant changes in PF-EPSC amplitude in *Elovl5*$^{-/-}$ mice (gray) compared to control littermates (black) at any stimulus imposed. **(C)** Representative traces of induced paired pulse facilitation in PFs-PC synapse in wild type (black) and *Elovl5*$^{-/-}$ (gray) mice. **(D)** Paired-pulse facilitation is comparable between wild type (black) and *Elovl5*$^{-/-}$ (right gray) mice.

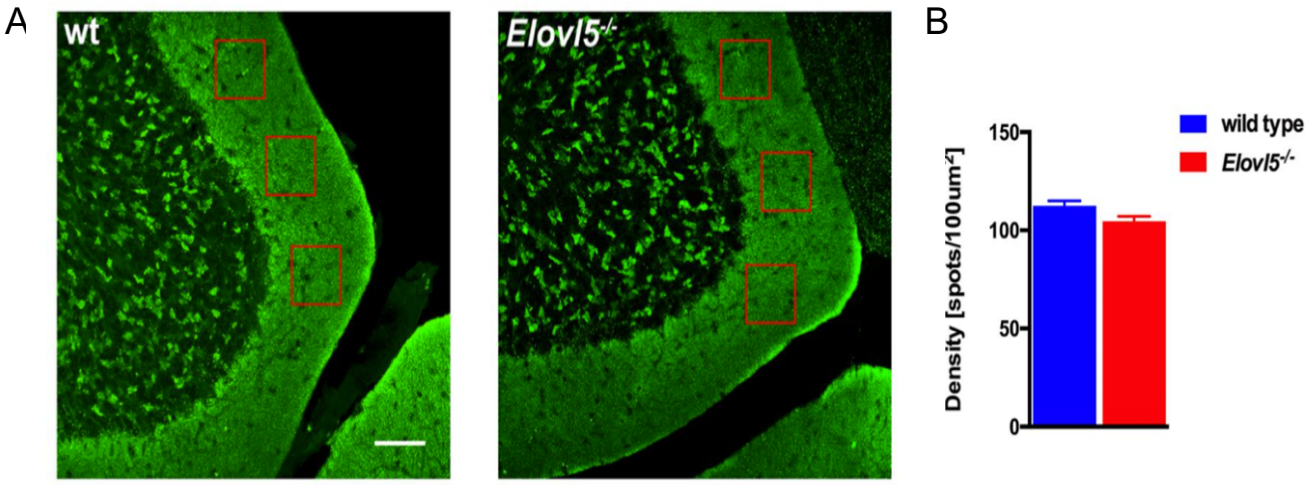

Figure 28. Preserved VGLUT1 expression in *Elovl5*$^{-/-}$ mice. (A) Representative images showing the expression of VGLUT1 in the molecular layer of the cerebellar cortex in wild type (left) and *Elovl5*$^{-/-}$ mice (right). **(B)** Plot indicating the comparable density of puncta of VGLUT1 unchanged in *Elovl5*$^{-/-}$ mice compared to the wild type. Scale bar: 100 μm

3.3.3 Conserved excitatory postsynaptic current of CF-PC synapse in Elovl5$^{-/-}$ *mice*

A second fundamental excitatory synaptic input to the PCs comes from the CFs, which generate complex spikes in PCs and are critical for motor learning (Ito et al., 2006). The CF-PCs synapse is characterized by a short-term depression when a paired-pulse stimulation protocol is applied (the interpulse interval ranged from 50 to 3200 ms). (**Fig. 29**). At intervals between 200 and 800 ms, *Elovl5*$^{-/-}$ PCs displayed a higher short-term depression relative to wild type (**Fig. 29 A, B**). The time course of short-term depression was described by double exponential functions. *Elovl5*$^{-/-}$ PCs, compared to wild type, showed a lower proportion and a lengthening of the fast time constant (wild type: $\tau f = 115$ ms, 46%; *Elovl5*$^{-/-}$: and $\tau f = 1138$ ms, 25.4%), in line with the higher depression at intermediate intervals.

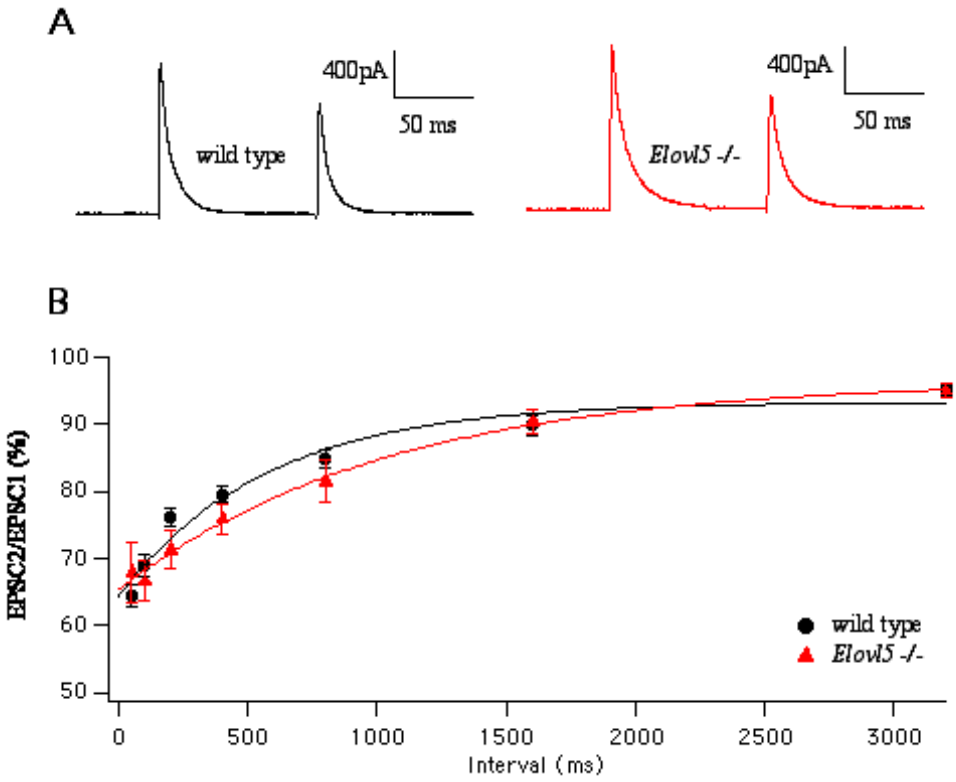

Figure 29. CF-EPSCs in wild-type and *Elovl5*$^{-/-}$ PCs. (A) Representative traces of excitatory postsynaptic currents evoked by climbing fiber paired-pulse stimulation with an interpulse interval of 100 ms in wild type (black) and *Elovl5*$^{-/-}$ (red) mice. **(B)** Time course of paired-pulse depression of CF-EPSC in wild type (black circles, n=8) and *Elovl5*$^{-/-}$mice (red triangles, n=3). The lines are double exponentials fittings of wild type and *Elovl5*$^{-/-}$ data points. The paired-pulse depression is expressed as the percentage of the amplitude of the second EPSC relative to the first one (mean ± SEM) and is plotted as a function of interpulse intervals.

To further study the correct functioning of the CF-PC synapse immunofluorescence reaction were performed and the intensity of the signal of vesicular glutamate transporter 2 (VGLUT2) was evaluated in both *Elovl5*$^{-/-}$ and wild type mice. We found that VGLUT2 expression showed a higher trend in both anterior and posterior lobes, but not in a significant way (Unpaired Student's t-test $p > 0.05$, **Fig. 30**).

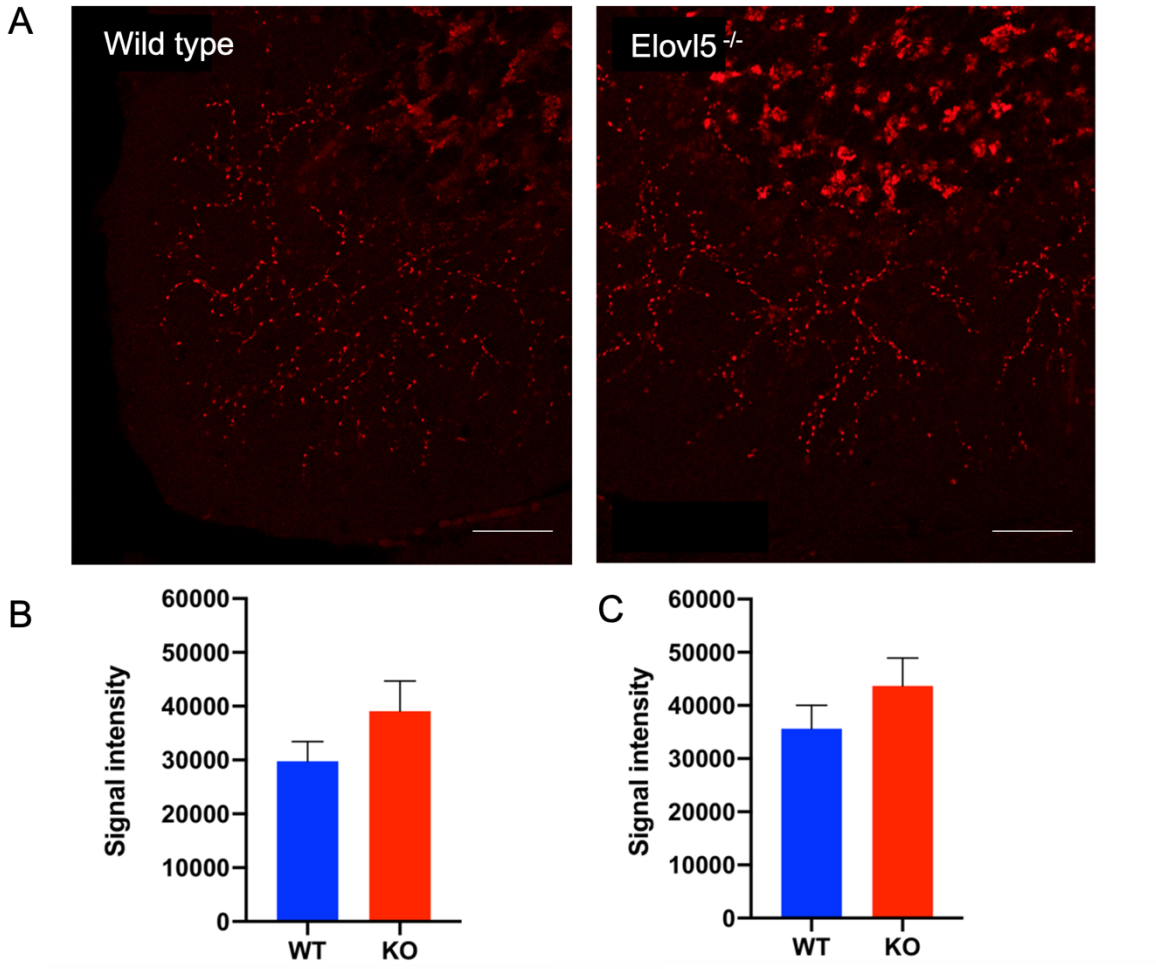

Figure 30. VGLUT2 expression in wild-type compared to *Elovl5*$^{-/-}$. (A) Immunofluorescent staining on cerebellar sagittal slices shows unaltered expression of VGLUT2 in the molecular layer of the cerebellar cortex between wild-type (left) and *Elovl5*$^{-/-}$ mice (right). Scarebars: 200 µm **(B)** The right graph represents the signal intensity for posterior lobules of the cerebellum, the left one for the anterior ones. The mean number of puncta of VLGUT2 is unvaried in *Elovl5*$^{-/-}$ mice compared to wild type. ($p > 0.05$, Student's t-test).

3.3.4 mGlu1-mediated slow EPSC is conserved in Elovl5$^{-/-}$ mice

Another essential player in cerebellar network functioning is mGluR1, critical for PCs plasticity (Aiba et al., 1994). Activation of mGluR induces an excitation of cerebellar PCs, where mGluR1 is expressed at high levels presynaptically in the dendritic spines (Tempia et al., 2001). We applied trains of stimulation (100 Hz with 4, 8, 12 and 16 pulses) to PFs to evoke slow EPSCs induced by activation of mGluR1 (**Fig. 31A**). We found that the mGluR1 responses in *Elovl5*$^{-/-}$ mice were comparable with those recorded in wild type mice regardless of the number of pulses delivered (two-way ANOVA repeated measures P>0.05, **Fig. 31B**). We also performed immunohistochemical staining of mGluR1 on sagittal slices of wild type and *Elovl5*$^{-/-}$ mice and found that mGluR1 presence in the molecular layer is not affected upon genetic deletion of *Elovl5* (Unpaired Student's t-test P>0.05; **Fig. 31C** and **D**).

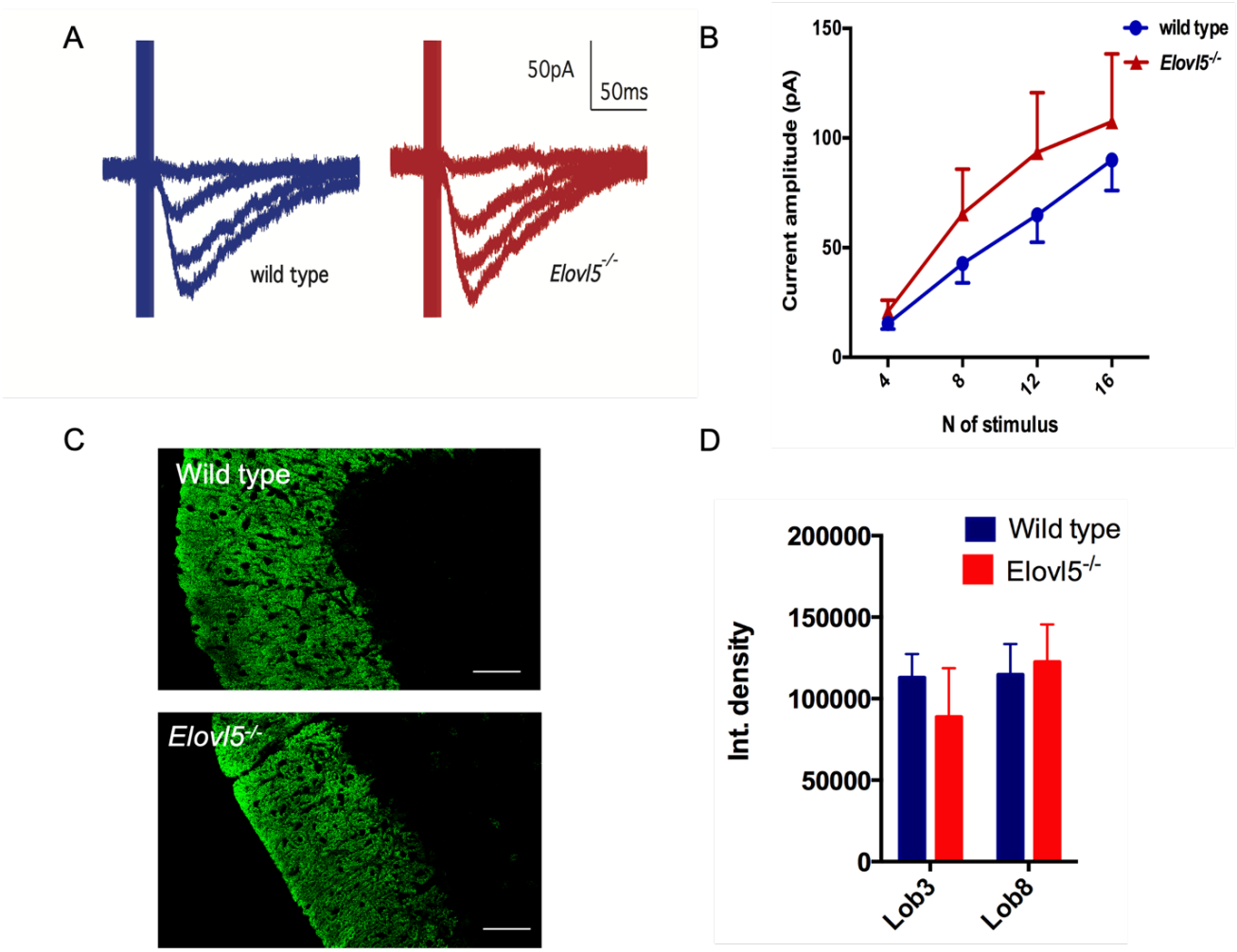

Figure 31. Conserved mGluR1 current and receptor density. (A) Representative traces showing mGluR1 current in wild type (blue) and *Elovl5*$^{-/-}$ mice (red). **(B)** No significant differences between

Elovl5$^{-/-}$ and wild type mice mGluR1 current. **(C)** Representative images of mGluR1 signal in cerebellar molecular layer in wild type (upper image) and *Elovl5*$^{-/-}$ mice (lower image). **(D)** Bar graphs of mean fluorescence intensity ±SEM of mGlu1 expression Scale bars: 100 μm

3.3.5 Altered short-term plasticity endocannabinoid-dependent in Elovl5$^{-/-}$ *mice*

eCBs are biologically active derivatives of a long-chain PUFA, specifically ARA, which have an important role in modulating synaptic transmission (Cascio, 2013). In the cerebellum, eCBs released by PCs retrogradely inhibit excitatory and inhibitory synapses that the PC receives. So, we hypothesized that lack of Elovl5 in mice could have a negative effect in the eCB system in the cerebellum. We stimulated PFs and recorded the EPSPs in current clamp mode from PCs. PFs were recorded with the following stimulus pattern: 0.5 Hz preceded and followed a train of ten stimuli at 200 Hz (**Fig. 32A**). This train of stimuli reduced the magnitude of subsequent EPSPs in both wild type and *Elovl5*$^{-/-}$ mice (**Fig. 32B, C**). The reduction of the EPSP immediately after the train stimuli was of 49.64 % for wild type and of 35.98 % for *Elovl5*$^{-/-}$ mice. The reduction was present in both genotypes but with a minor suppression of the response in the *Elovl5*$^{-/-}$ mice. The EPSP amplitude reduction recovered by 30 seconds to the level of the pre-train EPSP for wild type and by 15 seconds for *Elovl5*$^{-/-}$ mice ($P<0.001$, two-way ANOVA repeated measures; **Fig. 33D**). The shorter time of recovery of the EPSP amplitude indicate an alteration of the endocannabinoid response.

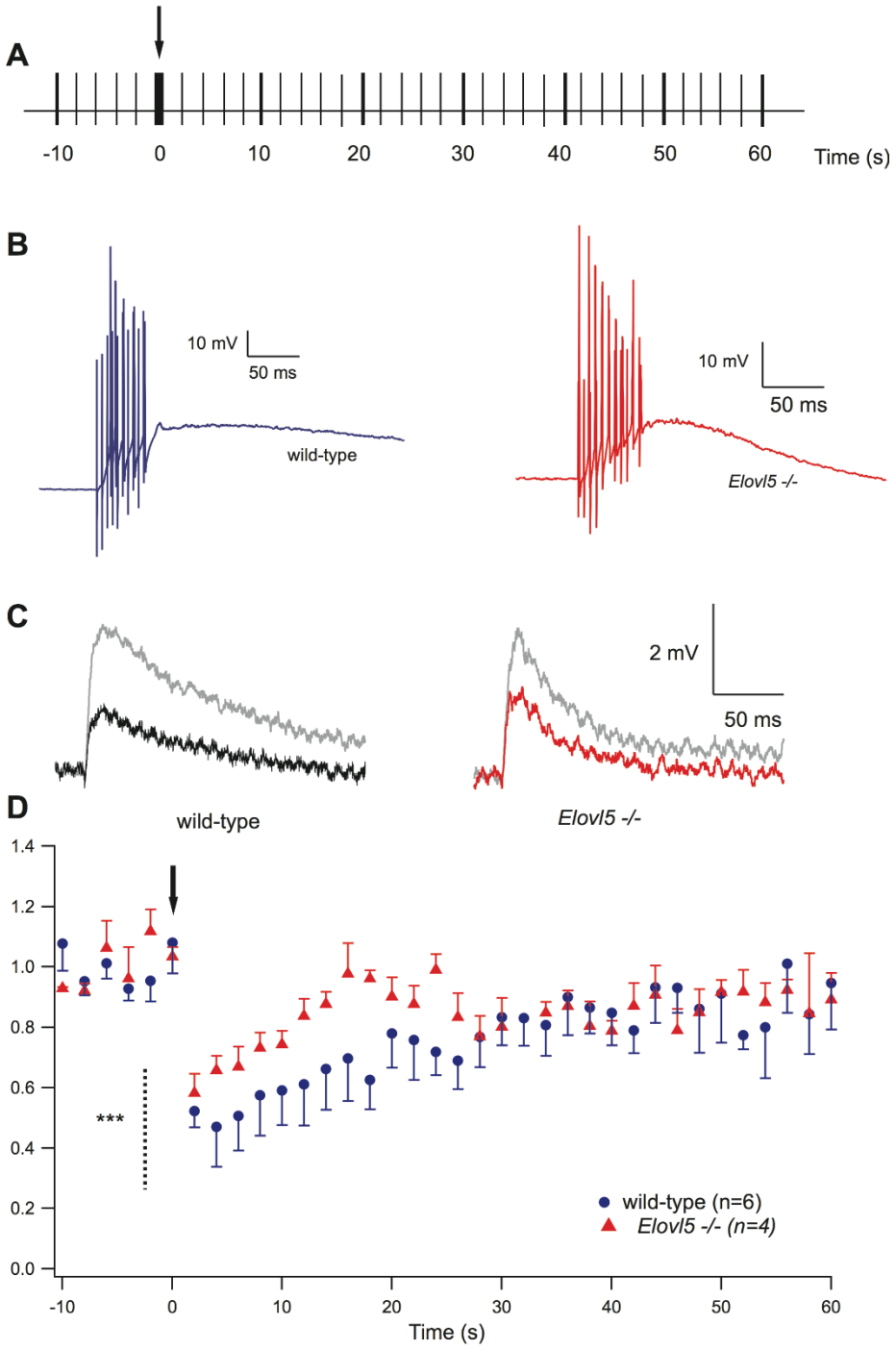

Figure 32. Synaptically evoked suppression of excitation (SSE). (A) The stimulation protocol applied to PFs to evoke endocannabinoid release from PCs. The PF were stimulated at low frequency except for a train of ten stimuli at 200 Hz (arrow). **(B)** Representative traces of train stimuli applied for both genotypes. **(C)** The PF- EPSP 2s before the train (gray trace) and 2s after the train (blue trace for wild type and red trace for *Elovl5*$^{-/-}$ PCs). **(D)** the normalized peak EPSP is plotted as a function of time for wild type (blue) and *Elovl5*$^{-/-}$ PCs (red) ($P<0.001$). The arrow indicates the brief train applied

3.3.6 Maintained long term-depression in Elovl5$^{-/-}$ mice

Long term plasticity mechanisms are essential for motor learning. In particular, LTD, an hour-lasting decrease in strength on synaptic contact, fundamental for the error-based correction of movement (Hansel et al., 2001). We looked at the long-term depression mechanism in both *Elovl5*$^{-/-}$ and wild type mice by stimulating PF-PC synapses. We found that in *Elovl5*$^{-/-}$ mice LTD was induced (normalized PF EPSC amplitude at 30 min after induction: 71.02 ± 2.56%, n = 3) to the same degree as in wild type mice (58.87 ± 15.06% n = 3; two-way ANOVA), indicating that Elovl5 loss does not alter this important plasticity mechanism (**Fig. 33**).

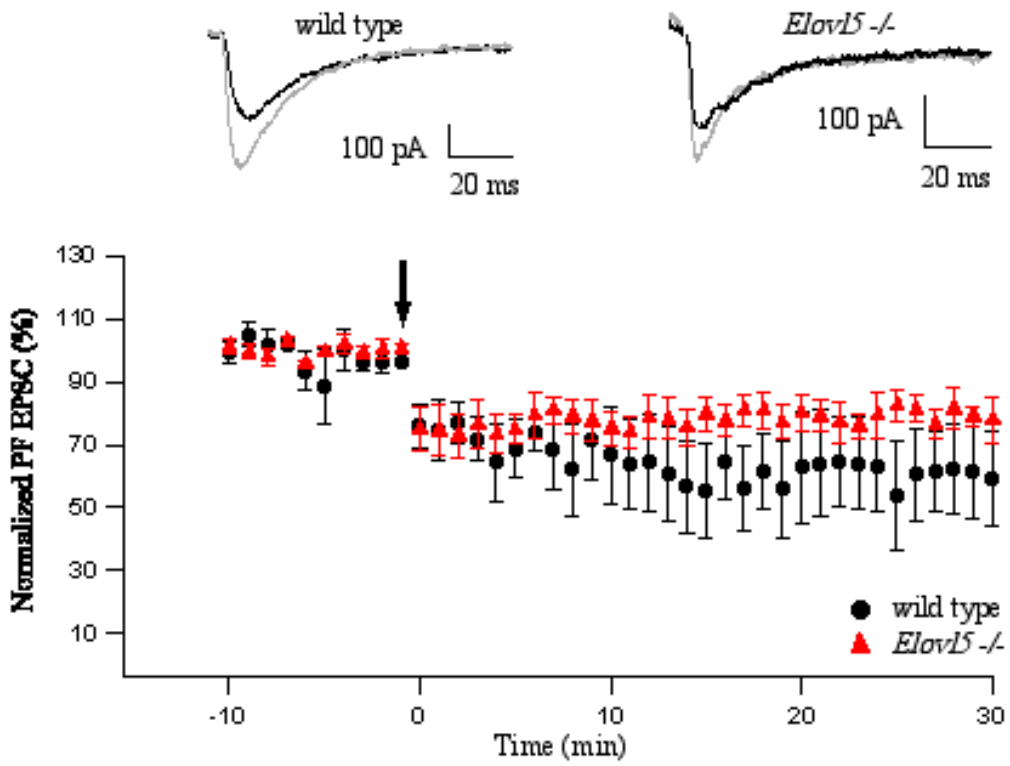

Figure 33. Long term depression induction in *Elovl5*$^{-/-}$ mice. Top: traces of AMPA receptor-mediated fast PF-evoked EPSCs before (gray) and after (black) induction of long-term synaptic plasticity (LTD; EPSC traces 30 min after the conjunctive stimuli). Bottom: pooled data of the fast EPSC amplitudes in wild type (black, n= 3 cells) and *Elovl5*$^{-/-}$ mice (red, n= 4 cells) normalized to the baseline period before the induction stimuli (arrow) of LTD.

3.3.7 Quantification of axon terminals

Once analyzed the afferents way to PC, we analyzed PC synaptic terminals in the DCNs, which receive the inhibitory contacts from PCs. We measured VGAT expression and localization to assess PC axon terminals integrity. We performed a double immunostaining of VGAT and Calbindin to visualize both the axon of the cell and the transporter located in the axon terminal. By analyzing the colocalization of these antibodies we found no significance difference between wild type and *Elovl5*$^{-/-}$ mice (Unpaired Student's t-test p > 0,05, **Fig. 34**).

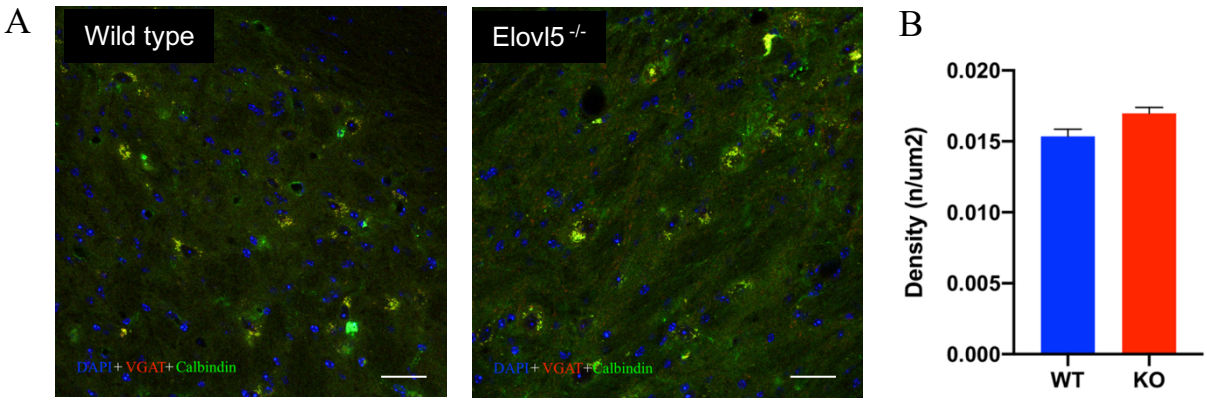

Figure 34. VGAT localization in PC axon terminals. (A) Immunofluorescent staining on cerebellar sagittal slices of wild type mice and *Elovl5*$^{-/-}$ mice. Nuclei are stained with DAPI (blue), PCs with Calbindin (green), VGAT with Cy3 (red). The arrow indicates a point of co-localization. Scalebars: 100 µm. **(B)** Schematic representation of VGAT density showing no significant difference in density of fluorescent signal in wild type mice and *Elovl5*$^{-/-}$ mice.

3.3.8 Increased nodal gap and paranode length in cerebellar axon of Elovl5$^{-/-}$ *mice*

The alteration in the axonal conductance in the peripheral nerve (see chapter 3.2.3 and 3.2.3) open the way to the hypothesis that a similar condition might be present also in the cerebellum. We started with the immunohistochemical analysis of the node/paranode complexes using Caspr labelling in *Elovl5*$^{-/-}$ mice and wild type littermates (**Fig. 35A** and **B**). Interestingly, we found that both nodal gap and paranode length were elongated in *Elovl5*$^{-/-}$ cerebellum (Kolmogorov Smirnov test P<0.0001, **Fig. 35 C-F**), this alteration induced an increase in the total length of the whole structure paranode-node-paranode (Kolmogorov Smirnov test P<0.0001, **Fig. 35G**). This increased nodal-paranodal length, suggests that also at cerebellar level Elovl5 lack influences the axonal action potential propagation.

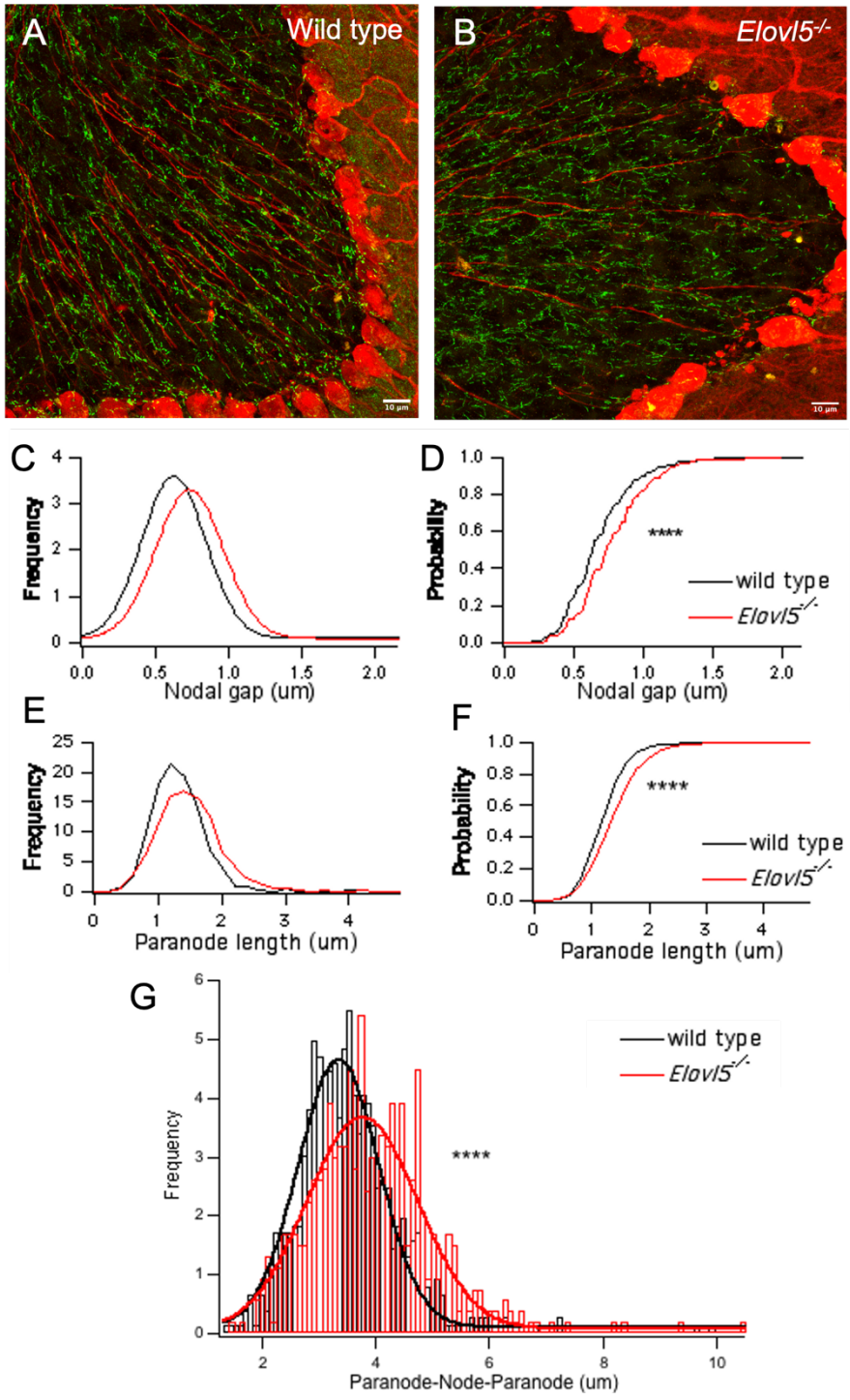

Figure 35. Increased node and paranode length in *Elovl5*$^{-/-}$ *mice.* (A) and **(B)** Representative images of the double staining Calbindin (red) which marks PCs soma and axons and Caspr (green) marking the paranodal section in both wild type and *Elovl5*$^{-/-}$mice. Scalebars: 10 µm. **(C)** and **(D)** Curves indicating the frequency and the probability of the nodal gap length found in wild type (black) and *Elovl5*$^{-/-}$mice

(red). The measurement reveals a significant increase in length of nodal gap in *Elovl5*$^{-/-}$mice. **(E)** and **(F)** Curves indicating the frequency and the probability of the paranodes length found in wild type (black) and *Elovl5*$^{-/-}$mice (red). The data indicate a significant increase in length of paranodes in *Elovl5*$^{-/-}$mice. **(G)** Frequency plot indicating the increase in length of *Elovl5*$^{-/-}$mice (red) paranode-node-paranode structure compared to wild type littermates (black).

3.3.9 Reduction of action potential antidromic propagation in Elovl5$^{-/-}$ *mice*

The conduction of action potential along axons is strongly influenced by the correct length of the node-paranode complexes. The stretched structure of the node-paranode suggests impaired action potential conduction. We stimulated the axon of PC and recorded the action potential in the PC soma (antidromic propagation of action potential) (**Fig. 36A**). We demonstrated that the conduction velocity of antidromic action potential was significantly lower in *Elovl5*$^{-/-}$ mice compared to those of wild type (0.125 ± 0.005 mm/sec, n=26) compared to those of wild type 0.141 ± 0.006 mm/sec, n=31) (Unpaired Student's t-test $P<0.05$; **Fig. 36B** and **C**).

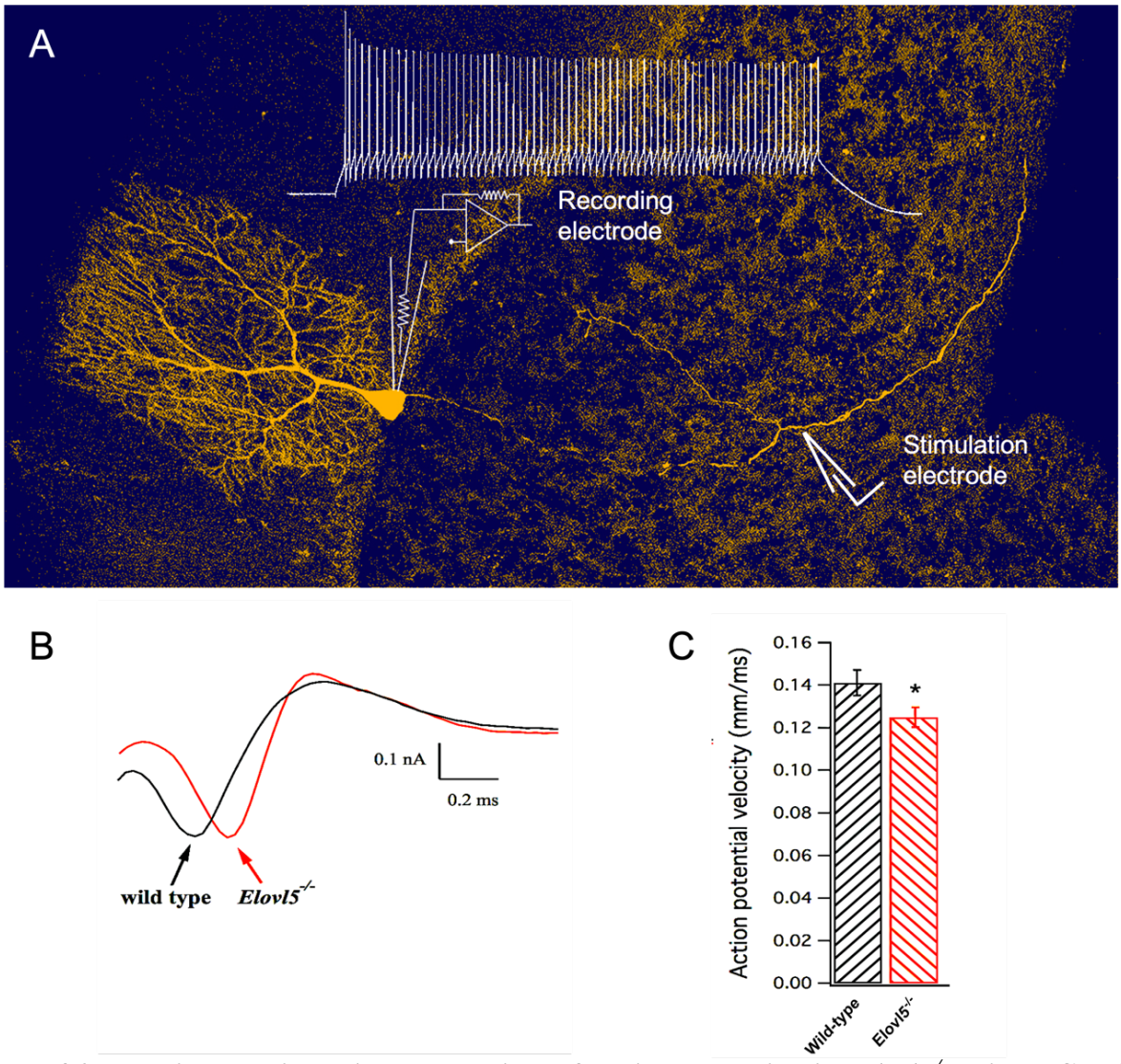

Figure 36. Impaired antidromic propagation of action potential in *Elovl5*$^{-/-}$ mice PCs. (A) Representative PC filled with biocytin and a schematic representation of antidromic recording. Stimulation electrode was placed on axon of PC while recording electrode was placed in the soma in order to evaluate the antidromic action potential conduction. **(B)** Representative antidromic action potentials evoked in PC in wild type (black trace) and *Elovl5*$^{-/-}$mice. **(C)** Bar graphs showing the mean antidromic action potential velocity of wild type and *Elovl5*$^{-/-}$mice ($P<0.05$).

3.4 PUFA-enriched diet supplementation as possible therapeutic approach for SCA38

Elovl5 correct functioning is essential for the biosynthesis of PUFAs, which are involved in many biological processes and play a key role in a healthy brain. The pathological condition of SCA38 is characterized by symptoms ascribable to an unbalance of PUFAs in the organism. Ideally, to rebalance this alteration, a supplementation of PUFAs could be the best way to approach patients' symptomatology. The studies performed by Manes and colleagues (2017 and 2019) (see chapter 1.2.3) showed that the administration of only DHA leads patients to long-term gait and posture ameliorations, improvement in cerebellar metabolism and no worsening of motor symptoms and peripheral neuropathy. Thus, we decided to investigate the effects of a complete diet-based therapy on *Elovl5*$^{-/-}$ mice by administering them not only DHA, the most common dietary supplement in many neurological disorder therapies (Bousquet et al., 2011; Abedi and Sahari et al., 2014; McNamara et al., 2018), but all downstream product of Elovl5. We divided mice into three groups: the negative control group, composed by *Elovl5*$^{-/-}$ mice and wild type littermates receiving the a diet providing them Elovl5 substrates (e.g. ALNA and LA), precursors for more complex PUFAs ("PUFA precursors only" group), which is expected to show SCA38 symptoms reported in Hoxha et al., 2017; a second group composed by *Elovl5*$^{-/-}$ mice and wild type littermates receiving a complete diet supplying both Elovl5 substrates and downstream products (i.e. both ALNA, LA and ARA, DHA, EPA) ("complete PUFA since birth" group); a third group composed by *Elovl5*$^{-/-}$ mice and wild type littermates, which receives the complete PUFA diet at weaning (1 month of age) ("complete PUFA since 1 month" group) (**Fig. 37**) (see **Table 1** for diet composition, chapter 2.1.1). We monitored our mice motor symptoms at different timepoints (1, 2, 3, 4, 6, 8 months of age) and then we sacrificed the mice in order to analyze their cerebellar architecture (**Fig. 37**).

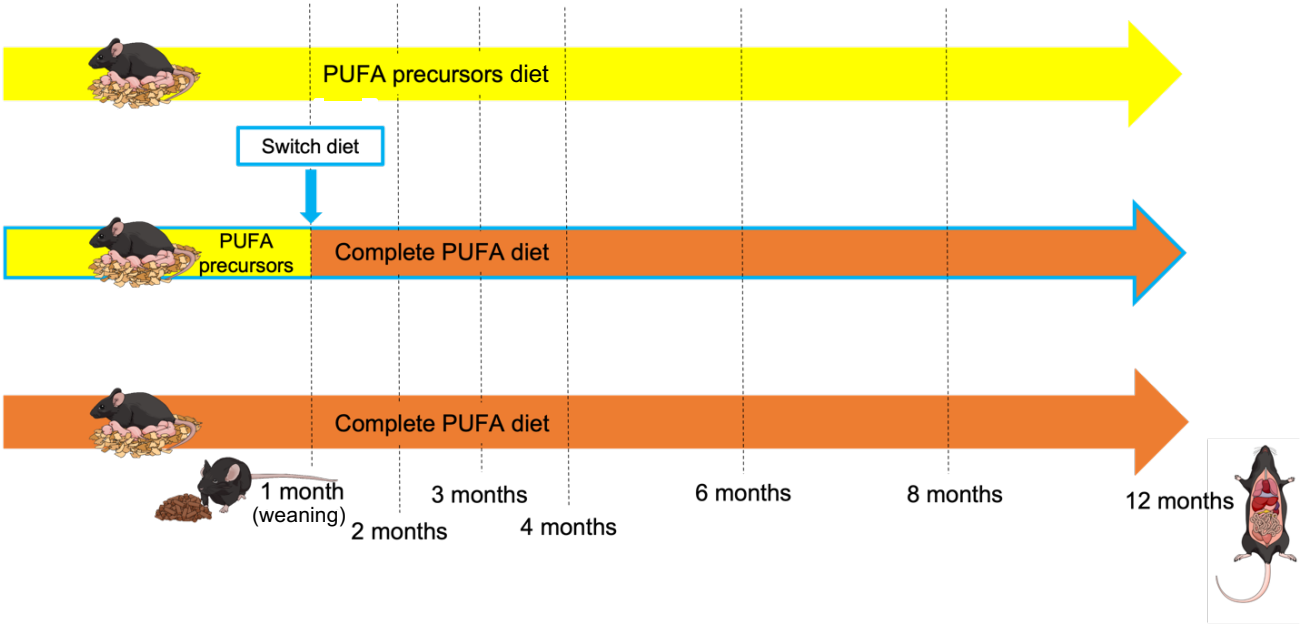

Figure 37. Experimental design. Experimental timeline representing the three different groups (yellow arrow = "PUFA precursors only" group: n female wild type = 13; n male wild type = 12; n female *Elovl5*$^{-/-}$ = 10; n male *Elovl5*$^{-/-}$ = 7; yellow-orange arrow = "complete PUFA since 1 month" group: n female wild type = 10; n male wild type = 10; n female *Elovl5*$^{-/-}$ = 11; n male *Elovl5*$^{-/-}$ = 11; orange arrow = "complete PUFA since birth" group: n female wild type = 11; n male wild type = 13; n female *Elovl5*$^{-/-}$ = 12; n male *Elovl5*$^{-/-}$ = 10;) with the age analyzed (indicated with segmented line at the bottom, 1(weaning)-2-3-4-6-8 months) and the age of the sacrifice (12 months of age). In PUFA precursors only group (yellow arrow at the top) and complete PUFA since birth (yellow arrow at the bottom) the diet is imposed to both dams and their progeny, while in complete PUFA since 1 month group dams are administered the diet providing the precursors of PUFAs and progeny at weaning are switched in the complete diet providing also the downstream products of Elovl5. (Mice images have been created with https://mindthegraph.com)

3.4.1 Progression of motor impairment with PUFA precursors diet

A deficit in the balance beam test was already present at the age of 1 month for *Elovl5*$^{-/-}$ mice, as shown by a higher number of paw placement errors compared to wild type littermates (**Fig. 38** and **Fig. 42**). The difference of motor performance between genotypes remained statistically significant throughout the ages analyzed ($P < 0.0001$, Two-way ANOVA; n = 38 wild type mice: 0.24 ± 0.04; n= 38 *Elovl5*$^{-/-}$ mice: 0.86 ± 0.11) (**Fig. 38** and **Fig. 42**). *Elovl5*$^{-/-}$ mice showed a progressive increase of motor errors with age, in agreement with the worsening of *Elovl5*$^{-/-}$ mice motor performance reported by Hoxha et al. (2017).

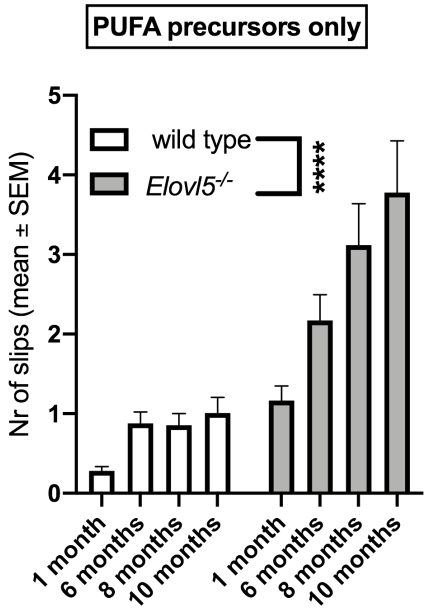

Figure 38. Progression of motor impairment in mice imposed a PUFA precursors diet. Bar graph showing the progression in time (from 1 to 10th month of age) of the motor deficit in *Elovl5*$^{-/-}$ mice (grey bars) and control littermates PUFA precursors only (white bars). As already showed in Hoxha et al., 2017, *Elovl5*$^{-/-}$ mice undergo a great worsening of motor coordination when imposed a diet providing them just the substrates of Elovl5 (e.g. LA and ALNA), while wild type mice present an almost unchanged mean of errors committed while traversing the experimental apparatus ($P < 0.0001$, Two-way ANOVA; n = 38 wild type mice: 0.24 ± 0.04; n= 38 *Elovl5*$^{-/-}$ mice: 0.86 ± 0.11)

3.4.2 Effects of the administration of a complete PUFA diet since birth

In wild type mice, the administration of a complete PUFA diet, also containing long chain PUFAs, improved motor performance at 1 ($P < 0.05$, Unpaired Student's t-test $t_{(53)}=2.02$; **Fig. 39A** and **B**) and 6 months ($P < 0.01$, Unpaired Student's t-test $t_{(34)}=3.29$; **Fig. 39D**), while at 8 months there was no significant difference ($P = 0.05$, Unpaired Student's t-test; **Fig. 39F**). In *Elovl5*$^{-/-}$ mice, at 1 month the complete PUFA diet did not significantly change the motor performance ($P > 0.05$, Unpaired Student's t-test; Fig. **39C**). However, at 6 and 8 months, *Elovl5*$^{-/-}$ mice with a complete PUFA diet showed significantly better performance compared to *Elovl5*$^{-/-}$ mice kept with PUFA precursors only (for 6 months old mice: $P < 0.05$, Unpaired Student's t-test $t_{(37)}=2.37$, **Fig. 39E**; for 8 months old mice: $P < 0.05$, Unpaired Student's t-test $t_{(36)}=2.03$; **Fig. 42**).

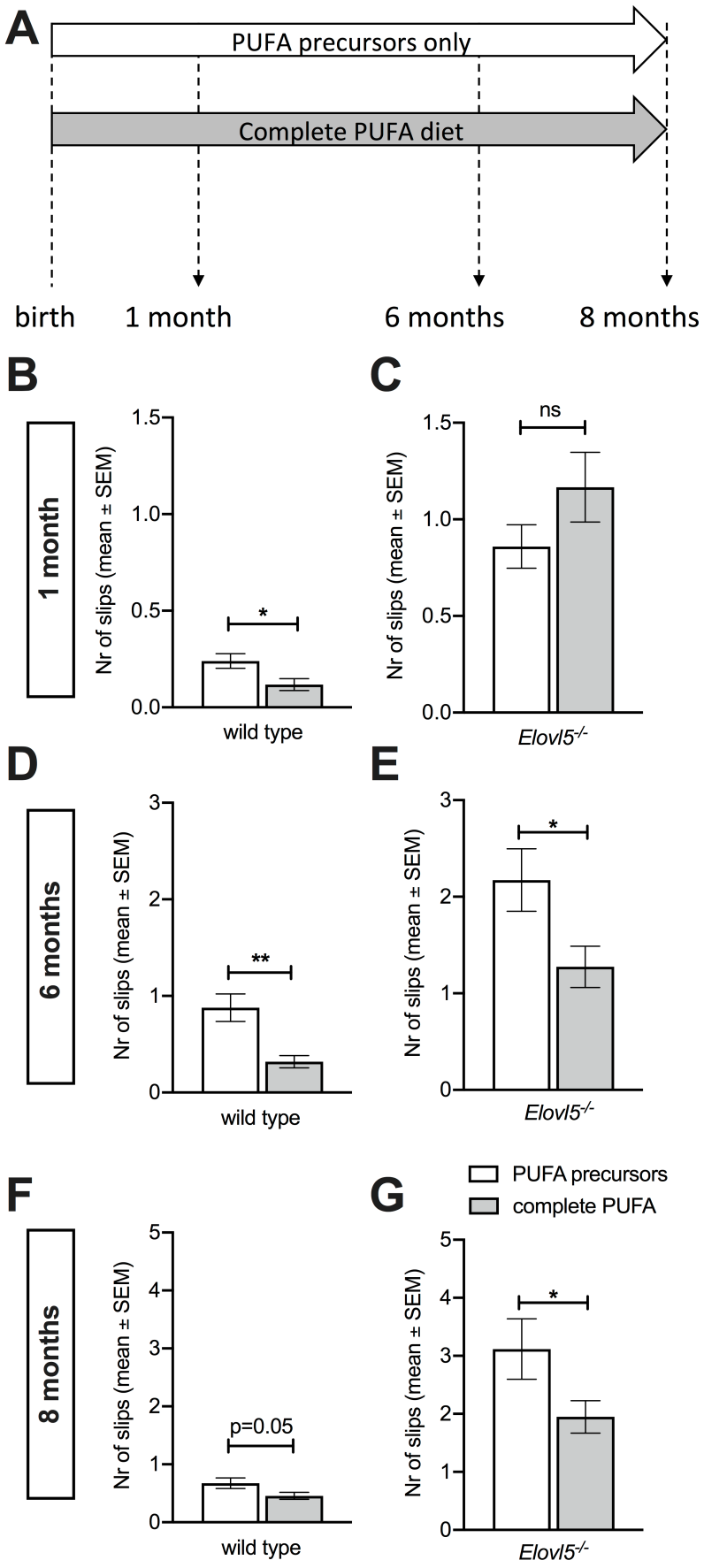

Figure 39. Slowdown of motor symptoms worsening in *Elovl5*$^{-/-}$ mice receiving a complete PUFA diet. (A) *Elovl5*$^{-/-}$ and wild type mice received from birth a diet providing them both Elovl5 substrates and

downstream products from birth (grey bars) were compared to genotype and age matched PUFA precursors only mice (white bars). **(B)** and **(C)** Graphs showing errors committed traversing the experimental apparatus at 1 month of age both wild type and *Elovl5*$^{-/-}$mice when receiving the complete PUFA diet compared to negative control group ($P < 0.05$, Unpaired Student's t-test $t_{(53)}=2.02$). **(D)** and **(E)** Motor performances of *Elovl5*$^{-/-}$mice and healthy littermates compared to PUFA precursors mice at 6 months of age ($P < 0.01$, Unpaired Student's t-test $t_{(34)}=3.29$) and 8 months of age ($P < 0.05$, Unpaired Student's t-test $t_{(36)}=2.03$) **(F)** and **(G)**.

3.4.3 Effects of the administration of a complete PUFA diet at later ages

The administration to wild type mice of a complete PUFA diet starting at 1 month of age significantly improved motor performance compared to wild-type mice fed with PUFA precursors only (for 6 months old mice: $P < 0.01$, Unpaired Student's t-test $t_{(37)}=3.18$, **Fig. 40A** and **B**; for 8 months old mice: $P < 0.01$, Unpaired Student's t-test $t_{(30)}=3.52$, Fig. **40D**; **Fig. 42**). In contrast, the complete PUFA diet stating at 1 month of age, failed to improve the motor performance of *Elovl5*$^{-/-}$ mice ($P > 0.05$, Unpaired Student's t-test; **Fig. 40C** and **E**), although at 8 months there was a trend to perform fewer errors than *Elovl5*$^{-/-}$ mice with PUFA precursors only (**Fig. 40E**). However, it should be noticed that PUFA precursors *Elovl5*$^{-/-}$ mice have a tendency to worsen their performance from 6 to 8 months, while, in the same period, *Elovl5*$^{-/-}$ mice with complete PUFAs since 1 month retained the same performance level, without worsening.

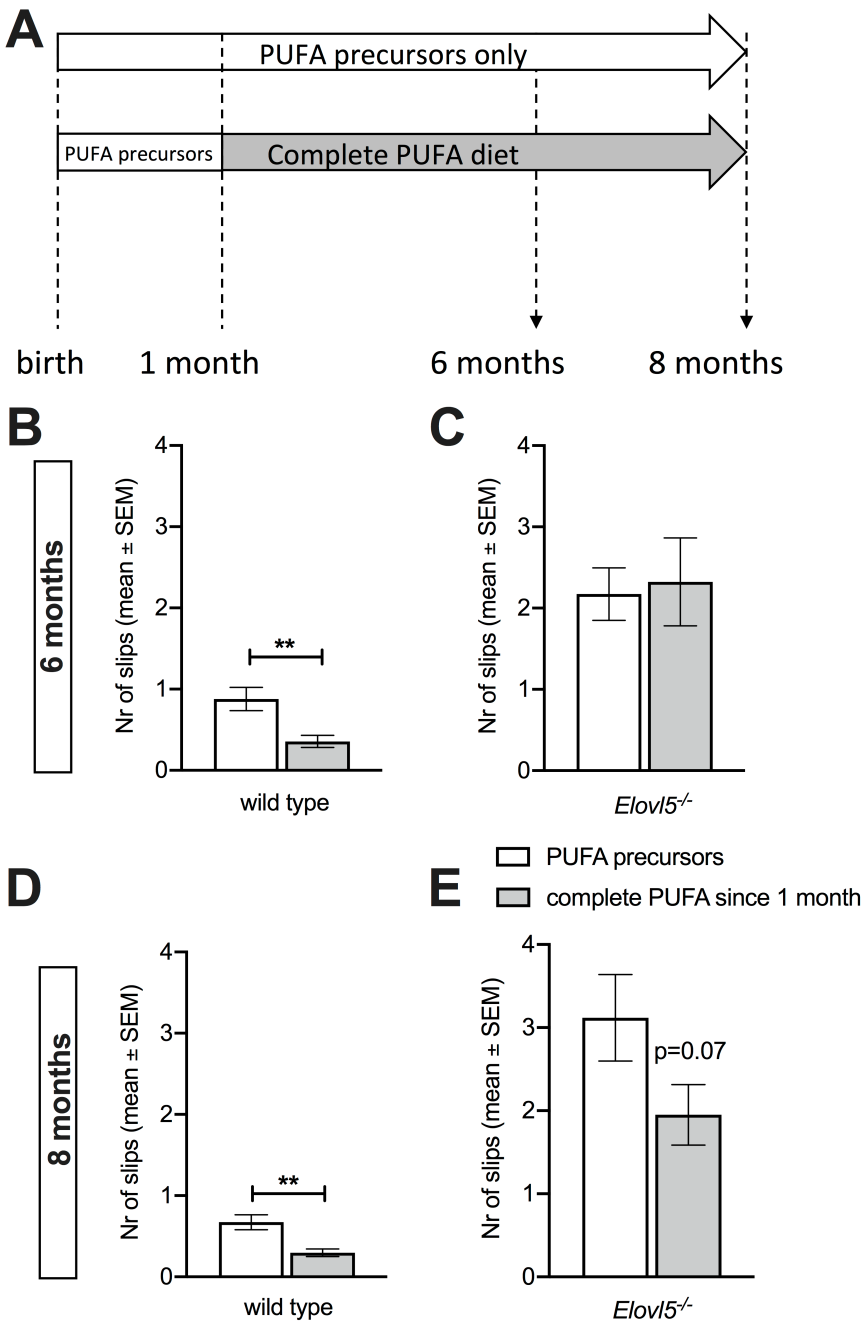

Figure 40. Effects of a complete PUFA diet from 1 month of age in *Elovl5*$^{-/-}$ and wild type mice. (A) *Elovl5*$^{-/-}$ and wild type mice received from the first month of age a diet providing them both Elovl5 substrates and downstream products from birth (grey bars) were compared to genotype and age matched PUFA precursors only mice (white bars). **(B)** and **(C)** Motor performances of both *Elovl5*$^{-/-}$ and wild type littermates when receiving the complete PUFA diet from 1 month of age at 6 months ($P < 0.01$, Unpaired Student's t-test $t_{(37)}=3.18$). **(D)** and **(E)** Graphs showing errors committed traversing the experimental apparatus at 8 months of age both wild type and *Elovl5*$^{-/-}$mice when receiving the complete PUFA diet since 1 month of age compared to negative control group ($P < 0.01$, Unpaired Student's t-test $t_{(30)}=3.52$).

In order to understand whether a later start of the complete PUFA diet could provide a benefit, similar to a therapy started after diagnosis of SCA38 in an adult individual, in a separate group we administered the complete PUFA diet since 10 months of age and continued for two months. With this protocol, neither wild type nor *Elovl5*$^{-/-}$ mice showed an improvement relative to the respective controls receiving PUFA precursors only ($P > 0.05$, Unpaired Student's t-test; **Fig. 41A**, **B** and **C**).

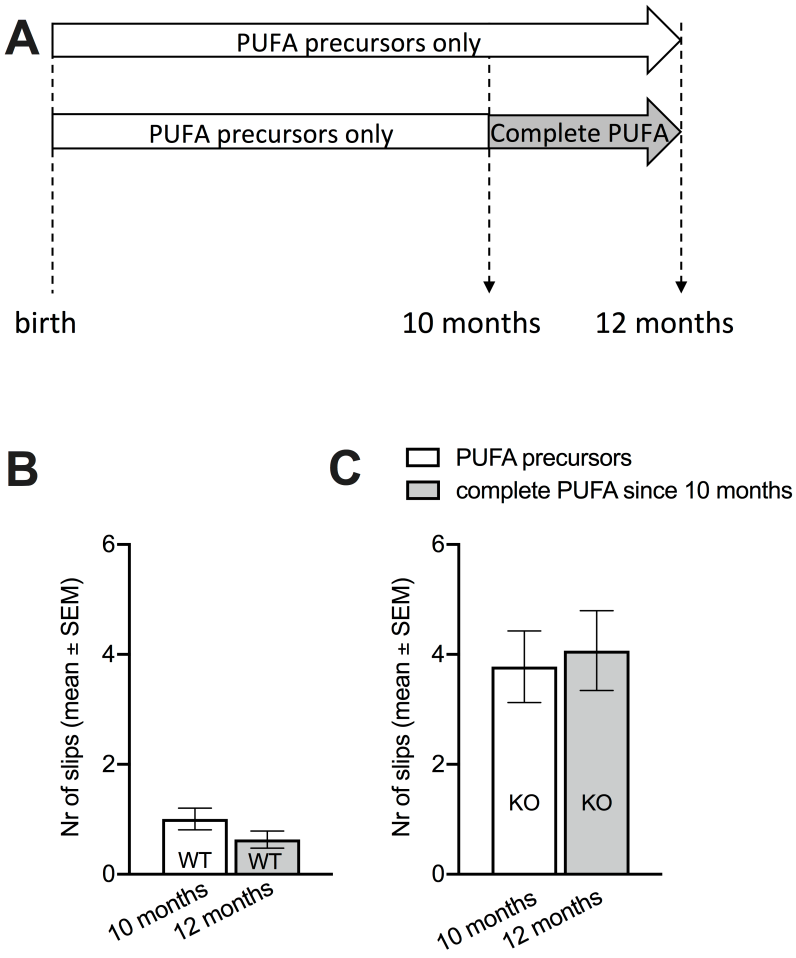

Figure 41. Complete PUFA diet in late adulthood does not restore motor deficits. (A) Schematic representation of the experimental design. *Elovl5*$^{-/-}$ and wild type mice received switched from a PUFA precursors only diet to a complete PUFA diet at 10 months of age and we checked the motor impairment after two months of treatment (12 months). **(B)** and **(C)** Mean number of errors committed traversing the experimental apparatus of both wild type and *Elovl5*$^{-/-}$ mice at 10 (white bars) and 12 months (grey bars). As shown, the diet supplementation fails to rescue motor coordination impairment ($P > 0.05$, Unpaired Student's t-test).

3.4.4 Effects of the complete PUFA diet on the cerebellar morphological parameters

In a previous report (Hoxha et al., 2017) we showed that *Elovl5*$^{-/-}$ cerebellar cortex has a shorter length of the PC layer and a reduced section area of the cerebellar white matter. Therefore, we studied the effects of the complete PUFA diet administered either since birth or since 1 month of age on these morphological parameters. The complete PUFA diet failed to affect these parameters in either wild type or *Elovl5*$^{-/-}$ mice. Thus, in *Elovl5*$^{-/-}$ the complete PUFA diet, even since birth, failed to increase either the PC layer length (PUFA precursors diet: n = 8 mice, 20.11 ± 0.55 mm; complete PUFAs since birth: n = 8 mice, 19.86 ± 0.30 mm; complete PUFAs since 1 month: n = 11 mice, 20.17 ± 0.22 mm; $P > 0.05$, Unpaired Student's t-test) or the white matter area (PUFA precursors diet: n = 8 mice, 0.12 ± 0.003; complete PUFAs since birth: n = 8 mice, 0.12 ± 0.003; complete PUFAs since 1 month: n = 11 mice, 0.11 ± 0.004; $P > 0.05$, Unpaired Student's t-test).

CHAPTER 4 – DISCUSSION

The current thesis work is aimed at deepening the knowledge about the physiological role of Elovl5 in central and peripheral nervous system, starting from a pathological mouse model lacking this enzyme. The study of the physiological mechanisms altered in SCA38-representing mice could give a hint to new clinical trials on patients, currently requiring an efficient therapy.

4.1 Elovl5 expression in the Central Nervous System is region- and cell-type specific (Balbo et al., 2021)

First goal of this work was to provide a comprehensive description of Elovl5 cell- and region-specific localization in the adult mouse brain. By immunohistochemistry, we showed that there are no rostro-caudal and ventro-dorsal differences in the expression of Elovl5 throughout the brain. Interestingly, big soma projecting neurons (e.g., mitral cells, cerebellar PCs, and cortical/hippocampal pyramidal cells) and glial cells showed a prominent expression of Elovl5. XGal staining and immunohistochemistry revealed subtle discrepancies between Elovl5 promoter activity and Elovl5 protein expression. Indeed, we observed that the XGal staining was very strong and homogeneous in the hippocampal pyramidal neurons, while the fluorescent signal was only moderately intense in CA2 and CA3 pyramidal cells and lower in the other hippocampal fields. On the other hand, in the thalamus, XGal analysis showed a low signal, while the fluorescent signal was stronger in all thalamic nuclei. These results suggest the existence of transcriptional or post-transcriptional regulation of Elovl5 expression. Notably, it is reported that estrogens can act as negative regulators of miRNAs which downregulate Elovl5 at a post-trascriptional level (Zhang et al., 2017). Elovl5 distribution in distinct CNS areas and in specific cell types suggests a unique role of this enzyme in the local synthesis of PUFAs subserving specific neuronal/glial processes and CNS functions. In the olfactory areas of the telencephalon, mitral cells showed the most prominent expression of Elovl5 protein, in contrast with a lack of labeling in the granular layer. Furthermore, strong positivity for Elovl5 was found in pyriform cortex, olfactory tubercle and anterior olfactory nucleus, which are part of the olfactory system. These findings are in line with the loss of the sense of smell found in SCA38 patients and in *Elovl5*$^{-/-}$ mice (Borroni et al., 2016; Hoxha et al., 2017), suggesting a crucial role of Elovl5 in olfaction, in line with the reported importance of PUFAs availability for a correct olfactory discrimination and a proper olfactory tissue integrity (Greiner et al., 2001; Le Bon et al., 2018; Khoury et al., 2020). A pattern similar to the olfactory bulb was also observed in the

cerebellar cortex. PCs were strongly positive for Elovl5, whereas granular cells were negative. This expression pattern well correlates with the gait abnormality and balance deficits observed in SCA38 patients with ELOVL5 mutation and in the *Elovl5*$^{-/-}$ mouse model (Borroni et al., 2016; Hoxha et al., 2017). By studying this pathological mouse model, it has been shown that the absence of Elovl5 in PCs led to a shrinkage of the dendritic tree causing molecular layer atrophy (Hoxha et al., 2017). This evidence suggests an important role of Elovl5 for the correct maintenance of PC dendritic morphology, a necessary requirement for cerebellar function. In the hippocampus, Elovl5 showed a peculiar expression pattern: labeling was specific for pyramidal cells and interneurons of the strata oriens and radiatum. The involvement of PUFAs in hippocampal synaptic plasticity has been largely described in the literature (Fukaya et al., 2007; Cutuli et al., 2014; Thomazeau et al., 2017) suggesting that the Elovl5 expression in this region is required for proper functioning and refinement of the circuits. The characterization of Elovl5 expression in the brainstem was challenging because of the huge density of cells and nuclei. In general, the most prominent labeling was shown by nuclei functionally and anatomically connected to the cerebellum (e.g., the red nucleus in the midbrain and the vestibular nuclei in the medulla). An interesting finding is that Elovl5 expression is not restricted to neurons but is extended to glial cells. The expression by both mature and immature oligodendrocytes suggests that Elovl5 downstream products might be important players in myelination and other oligodendroglia functions. Along with oligodendrocytes, microglial cells showed a prominent expression of Elovl5, consistent with the observation that some Elovl5 downstream products, omega-3 PUFAs, play a major role in the resolution of neuroinflammation and in enhancing beneficial immune response (Ebert et al., 2009; Chen et al., 2014; Joffre et al., 2019). Astrocytes instead showed no or little Elovl5 immunolabeling. However, a subpopulation of astrocytes was found positively marked, suggesting a local regulation of fatty acid production that could be possibly exploited for signaling or expansion of local membranes in astrocytes (Sakers et al., 2017). Furthermore, it has been recently shown that, while undergoing a neurogenic program, some astrocytes need to upregulate genes encoding for enzymes essential for lipid metabolisms, including Elovl5 (Magnusson et al., 2020).

The expression pattern of Elovl5 in the CNS is similar to the expression of Elovl4 (Sherry et al., 2017). Mutations of ELOVL5 or ELOVL4 cause spinocerebellar ataxia 38 and 34, respectively (Ozaki et al., 2015; Borroni et al., 2016) with common neurological symptoms which might be explained by the regional expression similarity between the two enzymes. Interestingly, both

enzymes are expressed in neurons and glial cells. Elovl5 is expressed by oligodendroglial cells, microglia and is heterogeneously in vivo expressed by astrocytes while Elovl4 is reported to be weakly expressed by astrocytes and presumably by oligodendrocytes (Sherry et al., 2017).
However, their cell-specific expression differs in some brain areas. In the cerebellum Elovl5 is expressed by PCs but not granule cells while Elovl4 is expressed mainly by granule cells with a low positivity in PCs (Sherry et al., 2017). Furthermore, in the olfactory bulb Elovl5 is expressed by mitral cells but not by granule cells while Elovl4 is expressed the most by granule cells with a low expression by mitral cells (Sherry et al., 2017). It is not clear how this difference in expression determines the onset of some neurological symptoms which are specific for SCA38 or SCA34, for instance the hyposmia in the SCA38 patients (Borroni et al., 2016).
Overall, the region-/cell-specific expression of Elovl5 suggests a special requirement of local production of VLCF with signaling or structural functions, in specific neuronal and glial cell types. However, further functional studies are needed to dissect the context-dependent role of Elovl5 and of its downstream products in neural cell physiology.

4.2 Elovl5 presence is essential for proper action potential propagation in peripheral myelinated fibers (Hoxha et al., 2021)

Once identified the cell types and the regions expressing Elovl5, we looked at the consequences of Elovl5 deficiency starting from the peripheral nerves. We exploited *Elovl5*$^{-/-}$ mice and show that the lack of Elovl5 enzymatic activity in mice leads to biochemical and structural changes in myelin, which have functional consequences in the velocity of action potential conduction along axons. Our lipidomic analysis, in line with the lack of Elovl5, revealed an accumulation of phospholipids consisting of 16 or 18 carbons fatty acids (Elovl5 substrates) with at most two or three unsaturations. On the other hand, *Elovl5*$^{-/-}$ fibers showed a strong reduction of phospholipids with fatty acids with 20 or more than 20 carbons carrying multiple unsaturations (Elovl5 products). More specifically, the strong alteration of the plasmalogens observed in *Elovl5*$^{-/-}$ mice is in line with the finding of a less compacted myelin. Indeed, plasmalogens represent a substantial part of phospholipids and are reported to protect myelin structure from oxidative stress, so that changes in their quantity can influence myelin-packing properties (Luoma et al., 2015). Noteworthy, the most prominent effect of the lack of Elovl5 on the lipidic profile is a reduced ratio between polyunsaturated versus saturated and monounsaturated fatty

acids. Interestingly, impaired PUFA levels, in the liver, are shown to increase the activity of the sterol regulatory element-binding protein (Srebp-1c) that pushes the expression of different lipogenic genes implicated in the monounsaturated and saturated fatty acid synthesis in *Elovl5*$^{-/-}$ mice (Moon et al., 2009). However, our analysis in the sciatic nerve did not reveal changes in the Srebp-1c and proteins involved in synthesis of phospholipids (data not shown). Actually, we found that Schwann cells themselves express Elovl5 indicating local PUFAs synthesis (Figure 20). This finding raises the question of the role of intrinsic synthesis relative to the uptake of preformed lipids from the bloodstream. From a functional point of view, saturated fatty acids lead to stronger lipid-lipid interactions and make membranes more rigid and tightly packed, while PUFAs fluidize membranes (Harayama & Riezman, 2018; Sezgin et al., 2017; van Meer et al., 2008). Moreover, the lack of Elovl5 revealed an important accumulation of sphingolipids, which are structural lipids highly enriched in nervous cells, and beyond their role in the architecture of membranes, they also participate in different cellular pathways (Venkataraman & Futerman, 2000). A 30% increase of sphingomyelin and galactosylceramide in lipid bilayer models is sufficient to cause an increase of the membrane stiffness and reduced flexibility (Saeedimasine et al., 2019). Sphingomyelin rich bilayers tend to form hydrogen bonding together (Niemelä et al., 2004), while galactosylceramides tend to pack together via sugar-sugar bonding and to make strong interactions with phospholipids, thus causing thickening of the membrane (Saeedimasine et al., 2019). Indeed, the accumulation of sphingolipids is the main feature of lipid storage diseases (Sural-Fehr & Bongarzone, 2016; Zheng et al., 2006), which are associated with aberrant myelination and peripheral neuropathy (Bagel et al., 2013; Higashi et al., 1995; Ramakrishnan et al., 2007). Even though there are several studies demonstrating that some specific lipids influence structural stability of myelin, there is insufficient information on how changes of the whole lipid composition impact the structure and function of myelin, mainly due to technical difficulties. Advances in lipidomic investigation highlight the fact that a deranged lipid homeostasis accompanied by myelin defects and axonal conduction deficits are common features for different neurodegenerative diseases (Harel et al., 2018; Horibata et al., 2018; Karsai et al., 2019; Kutkowska-Kazmierczak et al., 2018; Pujol-Lereis, 2019; Vaz et al., 2019). In line with alterations of phospholipid profile, in *Elovl5*$^{-/-}$ nerves, myelin thickness was increased, and the layer periodicity was enlarged. This corresponds to a deficit in myelin compactness, which is required to provide better electrical insulation, reduction of membrane capacitance and faster action potential conduction (Schmidt & Knösche, 2019). Interestingly, an

increase in myelin periodicity is reported in mice with defects in fatty acid synthesis (Cermenati et al., 2015) and in mice with deficiency of plasmalogens (da Silva et al., 2014). The node/paranode structure is strongly dependent on the lipid composition (Thaxton and Bhat, 2009). Accordingly, the nodal gap and the paranode length are increased in *Elovl5*$^{-/-}$ nerves, suggesting a role of Elovl5-dependent phospholipids in the maintenance of integrity of nodes and paranodes. It is well reported that the lack of sulfatides causes nodal and paranodal junction abnormalities in mice (Ishibashi et al., 2002; Marcus et al., 2006; Takano et al., 2012). Unsurprisingly, in *Elovl5*$^{-/-}$ mice, such deficits in myelin compactness and length of nodes and paranodes were associated with a slower conduction velocity of action potentials. Given the importance of myelin thickness, node and paranode length in influencing the velocity of action potentials (Schmidt & Knösche, 2019), it is not surprising to find that the alteration of even one of these parameters will cause deficits in the action potential conduction along axons (Arancibia-Carcamo et al., 2017; Li, 2015). The high amount of lipids in myelin renders them important players in determining structural integrity of myelin therefore influencing the conduction of action potentials. In summary, our findings strengthen the notion that the Elovl5 enzyme is necessary for a correct maintenance of the homeostasis of fatty acids in peripheral myelin, which is crucial to assure the correct biophysical properties of the membrane.

4.3 Elovl5 loss influences the correct function of the cerebellar circuitry

Ataxia is one of the main characteristic clinical features of SCA38 patients (Borroni et al., 2016). In a similar way, *Elovl5* loss in mice induces motor coordination and balance impairment (Hoxha et al., 2017). These findings suggest that *Elovl5*$^{-/-}$ mice can be used as model of SCA38 in order to understand the consequences of Elovl5 lack in central nervous system. We focused our study on the cerebellum, in particular on PCs, by questioning ourselves on the mechanisms underlying the motor impairment observed in *Elovl5*$^{-/-}$ mice. There are lot of examples in literature describing alterations in PC firing connected to various diseases, starting of course from ataxias to Huntington Disease and autism spectrum disorders (Cook et al., 2020). So, we started by looking at the PCs ability to generate action potentials. Altered PC firing properties have been observed in mouse models of various ataxia types. For instance, for SCA1, SCA2, SCA3, SCA5 and SCA6 a reduced firing frequency has been reported, while reduced firing regularity has been observed in SCA6, SCA7, Autosomal recessive spastic ataxia of Charlevoix-

Saguenay (ARSACS) and episodic ataxia type 2 (EA2) (Hourez et al., 2011; Hansen et al., 2013; Dell'Orco et al., 2017; Kasumu and Bezprozvanny, 2012; Liu et al., 2009; Shakkottai et al., 2011; McLoughlin et al., 2018; Perkins et al., 2010; Jayabal et al., 2016; Stoyas et al., 2020; Walter et al., 2006; Alviña and Khodakhah, 2010; Ady et al., 2018). In *Elovl5*$^{-/-}$ mice we found an alteration in spike frequency adaptation, suggesting impaired capabilities of PCs to compensate with a reduction of the firing when stimulated with excitatory signals for long periods.

Since many cerebellar disorders appear to be caused by a malfunction of synaptic connections (Koeppen, 2018; Roccaro-Waldmeyer et al., 2018), we then focused on the main synapses formed with PCs, the PFs-PC and the CF-PCs ones. We evaluated EPSCs and pre-synaptic terminal functioning in *Elovl5*$^{-/-}$ and control littermates and we discovered that the basal mechanism is preserved when Elovl5 is lacking. We further ruled out the involvement of this type of synapse by analyzing VGLUT1 expression in the mice cerebellum. In fact, as showed by other examples in literature, VGLUT1-specific PF synaptic deficits might contribute to abnormal cerebellar circuit development (Lin et al., 2017). However, we found intact localization and expression of VGLUT1 in *Elovl5*$^{-/-}$ mice were intact. Altogether our results lead us to conclude that the motor impairment in SCA38 mice is not due to alterations in PF-PC synapses.

Another important player in PFs-PC synapse is mGluR1-mediated signaling, which is activated when PFs are repeatedly stimulated (Hoxha et al., 2018). Many ataxic diseases reported dysfunction in mGluR1-mediated synaptic activity, showing both increased (e.g. SCA2 mouse model) and decreased signaling (e.g. SCA1 mouse model) (Kano and Watanabe, 2017; Shuvaev et al., 2017; Hoxha et al., 2018). Differently from these examples, we did not find any alterations in the mGluR1-mediated current in PCs nor in receptor expression in *Elovl5*$^{-/-}$ mice compared to control one.

The other important synapse formed with PC, is the one with CF. Changes in CF-PC synaptic connections have been found in various degenerative movement disorders, like Parkinson's disease (PD), multiple system atrophy (MSA) and essential tremor (Kuo et al., 2017). Moreover, impairment in CFs activity is a hallmark of some forms of SCA, like SCA1, SCA7, SCA14 and SCA23 (Ebner et al., 2013; Smeets and Verbeek, 2016). By voltage-clamp recordings we assessed the amplitude of the CF-evoked EPSC, as well as the paired-pulse depression. We found a preserved amplitude of the CF-evoked EPSC suggesting a normal function of the

dendritic spines occupied by CF varicosities. On the other hand, *Elovl5*$^{-/-}$ mice showed a reduced paired- pulse depression, suggesting a presynaptic mechanism (Hashimoto and Kano, 1998).
In fact, from observations accomplished on Elovl4 deficient mice, which have a reduction of very long-chain fatty acids (VLC-FA, ≥ 28 carbons), it is known that PUFAs increase membrane fusion at presynaptic level, in particular inducing faster fusion and turnover of vesicle released neurotransmitters pool in the synaptic cleft (Gedalya et al., 2009; Hopiavuori et al., 2018). Consequently, Elovl5 lack might lead to a decreased velocity of vesicle fusion and recycling at presynaptic level. To deepen the analysis, we performed an immunostaining of VGLUT2, the only glutamatergic transporter present on CF and often abnormally localized or expressed in ataxias and similar pathological conditions (Fremeu et al., 2001; Kuo et al., 2017; Hoxha et al., 2018). By comparing the intensity of expression of this transporter in *Elovl5*$^{-/-}$ mice with wild type littermates we found out that it is expressed in a similar way, with a tendency toward the increase.
It is widely assumed that gain control within cerebellar circuits is made possible by forms of synaptic plasticity (Rinaldo and Hansel, 2010). So, we then investigated the possibility of a disruption of LTD being the cause of the motor impairment observed in *Elovl5*$^{-/-}$ mice. LTD at PF-PC synapses results in a reduction of the excitatory inputs received by PCs, which in turn reduces the inhibition delivered to the deep cerebellar nuclei. In mice with an impairment in cerebellar motor learning, deficits in cerebellar synaptic plasticity were discovered (Aiba et al., 1994; De Zeeuw et al., 1998; Feil et al., 2003; van Woerden et al., 2009). So, we wondered whether Elovl5 loss could induce alteration in this mechanism, which could be involved in the motor impairment found in *Elovl5*$^{-/-}$ mice. What resulted from inducing LTD at PF-PC synapses was that *Elovl5*$^{-/-}$ mice did not present differences from wild type littermates. Therefore, it is possible to rule out the presence of an LTD impairment when Elovl5 is lacking. Remarkably, in contrast, deletion of Elovl4 induces disruption in both LTD and LTP, accompanied by alteration in synchronization of the cerebellar network due to impaired presynaptic activity of PFs (Nagaraja et al., 2021). These differences compared to the situation originated from Elovl5 mutations could be due to the different pattern of expression of Elovl4 and Elovl5. In fact, Elovl4 is expressed in granule cells (Sherry et al., 2017), so its absence could impair their basal activity and PFs-mediated plasticity. Since Elovl5 is involved in the biosynthesis of PUFAs, including ARA and DHA, which are essential modulators of neuronal excitability (Vreugdenhil et al., 1996; Young et al., 2000), we also assessed a plasticity form which involves the

endocannabinoid system, the SSE. eCBs bind the receptors CB1, the most widespread G protein-coupled receptor (GPCR) in the mammalian cerebellum (Stephens, 2016). Highly expressed at presynaptic level, CB1Rs are able to inhibit evoked and spontaneous IPSCs at interneuron-PC synapses or EPSCs at CF-PC and PF-PC synapses (Stephens, 2016). Our results show that a lack of Elovl5 in mice causes the dysregulation of the eCB-mediated inhibition of presynaptic transmission at the PF-PC synapse. The alteration found could be due to a reduced production of eCBs, deriving from a reduced pool of products downstream Elovl5. A similar result was obtained in a mouse model of SCA1, which showed a duration of the SSE dramatically reduced (Shuvaev et al., 2017). However, we cannot exclude the hypothesis that this reduced response might be due to a reduced number of CB1 receptors. Indeed, studies on post-mortem cerebellar tissues of patients with different SCAs showed an increased level of MAGL enzyme levels, a key player for hydrolysis of eCBs, and an up regulation of CB1 receptor on PC soma in SCA patients (Rodrıguez-Cueto et al. 2014b and 2014a).

Elovl5$^{-/-}$ mice presented reduced velocity in conducting action potentials in peripheral nerves (see chapter 3.2.3 and 3.2.4). Interestingly, we found a decreased velocity of propagation of the antidromic action potential in *Elovl5*$^{-/-}$ PC axons compared to control littermates. This reduced velocity of propagation is in part due the increased length of both nodes and paranodes on PCs axon. The cause of the instability of node-paranode complexes might be due to the different lipid composition of myelin.

We hypothesized that PCs deficits were not confined to the axonal conduction capabilities but also at the level of synaptic contacts between PC and their target cells in deep cerebellar nuclei. We evaluated PC axon terminal in deep cerebellar nuclei with vesicular GABA transporter (VGAT) immunostaining. It is well known that VGAT deficiency causes motor dysfunction in mice (Kayakabe et al., 2013). However, we did not observe changes of VGAT expression in the deep cerebellar nuclei ruling out that PC-deep cerebellar nuclei cells synapse is involved in motor dysfunction of *Elovl5*$^{-/-}$ mice.

Taken together these data suggest that ELovl5 lack impact several components of the cerebellar cortex, including here: intrinsic excitability of PCs, eCB-dependent synaptic plasticity of PFs and short-term plasticity of CFs. These changes are associated with a slowed down conduction of action potentials along axons of PCs. It is difficult to understand which of these changes is a compensatory or a causative mechanism, since *Elovl5*$^{-/-}$ mice lack Elovl5 throughout

development. Additional experiments are necessary to understand which of these mechanisms has a causal link with motor impairment.

4.4 PUFA-enriched diet supplementations as a possible therapeutic approach for SCA38

Once having identified some of the mechanisms altered when Elovl5 is lacking, we assessed the effect of an early administration versus an administration of PUFAs during the turning from adolescence to young adulthood, and we verified possible differences. Clinical trials on SCA38 patients showed that the administration of DHA only, one of the PUFAs downstream Elovl5, leads patients to gait and posture amelioration, increase in cerebellar metabolism and no worsening of motor impairment and peripheral neuropathy (Manes et al., 2017 and 2019). So, we wondered whether an earlier assumption of all the downstream products of Elovl5 (including ARA, DHA and EPA) could lead to better improvement. Actually, it is widely known that PUFAs omega 3 and 6 are critical for the correct development of the brain and its function (Innis et al., 2007), so the administration of a complete PUFA diet to dams could give *Elovl5*$^{-/-}$ mice the possibility for a quicker recovery of motor symptoms and cerebellar atrophy. Despite these expectations, analysis performed at 1 month of age revealed that *Elovl5*$^{-/-}$ mice fed with the complete PUFA diet from birth did not show a rescue of the motor phenotype neither when compared to wild type littermates, nor to *Elovl5*$^{-/-}$ PUFA precursors only mice. At later timepoints, (6 and 8 months), we found that the diet supplementation in knockout mice led to a slowdown of the impairment (**Fig. 42)** while the *Elovl5*$^{-/-}$ PUFA precursors only mice showed a progressive worsening of balance, as previously reported (Hoxha et al., 2017). On the other hand, mice that received the complete PUFA diet from weaning showed a significant amelioration of motor coordination shifted to the latest timepoint analyzed **(Fig. 42)**. This last evidence highlights the importance of the time at which the treatment is started and ended: this kind of approach seems much more effective when started early. This finding is supported by the results obtained with the diet supplementation with PUFA in late adulthood of *Elovl5*$^{-/-}$ mice (10 months of age) and the symptoms assessment after only two months of administration. Interestingly, *Elovl5*$^{-/-}$ mice receiving complete PUFA diet either from birth or from weaning showed amelioration in motor performance with a reduced number of foot-slips from the beam, but no amelioration in latency was observed. Hence, mice receiving the diet supplementation displayed a rescue of the motor balance and coordination. This condition could be due to a

potential enhancement of the action potential conduction along peripheral myelinated axons. Indeed, as showed before, Elovl5 has an essential role in peripheral and central nervous system in supporting the correct structure of myelin, hence, proper action potential conduction (see chapter 3.2, 3.3 and 4.2, 4.3; Hoxha et al., 2021). Impaired PUFAs levels due to Elovl5 loss likely lead to a stronger lipid-lipid interaction and makes membranes more rigid. Since PUFAs are the primary components of myelin and are involved in membrane fluidification (Harayama & Riezman, 2018; Sezgin et al., 2017; van Meer et al., 2008), we can speculate that a balanced replacement treatment by PUFAs might restore the correct myelin compactness required to provide better axonal insulation and faster action potential conduction in *Elovl5*$^{-/-}$ mice.

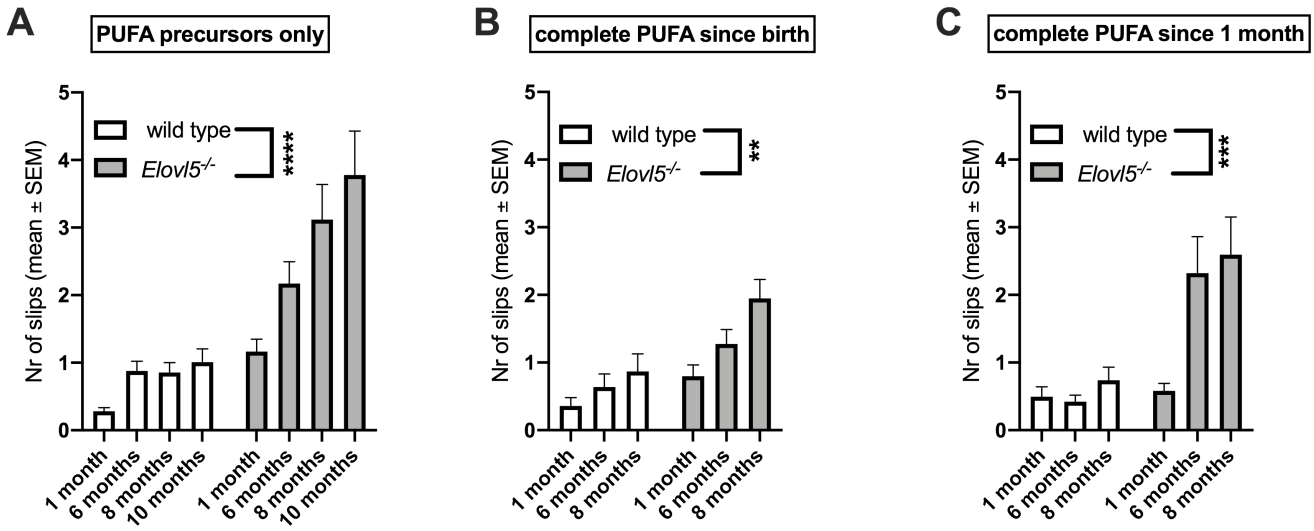

Figure 42. Pathology progression in *Elovl5*$^{-/-}$ mice compared to wild type littermates. (A) Graph showing the great motor worsening showed by *Elovl5*$^{-/-}$ mice (grey bars) when receiving the PUFA precursors only diet compared to control littermates (white bars) from the first to the 10th month of age. **(B)** Comparison between *Elovl5*$^{-/-}$ mice (grey bars) and wild type controls (white bars) imposed the complete PUFA diet from birth, showing a mild worsening with age of the motor coordination (1st – 8th month of age). **(C)** Graph representing the motor skill worsening of *Elovl5*$^{-/-}$ mice (grey bars) with age (1st – 8th month of age) compared to control littermates (white bars).

We decided also to check whether the complete PUFA diet is sufficient to induce amelioration in cerebellar atrophy of *Elovl5*$^{-/-}$ mice (Hoxha et al., 2017). We found that the administration of this complete PUFA diet from birth does not restore the normal amount of white matter area in the cerebellum of *Elovl5*$^{-/-}$ mice nor ameliorate the general cerebellar shrinkage, as evident from the

Purkinje layer length measurement. This result suggests that in this pathological condition the lipidic balance of diet is not enough to induce structural changes in the cerebellum. On the other side, previous data show that when imposing a diet poor in PUFAs, the myelination process is disrupted, by inducing a thinning of myelin sheaths and altering white matter organization (Salvati et al., 2008; Tian et al., 2011; Witte et al., 2014; Gu et al., 2016; McNamara et al., 2017; McNamara et al., 2018; Leyrolle et al., 2021). This could be caused by an impaired maturation of oligodendrocytes, since, as reported in literature, n-3 PUFA and their derivatives have been shown to promote OPCs differentiation (Minghetti et al., 2014; Bernardo et al., 2017). Moreover, Elovl5 is strongly expressed by OPCs and oligodendrocytes (see chapter 3.1.3; Balbo et al., 2021), so its loss could alter their functionality and impair the myelin production. Nevertheless, further studies are essential to understand why this diet supplementation lead this mice to functional recovery without a structural ameliorations.

Diet supplementation with PUFAs is widely known to have beneficial effects in treatment of many neurodegenerative disease and pathological conditions (Delattre et al., 2010; Hacioglu et al., 2012; Luchtman et al., 2012; Chen et al., 2014; Beblo et al., 2017; Yassine et al., 2017; Mondal et al., 2021). On the other hand, PUFA deficiency situations lead to major impairments both during development and in adolescence (Carrié et al., 2000; Larrieu et al., 2012; Bondi et al., 2014; Janssen et al., 2015; Lozada et al., 2017; Manduca et al., 2017; Robertson et al., 2017). This evidence suggests that a correct balance of PUFA is essential for the correct functions of brain, especially in such a critical period like development or adolescence. Therefore, our results suggest that an implementation with a complete PUFA diet from birth is the most effective approach to slow down SCA38 progression. While, on the contrary, the intervention in late adulthood might be insufficient to lead to satisfactory comparable result. Taken together these findings highlight the need of a better diagnosis tool which could lead SCA38 patients and their families to an earlier approach like a complete diet supplementation with PUFAs, which is safe and easy to practice. In fact, the choice to administer a diet providing all the products downstream Elovl5, including ARA, did not lead to adverse effects. Nonetheless, a systematic evaluation of literature provided by Calder et al. (2019) suggests that a supplementation of ARA is not necessarily linked to increased inflammatory events or platelet aggregation in humans. However, it must be said that this kind of treatment is not as precise as a pharmaceutical one, so maybe greater effects could be observed by an administration of a precise dosage of PUFAs as a supplementation to a balanced diet.

CHAPTER 5 – CONCLUSIONS AND FUTURE PERSPECTIVES

In this thesis work, we tried to identify the physiological role of Elovl5 in central and peripheral nervous system, by means of the *Elovl5*$^{-/-}$ mouse, which is a model of SCA38. Our results showed that Elovl5 is abundantly expressed at both central and peripheral level, with a cell- and region-specific pattern, that its loss induces changes in myelin, alters action potential propagation and, finally, that the motor impairment induced by its lack could be overcome by an early administration of a complete PUFA diet. Alterations in enzymes involved in biosynthesis of PUFAs greatly impair brain composition and cause severe consequences for human health (Rizzi et al., 2013; Freemantle et al., 2012; Kutkowska-Kaźmierczak, et al., 2018; Mueller et al., 2019; Sun et al., 2018; Cadieux-Dion et al., 2014; Bourassa et al., 2015; Ozaki et al., 2015; Bernstein et al., 2001; Edwards et al., 2001; Zhang et al., 2001; Sailer et al., 2016; Li et al., 2018; Keo et al., 2020). The brain is one of the most lipid-rich tissues in the organism, second only at adipose tissue (Adibhatla et al., 2007). So, it should not be surprising that an imbalance of lipids due to lack of Elovl5 leads to a neurological deficit like SCA38, which, as showed during this thesis work, impacts not only on the central but also on the peripheral nervous system, both at morphological and functional level. This concept is confirmed by the benefic effect, of a rebalance of PUFAs in diet, in restoring the correct functionality of the brain. Taken the data obtained all together, Elovl5 revealed to have a complex function in the nervous system, not completely understood yet. The aim of this thesis work was to provide a more accurate understanding of Elovl5 physiological roles in order to give a more detailed insight on the pathological alterations risen by its loss.

In this work, we showed that a deficit of PUFAs with an increase in saturates fatty acids due to Elovl5 lack alters myelin and slows action potentials, while the specific effect of alterations in fatty acid chain length and different types of phospholipids (sphingomyelins, plasmalogens, phosphatidylcholines, phosphatidylethanolamines, phosphatidylserines) in brain functionality remains to be investigated. Moreover, studies still need to clarify the impairment of the paired pulse depression of CFs, which we hypothesize being due impaired velocity of either vesicle fusion or recycling at presynaptic level. So, it would be interesting to study the dynamics of recruitment and release of synaptic vesicles from presynaptic terminals of CFs affected by Elovl5 loss. Another point that should be deepened is the rescue of the phenotype induced by the complete PUFA diet administration. In fact, it is not clear whether this approach leads to amelioration of other signs of SCA38, like the peripheral neuropathy or the hyposmia, in

addition to motor deficits. Moreover, clinical studies focused only on DHA administration (Manes et al., 2017; Manes et al., 2019), while our results showed effective results with the administration of both omega-3 and omega-6 PUFAs, with only one relative amount ratio. It would be interesting to study different ratios omega-3/omega-6 and investigate the efficacy of the treatment. Importantly, these preliminary data could put the basis for an optimization of a therapeutic intervention on SCA38 patients.

CHAPTER 6 – REFERENCES

Abedi, E., & Sahari, M. A. (2014). Long-chain polyunsaturated fatty acid sources and evaluation of their nutritional and functional properties. *Food science & nutrition*, 2(5), 443–463. https://doi.org/10.1002/fsn3.121

Adibhatla, R. M., & Hatcher, J. F. (2007). Role of Lipids in Brain Injury and Diseases. *Future lipidology*, *2*(4), 403–422. https://doi.org/10.2217/17460875.2.4.403

Ady, V., Toscano-Márquez, B., Nath, M., Chang, P. K., Hui, J., Cook, A., Charron, F., Larivière, R., Brais, B., McKinney, R. A., & Watt, A. J. (2018). Altered synaptic and firing properties of cerebellar Purkinje cells in a mouse model of ARSACS. *The Journal of physiology*, 596(17), 4253–4267. https://doi.org/10.1113/JP275902

Ahn, A. H., Dziennis, S., Hawkes, R., Herrup, K. (1994). The cloning of zebrin II reveals its identity with aldolase C. *Development* 120, 2081–2090.

Aiba, A., Kano, M., Chen, C., Stanton, M. E., Fox, G. D., Herrup, K., Zwingman, T. A., & Tonegawa, S. (1994). Deficient cerebellar long-term depression and impaired motor learning in mGluR1 mutant mice. *Cell*, 79(2), 377–388.

Albus, J. S. (1971). A theory of cerebellar function. *Math. Biosci*. 10, 25–61. doi: 10. 1016/0025-5564(71)90051-4

Alviña, K., & Khodakhah, K. (2010). KCa channels as therapeutic targets in episodic ataxia type-2. *The Journal of neuroscience: the official journal of the Society for Neuroscience*, 30(21), 7249–7257. https://doi.org/10.1523/JNEUROSCI.6341-09.2010

Andreone, B. J., Chow, B. W., Tata, A., Lacoste, B., Ben-Zvi, A., Bullock, K., Deik, A., A., Ginty, D., D., Clish, C., B., Gu, C. (2017). Blood-Brain barrier permeability is regulated by lipid transport- dependent suppression of caveolae-mediated transcytosis. *Neuron* 94, 581–594.e5. doi: 10.1016/j.neuron.2017.03.043

Antonny, B., Vanni, S., Shindou, H., and Ferreira, T. (2015). From zero to six double bonds: phospholipid unsaturation and organelle function. *Trends Cell Biol.* 25, 427–436. doi: 10.1016/j.tcb.2015.03.004

Arancibia-Carcamo, I. L., Ford, M. C., Cossell, L., Ishida, K., Tohyama, K., & Attwell, D. (2017). Node of Ranvier length as a potential regulator of myelinated axon conduction speed. *eLife*, 6, e23329. https://doi.org/ 10.7554/eLife.23329

Armstrong, D. M. & Schild, R. F. (1970). A quantitative study of the Purkinje cells in the cerebellum of the albino rat. *J. Comp. Neurol*. 139, 449–456.

Bagel, J. H., Sikora, T. U., Prociuk, M., Pesayco, J. P., Mizisin, A. P., Shelton, G. D., & Vite, C. H. (2013). Electrodiagnostic testing and histo- pathologic changes confirm peripheral nervous system myelin abnor- malities in the feline model of niemann-pick disease type C. *Journal of Neuropathology and Experimental Neurology*, 72(3), 256–262. https:// doi.org/10.1097/NEN.0b013e318286587f

Bakiri, Y., Káradóttir, R., Cossell, L., & Attwell, D. (2011). Morphological and electrical properties of oligodendrocytes in the white matter of the corpus callosum and cerebellum. *The Journal of Physiology*, 589(Pt 3), 559–573. https://doi.org/10.1113/jphysiol.2010.201376

Balbo, I., Montarolo, F., Boda, E., Tempia, F. and Hoxha, E. (2021) Elovl5 Expression in the Central Nervous System of the Adult Mouse. *Front. Neuroanat*. 15:669073. doi: 10.3389/fnana.2021.669073

Bazinet, R. P., and Layé, S. (2014). Polyunsaturated fatty acids and their metabolites in brain function and disease. *Nat. Rev. Neurosci*. 15, 771–785. doi: 10.1038/ nrn3820

Beblo, S., Reinhardt, H., Demmelmair, H., Muntau, A. C., & Koletzko, B. (2007). Effect of Fish Oil Supplementation on Fatty Acid Status, Coordination, and Fine Motor Skills in Children with Phenylketonuria. *The Journal of Pediatrics*, 150(5), 479–484. https://doi.org/10.1016/J.JPEDS.2006.12.011

Bernardo, A., Giammarco, M. L., De Nuccio, C., Ajmone-Cat, M. A., Visentin, S., De Simone, R., & Minghetti, L. (2017). Docosahexaenoic acid promotes oligodendrocyte differentiation via PPAR-γ signalling and prevents tumor necrosis factor-α-dependent maturational arrest. *Biochimica et Biophysica Acta - Molecular and Cell Biology of Lipids*, 1862, 1013–1023.

Bernstein, P. S., Tammur, J., Singh, N., Hutchinson, A., Dixon, M., Pappas, C. M., Zabriskie, N. A., Zhang, K., Petrukhin, K., Leppert, M., Allikmets, R. (2001). Diverse macular dystrophy phenotype caused by a novel complex mutation in the ELOVL4 gene. *Investig. Ophthalmol. Vis. Sci*. 42, 3331–3336

Bhattacharjee, S., Jun, B., Belayev, L., Heap, J., Kautzmann, M. A., Obenaus, A., Menghani, H., Marcell, S. J., Khoutorova, L., Yang, R., Petasis, N. A., & Bazan, N. G. (2017). Elovanoids are a novel class of homeostatic lipid mediators that protect neural cell integrity upon injury. *Science Advances*, 3(9). https://doi.org/10.1126/SCIADV.1700735

Boda, E., Viganò, F., Rosa, P., Fumagalli, M., Labat-Gest, V., Tempia, F., Abbracchio, M. P., Dimou, L., & Buffo, A. (2011). The GPR17 receptor in NG2 expressing cells: Focus on in vivocell maturation and participation in acute trauma and chronic damage. *Glia*, 59(12), 1958–1973. https://doi.org/10.1002/glia.21237

Boda, E., Di Maria, S., Rosa, P., Taylor, V., Abbracchio, M. P., and Buffo, A. (2015). Early phenotypic asymmetry of sister oligodendrocyte progenitor cells after mitosis and its modulation by aging and extrinsic factors. Glia 63, 271–286. doi: 10.1002/glia.22750

Bondi, C. O., Taha, A. Y., Tock, J. L., Totah, N. K. B., Cheon, Y., Torres, G. E., Rapoport, S. I., & Moghaddam, B. (2014). Adolescent Behavior and Dopamine Availability Are Uniquely Sensitive to Dietary Omega-3 Fatty Acid Deficiency. *Biological Psychiatry*, 75(1), 38–46. https://doi.org/10.1016/j.biopsych.2013.06.007

Borjesson, S.I., Hammarstrom, S., Elinder, F. (2008). Lipoelectric modification of ion channel voltage gating by polyunsaturated fatty acids. *Biophys J* 95:2242–2253.

Borroni, B., Di Gregorio, E., Orsi, L., Vaula, G., Costanzi, C., Tempia, F., Mitro, N., Caruso, D., Manes, M., Pinessi, L., Padovani, A., Brusco, A., Boccone, L. (2016) Clinical and neuroradiological features of spinocerebellar ataxia 38 (SCA38). *Parkinsonism Relat Disord.* 28:80-6. doi: 10.1016/j.parkreldis.2016.04.030.

Bourassa, C. V., Raskin, S., Serafini, S., Teive, H. A. G., Dion, P. A., and Rouleau, G. A. (2015). A New ELOVL4 mutation in a case of spinocerebellar ataxiawith erythroke *JAMA Neurol*. 72, 942–943. doi: 10.1001/jamaneurol. 2015.0888

Bousquet, M., Calon, F., & Cicchetti, F. (2011). Impact of omega-3 fatty acids in Parkinson's disease. In Ageing Research Reviews (Vol. 10, Issue 4, pp. 453–463). *Ageing Res Rev*. https://doi.org/10.1016/j.arr.2011.03.001

Bradl, M. (1999). Myelin dysfunction/degradation in the central nervous system: Why are myelin sheaths susceptible to damage? *Journal of Neural Transmission. Supplementum,* 55, 9–17. https://doi.org/10. 1007/978-3-7091-6369-6_2

Braitenberg, V. & Atwood, R. P. (1958). Morphological observations on the cerebellar cortex. *J. Comp. Neurol*. 109, 1–33

Brochu, G., Maler, L., Hawkes, R. (1990) Zebrin II: a polypeptide antigen expressed selectively by Purkinje cells reveals compartments in rat and fish cerebellum. *J. Comp. Neurol*. 291, 538–552

Brown, S. P., Brenowitz, S. D., & Regehr, W. G. (2003). Brief presynaptic bursts evoke synapse-specific retrograde inhibition mediated by endogenous cannabinoids. *Nature Neuroscience*, 6(10), 1048–1057. https://doi.org/10.1038/nn1126

Cadieux-Dion, M., Turcotte-Gauthier, M., Noreau, A., Martin, C., Meloche, C., Gravel, M., Drouin, C. A., Rouleau, G. A., Nguyen, D. K., Cossette, P. (2014). Expanding the clinical phenotype associated with ELOVL4 mutation: study of a large French-Canadian family with

autosomal dominant spinocerebellar ataxia and erythrokeratodermia. *JAMA Neurol*. 71, 470–475. doi: 10.1001/jamaneurol.2013.6337

Calder, P., Campoy, C., Eilander, A., Fleith, M., Forsyth, S., Larsson, P., . . . Mensink, R. (2019). A systematic review of the effects of increasing arachidonic acid intake on PUFA status, metabolism and health-related outcomes in humans. *British Journal of Nutrition*, 121(11), 1201-1214. doi:10.1017/S0007114519000692

Campagnoni, A. T., & Skoff, R. P. (2006). The pathobiology of myelin mutants reveal novel biological functions of the MBP and PLP. *Genes Brain Pathol*, 11(1), 74–91. https://doi.org/10.1111/j.1750-3639. 2001.tb00383

Carrié, I., Clément, M., de Javel, D., Francès, H., & Bourre, J.-M. (2000). Phospholipid supplementation reverses behavioral and biochemical alterations induced by n-3 polyunsaturated fatty acid deficiency in mice. *Journal of Lipid Research*, 41(3), 473–480. https://doi.org/10.1016/S0022-2275(20)34486-2

Cascio, M.G. (2013). PUFA-derived endocannabinoids: an overview. *Proceedings of the Nutrition Society*, 72(4):451-9. doi: 10.1017/S0029665113003418.

Castillo, P. E., Younts, T. J., Chávez, A. E., & Hashimotodani, Y. (2012). Endocannabinoid Signaling and Synaptic Function. *Neuron.* https://doi.org/10.1016/j.neuron.2012.09.020

Cerminara, N. L., Lang, E. J., Sillitoe, R. V, & Apps, R. (2015). Redefining the cerebellar cortex as an assembly of non-uniform Purkinje cell microcircuits. *Nature Reviews Neuroscience*, 16(2), 79–93.

Cermenati, G., Audano, M., Giatti, S., Carozzi, V., Porretta-Serapiglia, C., Pettinato, E., Ferri, C., Antonio, M., Fabiani, E., Crestani, M., Scurati, S., Saez, E., Azcoitia, I., Cavaletti, G., Garcia-Segura, L.-M., Melcangi, R. C., Caruso, D., & Mitro, N. (2015). Lack of sterol regulatory element bind- ing factor-1c imposes glial fatty acid utilization leading to peripheral neuropathy. *Cell Metabolism*, 21(4), 571–583. https://doi.org/10. 1016/j.cmet.2015.02.016

Chen, C., Bazan, N.G. (2005). Endogenous PGE2 regulates membrane excitability and synaptic transmission in hippocampal CA1 pyramidal neurons. *J Neurophysiol* 93:929–41.

Chen, S., Zhang, H., Pu, H., Wang, G., Li, W., Leak, R. K., Chen, J., Liou, A. K., & Hu, X. (2014). n-3 PUFA supplementation benefits microglial responses to myelin pathology. *Scientific report.* https://doi.org/10.1038/srep07458

Constantin, L. The Role of MicroRNAs in Cerebellar Development and Autism Spectrum Disorder During Embryogenesis. *Mol Neurobiol* 54, 6944–6959 (2017). https://doi.org/10.1007/s12035-016-0220-9

Cook, A. A., Fields, E., & Watt, A. J. (2021). Losing the Beat: Contribution of Purkinje Cell Firing Dysfunction to Disease, and Its Reversal. *Neuroscience*, 462, 247–261. https://doi.org/10.1016/j.neuroscience.2020.06.008

Cutuli, D., de Bartolo, P., Caporali, P., Laricchiuta, D., Foti, F., Ronci, M., Rossi, C., Neri, C., Spalletta, G., Caltagirone, C., Farioli-Vecchioli, S., & Petrosini, L. (2014). n-3 polyunsaturated fatty acids supplementation enhances hippocampal functionality in aged mice. Frontiers in Aging Neuroscience, 6(AUG), 1–53. https://doi.org/10.3389/fnagi.2014.00220

D'Angelo, E., & Casali, S. (2013). Seeking a unified framework for cerebellar function and dysfunction: from circuit operations to cognition. *Frontiers in Neural Circuits*, 6, 116.

D'Angelo, E., Solinas, S., Mapelli, J., Gandolfi, D., Mapelli, L. and Prestori, F. (2013) The cerebellar Golgi cell and spatiotemporal organization of granular layer activity. *Front. Neural Circuits* 7:93. doi: 10.3389/fncir.2013.00093.

da Silva, T. F., Eira, J., Lopes, A. T., Malheiro, A. R., Sousa, V., Luoma, A., Avila, R. L., Wanders, R. J., Just, W. W., Kirschner, D. A., Sousa, M. M., & Brites, P. (2014). Peripheral

nervous system plasmalogens regulate Schwann cell differentiation and myelination. *The Journal of Clinical Investigation*, 124(6), 2560–2570. https://doi. org/10.1172/JCI72063

Danthi, S.J., Enyeart, J.A., Enyeart, J.J. (2005). Modulation of native T-type calcium channels by omega-3 fatty acids. *Biochem Biophys Res Commun* 327:485–493.

De Zeeuw, C. I., Hansel, C., Bian, F., Koekkoek, S. K., van Alphen, A. M., Linden, D. J., & Oberdick, J. (1998). Expression of a protein kinase C inhibitor in Purkinje cells blocks cerebellar LTD and adaptation of the vestibulo-ocular reflex. *Neuron*, 20(3), 495–508. https://doi.org/10.1016/s0896-6273(00)80990-3

Di Gregorio, E., Borroni, B., Giorgio, E., Lacerenza, D., Ferrero, M., Lo Buono, N., Ragusa, N., Mancini, C., Gaussen, M., Calcia, A., Mitro, N., Hoxha, E., Mura, I., Coviello, D.A., Moon, Y.A., Tesson, C., Vaula, G., Couarch, P., Orsi, L., Duregon, E., Papotti, M.G., Deleuze, J.F., Imbert, J., Costanzi, C., Padovani, A., Giunti, P., Maillet-Vioud, M., Durr, A., Brice, A., Tempia, F., Funaro, A., Boccone, L., Caruso, D., Stevanin, G., Brusco, A. (2014). ELOVL5 Mutations Cause Spinocerebellar Ataxia 38. *Am J HumGenet.* 7;95(2):209-17. doi: 10.1016/j.ajhg.2014.07.001.

Diana, M. A., & Marty, A. (2004). Endocannabinoid-mediated short-term synaptic plasticity: depolarization-induced suppression of inhibition (DSI) and depolarization-induced suppression of excitation (DSE). *British Journal of Pharmacology*, 142, 9–19. https://doi.org/10.1038/sj.bjp.0705726

Deák, F., Anderson, R. E., Fessler, J. L. and Sherry, D. M. (2019) Novel Cellular Functions of Very Long Chain-Fatty Acids: Insight From ELOVL4 Mutations. *Front. Cell. Neurosci.* 13:428. doi: 10.3389/fncel.2019.00428

Delattre, A. M., Kiss, Á., Szawka, R. E., Anselmo-Franci, J. A., Bagatini, P. B., Xavier, L. L., Rigon, P., Achaval, M., Iagher, F., de David, C., Marroni, N. A. P., & Ferraz, A. C. (2010). Evaluation of chronic omega-3 fatty acids supplementation on behavioral and neurochemical

alterations in 6-hydroxydopamine-lesion model of Parkinson's disease. *Neuroscience Research*, 66(3), 256–264. https://doi.org/10.1016/J.NEURES.2009.11.006

Dell'Orco, J. M., Wasserman, A. H., Chopra, R., Ingram, M. A., Hu, Y. S., Singh, V., Wulff, H., Opal, P., Orr, H. T., & Shakkottai, V. G. (2015). Neuronal Atrophy Early in Degenerative Ataxia Is a Compensatory Mechanism to Regulate Membrane Excitability. *The Journal of neuroscience: the official journal of the Society for Neuroscience*, 35(32), 11292–11307. https://doi.org/10.1523/JNEUROSCI.1357-15.2015

Durr, A. (2010). Autosomal dominant cerebellar ataxias: Polyglutamine expansions and beyond. *The Lancet Neurology*; 9(9):885-94. doi: 10.1016/S1474-4422(10)70183-6.

Dyall, S. C., Michael-Titus, A. T. (2008) Neurological Benefits of Omega-3 Fatty Acids. *Neuromol Med* 10, 219–235. https://doi.org/10.1007/s12017-008-8036-z

Ebert, S., Weigelt, K., Walczak, Y., Drobnik, W., Mauerer, R., Hume, D. A., Weber, B. H. F., & Langmann, T. (2009). Docosahexaenoic acid attenuates microglial activation and delays early retinal degeneration. *Journal of Neurochemistry*, 110(6), 1863–1875. https://doi.org/10.1111/j.1471-4159.2009.06286.x

Ebner, B. A., Ingram, M. A., Barnes, J. A., Duvick, L. A., Frisch, J. L., Clark, H. B., Zoghbi, H. Y., Ebner, T. J., & Orr, H. T. (2013). Purkinje Cell Ataxin-1 Modulates Climbing Fiber Synaptic Input in Developing and Adult Mouse Cerebellum. *The Journal of Neuroscience*, *33*(13), 5806 LP – 5820. https://doi.org/10.1523/JNEUROSCI.6311-11.2013

Eccles, J. C., Llinas, R., & Sasaki, K. (1966). The excitatory synaptic action of climbing fibres on the Purkinje cells of the cerebellum. *The Journal of Physiology*, 182(2), 268-296.

Eccles, J. C., Ito, M. & Szentagothai, J. (1967). *The cerebellum as a neuronal machine*. Berlin: Springer-Verlag

Edmond, J. (2001). Essential polyunsaturated fatty acids and the barrier to the brain: the components of a model for transport. *J. Mol. Neurosci*. 16, 181–193.

Edwards, A. O., Donoso, L. A., and Ritter, R. III (2001). A novel gene for autosomal dominant Stargardt-like macular dystrophy with homology to the SUR4 protein family. *Invest. Ophthalmol. Vis. Sci*. 42, 2652–2663.

Fernstrom, J. D. (1999). Effects of dietary polyunsaturated fatty acids on neuronal function. *Lipids*, *34*(2), 161–169. https://doi.org/10.1007/S11745-999-0350-3

Feil, R., Hartmann, J., Luo, C., Wolfsgruber, W., Schilling, K., Feil, S., Barski, J. J., Meyer, M., Konnerth, A., De Zeeuw, C. I., & Hofmann, F. (2003). Impairment of LTD and cerebellar learning by Purkinje cell-specific ablation of cGMP-dependent protein kinase I. *The Journal of cell biology*, 163(2), 295–302. https://doi.org/10.1083/jcb.200306148

Freemantle, E., Lalovic, A., Mechawar, N., & Turecki, G. (2012). Age and haplotype variations within FADS1 interact and associate with alterations in fatty acid composition in human male cortical brain tissue. *PloS one*, 7(8), e42696. https://doi.org/10.1371/journal.pone.0042696

Fujita, H., Aoki, H., Ajioka, I., Yamazaki, M., Abe, M., Arata, O., Sakimura, K., Sugihara, I. (2014) Detailed Expression Pattern of Aldolase C (Aldoc) in the Cerebellum, Retina and Other Areas of the CNS Studied in Aldoc-Venus Knock-In Mice. *PLOS ONE* 9(1): e86679. https://doi.org/10.1371/journal.pone.0086679

Fukaya, T., Gondaira, T., Kashiyae, Y., Kotani, S., Ishikura, Y., Fujikawa, S., Kiso, Y., & Sakakibara, M. (2007). Arachidonic acid preserves hippocampal neuron membrane fluidity in senescent rats. *Neurobiology of Aging*, 28(8), 1179–1186. https://doi.org/10.1016/j.neurobiolaging.2006.05.023

Gedalya, T. Ben, Loeb, V., Israeli, E., Altschuler, Y., Selkoe, D. J., & Sharon, R. (2009). α-Synuclein and polyunsaturated fatty acids promote clathrin-mediated endocytosis and

synaptic vesicle recycling. *Traffic*, 10(2), 218–234. https://doi.org/10.1111/j.1600-0854.2008.00853.x

Geuna, S., Tos, P., Battiston, B., Guglielmone, R. (2000). Verification of the two-dimensional disector, a method for the unbiased estimation of density and number of myelinated nerve fibers in peripheral nerves. *Annals of Anatolia,* 182(1), 23–34. https://doi.org/10.1016/S0940-9602(00)80117-X

Greiner, R. S., Moriguchi, T., Slotnick, B. M., Hutton, A., & Salem, N. (2001). Olfactory discrimination deficits in n - 3 fatty acid-deficient rats. *Physiology and Behavior*, 72(3), 379–385. https://doi.org/10.1016/S0031-9384(00)00437-6

Gu, Y., Vorburger, R. S., Gazes, Y., Habeck, C. G., Stern, Y., Luchsinger, J. A., Manly, J. J., Schupf, N., Mayeux, R., & Brickman, A. M. (2016). White matter integrity as a mediator in the relationship between dietary nutrients and cognition in the elderly. *Annals of Neurology*, 79, 1014–1025.

Guillou, H., Zadravec, D., Martin, P. G., and Jacobsson, A. (2010). The key roles of elongases and desaturases in mammalian fatty acid metabolism: insights from transgenic mice. *Prog. Lipid Res.* 49, 186–199. doi: 10.1016/j.plipres.2009. 12.002

Hacioglu, G., Seval-Celik, Y., Tanriover, G., Ozsoy, O., Saka-Topcuoglu, E., Balkan, S., & Agar, A. (2012). Docosahexaenoic acid provides protective mechanism in bilaterally MPTP-lesioned rat model of parkinson's disease. *Folia Histochemica et Cytobiologica*, *50*(2), 228–238. https://doi.org/10.5603/FHC.2012.0032

Hansel, C., Linden, D.J., D'Angelo, E. (2001) Beyond parallel fiber LTD: the diversity of synaptic and non-synaptic plasticity in the cerebellum. *Nat Neurosci* 4(5):467–475. https://doi.org/10.1038/87419

Hansen, S. T., Meera, P., Otis, T. S., & Pulst, S. M. (2013). Changes in Purkinje cell firing and gene expression precede behavioral pathology in a mouse model of SCA2. *Human Molecular Genetics*, 22(2). https://doi.org/10.1093/hmg/dds427

Harel, T., Quek, D. Q. Y., Wong, B. H., Cazenave-Gassiot, A., Wenk, M. R., Fan, H., Berger, I., Shmueli, D., Shaag, A., Silver, D. L., Elpeleg, O., & Edvardson, S. (2018). Homozygous mutation in MFSD2A, encoding a lysolipid transporter for docosahexanoic acid, is associated with microcephaly and hypomyelination. *Neurogenetics*, 19(4), 227–235. https://doi.org/10.1007/s10048-018-0556-6

Harayama, T., & Riezman, H. (2018). Understanding the diversity of membrane lipid composition. *Nature Reviews. Molecular Cell Biology*, *19*(5), 281–296. https://doi.org/10.1038/NRM.2017.138

Harayama, T., & Shimizu, T. (2020). Roles of polyunsaturated fatty acids, from mediators to membranes. *Journal of Lipid Research*, *61*(8), 1150–1160. https://doi.org/10.1194/JLR.R120000800

Hashimoto, K, Kano, M (1998) Presynaptic origin of paired-pulse depression at climbing fibre-Purkinje cell synapses in the rat cerebellum. *J Physiol* 506(Pt 2): 391–405.

Hekman, K. E., Gomez, C. M. (2015). The autosomal dominant spinocerebellar ataxias: emerging mechanistic themes suggest pervasive Purkinje cell vulnerability. J. *Neurol Neurosurg Psychiatry* 86(5):554-61. doi: 10.1136/jnnp-2014-308421.

Hernando, S., Requejo, C., Herran, E., Ruiz-Ortega, J. A., Morera-Herreras, T., Lafuente, J. V., Ugedo, L., Gainza, E., Pedraz, J. L., Igartua, M., & Hernandez, R. M. (2019). Beneficial effects of n-3 polyunsaturated fatty acids administration in a partial lesion model of Parkinson's disease: The role of glia and NRf2 regulation. *Neurobiology of Disease*, 121, 252–262. https://doi.org/10.1016/j.nbd.2018.10.001

Higashi, Y., Murayama, S., Pentchev, P. G., & Suzuki, K. (1995). Peripheral nerve pathology in Niemann-pick type C mouse. *Acta Neuropathologica*, 90(2), 158–163. https://doi.org/10.1007/BF00294315

Hopiavuori, B. R., Deak, F., Wilkerson, J. L., Brush, R. S., Rocha-Hopiavuori, N. A., Hopiavuori, A. R., Ozan, K. G., Sullivan, M. T., Wren, J. D., Georgescu, C., Szweda, L., Awasthi, V., Towner, R., Sherry, D. M., Anderson, R. E., Agbaga, M.-P. (2018). Homozygous expression of mutant ELOVL4 leads to seizures and death in a novel animal model of very long-chain fatty acid deficiency. *Mol. Neurobiol*. 55, 1795–1813. doi: 10.1007/s12035-017-0824-8

Hopiavuori, B. R., Anderson, R. E., and Agbaga, M. P. (2019). ELOVL4: very long- chain fatty acids serve an eclectic role in mammalian health and function. *Prog. Retin. Eye Res*. 69, 137–158. doi: 10.1016/j.preteyeres.2018.10.004

Horibata, Y., Elpeleg, O., Eran, A., Hirabayashi, Y., Savitzki, D., Tal, G., Mandel, H., & Sugimoto, H. (2018). Ethanolamine phosphotransferase 1 (selenoprotein I) is critical for the neural development and mainte- nance of plasmalogen in human. *Journal of Lipid Research*, 59(6), 1015– 1026. https://doi.org/10.1194/jlr.P081620

Hoxha, E., Boda, E., Montarolo, F., Parolisi, R., Tempia, F. (2012). Excitability and Synaptic Alterations in the Cerebellum of APP/PS1 Mice. *PLoS ONE* 7(4): e34726. https://doi.org/10.1371/journal.pone.0034726

Hoxha E., Tempia F., Lippiello P. and Miniaci M.C. (2016). Modulation, Plasticity and Pathophysiology of the Parallel Fiber-Purkinje Cell Synapse. *Front. Synaptic Neurosci*. 8:35. doi: 10.3389/fnsyn.2016.00035.

Hoxha, E., Gabriele, R.M.C, Balbo, I., Ravera, F., Masante, L., Zambelli, V., Albergo, C., Mitro, N., Caruso, D., Di Gregorio, E., Brusco, A., Borroni, B., Tempia, F. (2017). Motor deficits and cerebellar atrophy in Elovl5 knock out mice. *Front. Cell. Neurosci.*

Hoxha, E., Balbo, I., Parolisi, R., Audano, M., Montarolo, F., Ravera, F., Guglielmotto, M., Muratori, L., Raimondo, S., DiGregorio, E., Buffo, A., Brusco, A., Borroni, B., Mitro, N., Caruso, D., & Tempia, F. (2021). Elovl5 is required for proper action potential conduction along peripheral myelinated fibers. *Glia*, 1–10. https://doi.org/10. 1002/glia.24048

Hourez, R., Servais, L., Orduz, D., Gall, D., Millard, I., de Kerchove d'Exaerde, A., Cheron, G., Orr, H. T., Pandolfo, M., & Schiffmann, S. N. (2011). Aminopyridines correct early dysfunction and delay neurodegeneration in a mouse model of spinocerebellar ataxia type 1. *The Journal of neuroscience: the official journal of the Society for Neuroscience*, 31(33), 11795–11807. https://doi.org/10.1523/JNEUROSCI.0905-11.2011

Innis, S. M. (2007). Dietary (n-3) Fatty Acids and Brain Development. *The Journal of Nutrition*, 137(4), 855–859. https://doi.org/10.1093/jn/137.4.855

Ishibashi, T., Dupree, J. L., Ikenaka, K., Hirahara, Y., Honke, K., Peles, E., Popko, B., Suzuki, K., Nishino, H., & Baba, H. (2002). A myelin galactolipid, sulfatide, is essential for maintenance of ion channels on myelinated axon but not essential for initial cluster formation. *The Journal of Neuroscience*, 22(15), 6507–6514. https://doi.org/10.1523/ JNEUROSCI.22-15-06507.2002

Ito, M. (1984). *The cerebellum and neural control*. Blackwell Science Inc, New York.

Ito, M. (2000). Mechanisms of motor learning in the cerebellum. *Brain Research*. 15;886(1-2):237-245.

Ito, M. (2006). Cerebellar circuitry as a neuronal machine. *Prog Neurobiol* 78(3-5):272–303. https://doi.org/10.1016/j.pneurobio. 2006.02.006

Jakobsson, A., Westerberg, R., and Jacobsson, A. (2006). Fatty acid elongases in mammals: their regulation and roles in metabolism. *Prog. Lipid Res*. 45, 237–249. doi: 10.1016/j.plipres.2006.01.004

Janssen, C. I. F., Zerbi, V., Mutsaers, M. P. C., de Jong, B. S. W., Wiesmann, M., Arnoldussen, I. A. C., Geenen, B., Heerschap, A., Muskiet, F. A. J., Jouni, Z. E., van Tol, E. A. F., Gross, G., Homberg, J. R., Berg, B. M., & Kiliaan, A. J. (2015). Impact of dietary n-3 polyunsaturated fatty acids on cognition, motor skills and hippocampal neurogenesis in developing C57BL/6J mice. *Journal of Nutritional Biochemistry*, *26*(1), 24–35. https://doi.org/10.1016/j.jnutbio.2014.08.002

Jayadev, S., & Bird, T. D. (2013). Hereditary ataxias: overview. *Genetics in Medicine*, 15(9), 673– 683.

Jayabal, S., Chang, H. H., Cullen, K. E., & Watt, A. J. (2016). 4-aminopyridine reverses ataxia and cerebellar firing deficiency in a mouse model of spinocerebellar ataxia type 6. *Scientific reports*, *6*, 29489. https://doi.org/10.1038/srep29489

Joffre, C., Rey, C., & Layé, S. (2019). N-3 Polyunsaturated Fatty Acids and the Resolution of Neuroinflammation. *Front. Pharmacol* 10. https://doi.org/10.3389/fphar.2019.01022

Jun, B., Mukherjee, P.K., Asatryan, A., Kautzmann, M.-A., Heap, J., Gordon, W.C., Bhattacharjee, S., Yang, R., Petasis, N. A., Bazan, N. G. (2017) Elovanoids are novel cell-specific lipid mediators necessary for neuroprotective signaling for photoreceptor cell integrity. *Sci Rep* 7, 5279. https://doi.org/10.1038/s41598-017-05433-7

Kandel, E.R., Schwartz, J.H., Jessell, T.M., Siegelbaum, S.A., Hudspeth, A. J., (2013). *Principles of Neural Science, Fifth Edition.* McGraw-Hill Professional.

Kano, M., Hashimoto, K., & Tabata, T. (2008). Type-1 metabotropic glutamate receptor in cerebellar Purkinje cells: A key molecule responsible for long-term depression, endocannabinoid signalling and synapse elimination. *Philosophical Transactions of the Royal Society B: Biological Sciences,* 363(1500), 2173–2186. https://doi.org/10.1098/rstb.2008.2270

Kano, M., and Watanabe, T. (2017). Type-1 metabotropic glutamate receptor signaling in cerebellar Purkinje cells in health and disease. *F1000Research* 6. doi:10.12688/f1000research.10485.1.

Karsai, G., Kraft, F., Haag, N., Korenke, G. C., Hänisch, B., Othman, A., Suriyanarayanan, S., Steiner, R., Knopp, C., Mull, M., Bergmann, M., Schröder, J. M., Weis, J., Elbracht, M., Begemann, M., Hornemann, T., & Kurth, I. (2019). DEGS1-associated aberrant sphingolipid metabolism impairs nervous system function in humans. *The Journal of Clinical Investigation*, 129(3), 1229–1239. https://doi. org/10.1172/JCI124159

Kasumu, A., Bezprozvanny, I. Deranged Calcium Signaling in Purkinje Cells and Pathogenesis in Spinocerebellar Ataxia 2 (SCA2) and Other Ataxias. *Cerebellum* 11, 630–639 (2012). https://doi.org/10.1007/s12311-010-0182-9

Kayakabe, M., Kakizaki, T., Kaneko, R., Sasaki, A., Nakazato, Y., Shibasaki, K., Ishizaki, Y., Saito, H., Suzuki, N., & Yanagawa, Y. (2014). Motor dysfunction in cerebellar Purkinje cell-specific vesicular GABA transporter knockout mice. *Frontiers in Cellular Neuroscience* (Vol. 7, p. 286). https://www.frontiersin.org/article/10.3389/fncel.2013.00286

Keo, A., Mahfouz, A., Ingrassia, A. M. T., Meneboo, J. P., Villenet, C., Mutez, E., Comptaer, T., Lelieveldt, B.P.F., Figeac, M., Chartier-Harlin, M.-C., Van de Berg, W.D.J., Van Hilten, J.J., Reinders, M.J.T. (2020). Transcriptomic signatures of brain regional vulnerability to Parkinson's disease. *Commun. Biol*. 3:101. doi: 10.1038/s42003-020-0804-9

Khoury, S., Soubeyre, V., Cabaret, S., Merle, L., Grégoire, S., Deprêtre, N., Jarriault, D., Grosmaitre, X., Bretillon, L., Berdeaux, O., Acar, N., & Le Bon, A. M. (2020). Perinatal exposure to diets with different n-6:n-3 fatty acid ratios affects olfactory tissue fatty acid composition. *Scientific Reports*, 10(1), 1–15. https://doi.org/10.1038/s41598-020-67725-9

Kihara, A. (2012). Very long-chain fatty acids: elongation, physiology and related disorders. *J. Biochem.* 152, 387–395. doi: 10.1093/jb/mvs105

Kim, H. Y. & Spector, A. A. (2013). Synaptamide, endocannabinoid-like derivative of docosahexaenoic acid with cannabinoid-independent function. Prostaglandins *Leukot. Essent. Fatty Acids* 88, 121–125.

Kim, H. Y., Spector, A. A. & Xiong, Z. M. (2011). A synaptogenic amide N-docosahexaenoylethanolamide promotes hippocampal development. *Prostaglandins Other Lipid Mediators* 96, 114–120.

Kirchhausen, T., Boll, W., Van Oijen, A., and Ehrlich, M. (2005). Single-molecule live-cell imaging of clathrin-based endocytosis. *Biochem. Soc. Symp*. 72, 71–76. doi: 10.1042/bss0720071

Klockgether, T., Mariotti, C., & Paulson, H. L. (2019). Spinocerebellar ataxia. *Nature Reviews Disease Primers*, *5*(1), 1–21. https://doi.org/10.1038/s41572-019-0074-3

Koeppen, A. H. (2018). "The neuropathology of the adult cerebellum," in *Handbook of Clinical Neurology* (Elsevier B.V.), 129–149. doi:10.1016/B978-0-444-63956-1.00008-4.

Konnerth, A., Llano, I., Armstrong, C. M. (1990). Synaptic currents in cerebellar Purkinje cells. *Proceedings of the National Academy of Sciences*, 87(7), 2662-2665.

Konnerth, A., Dreessen, J., and Augustine, G. J. (1992). Brief dendritic calcium signals initiate long-lasting synaptic depression in cerebellar Purkinje cells. *Proceedings of the National Academy of Sciences. U S A* 89, 7051–7055. doi: 10.1073/pnas.89.15.7051

Kreitzer, A. C., & Regehr, W. G. (2001). Retrograde inhibition of presynaptic calcium influx by endogenous cannabinoids at excitatory synapses onto Purkinje cells. *Neuron*. https://doi.org/10.1016/S0896-6273(01)00246-X

Kuo, S. H., Lin, C. Y., Wang, J., Sims, P. A., Pan, M. K., Liou, J. you, et al. (2017). Climbing fiber-Purkinje cell synaptic pathology in tremor and cerebellar degenerative diseases. *Acta Neuropathol.* 133, 121–138. doi:10.1007/s00401-016-1626-1.

Kutkowska-Kaźmierczak, A., Rydzanicz, M., Chlebowski, A., Kłosowska-Kosicka, K., Mika, A., Gruchota, J., Jurkiewicz, E., Kowalewski, C., Pollak, A., Stradomska, T. J., Kmieć, T., Jakubowski, R., Gasperowicz, P., Walczak, A., Śladowski, D., Jankowska-Steifer, E., Korniszewski, L., Kosińska, J., Obersztyn, E., … Płoski, R. (2018). Dominant ELOVL1 mutation causes neurological disorder with ichthyotic keratoderma, spasticity,

hypomyelination and dysmorphic features. *Journal of Medical Genetics*, *55*(6), 408–414. https://doi.org/10.1136/jmedgenet-2017-105172

Lacombe, R. J. S., Chouinard-Watkins, R., and Bazinet, R. P. (2018). Brain docosahexaenoic acid uptake and metabolism. *Mol. Aspects Med*. 64, 109–134. doi: 10.1016/j.mam.2017.12.004

Lainé, J. & Axelrad, H., (1998). Lugaro cells target basket and stellate cells in the cerebellar cortex. *NeuroReport* 2399-2403

Larrieu, T., Madore, C., Joffre, C., & Layé, S. (2012). Nutritional n-3 polyunsaturated fatty acids deficiency alters cannabinoid receptor signaling pathway in the brain and associated anxiety-like behavior in mice. *Journal of Physiology and Biochemistry*, 68(4), 671–681. https://doi.org/10.1007/s13105-012-0179-6

Lauwers, E., Goodchild, R., and Verstreken, P. (2016). Membrane lipids in presynaptic function and disease. *Neuron* 90, 11–25. doi: 10.1016/j.neuron. 2016.02.033 2016.02.033

Layé, S. Polyunsaturated fatty acids, neuroinflammation and well being (2010). *Prostaglandins Leukot Essent. Fatty Acids* 82, 295–303.

Le Bon, A. M., Deprêtre, N., Sibille, E., Cabaret, S., Grégoire, S., Soubeyre, V., Masson, E., Acar, N., Bretillon, L., Grosmaitre, X., & Berdeaux, O. (2018). Comprehensive study of rodent olfactory tissue lipid composition. *Prostaglandins Leukotrienes and Essential Fatty Acids*, 131(March), 32–43. https://doi.org/10.1016/j.plefa.2018.03.008

Lein, E. S., Hawrylycz, M. J., Ao, N., Ayres, M., Bensinger, A., Bernard, A., Boe, A. F., Boguski, M. S., Brockway, K. S., Byrnes, E. J., Chen, L., Chen, L., Chen, T. M., Chin, M. C., Chong, J., Crook, B. E., Czaplinska, A., Dang, C. N., Datta, S., … Jones, A. R. (2007). Genome-wide atlas of gene expression in the adult mouse brain. *Nature,* 445(7124), 168–176. https://doi.org/10.1038/nature05453

Leonard, A. E., Bobik, E. G., Dorado, J., Kroeger, P. E., Chuang, L. T., Thurmond, J. M., Parker-Barnes, J., Das, T., Huang, Y., Mukerji, P. (2000). Cloning of a human cDNA

encoding a novel enzyme involved in the elongation of long-chain polyunsaturated fatty acids. *Biochem. J*. 350, 765–770. doi: 10.1042/0264-6021:3500765

Leonard, A. E., Pereira, S. L., Sprecher, H., and Huang, Y. S. (2004). Elongation of long-chain fatty acids. *Prog. Lipid Res*. 43, 36–54. doi: 10.1016/S0163-7827(03) 00040- 7

Leyrolle, Q., Decoeur, F., Dejean, C., Brière, G., Leon, S., Bakoyiannis, I., Baroux, E., Sterley, T.-L., Bosch-Bouju, C., Morel, L., Amadieu, C., Lecours, C., St-Pierre, M.-K., Bordeleau, M., De Smedt-Peyrusse, V., Séré, A., Schwendimann, L., Grégoire, S., Bretillon, L., Acar, N., Joffre, C., Ferreira, G., Uricaru, R., Thebault, P., Gressens, P., Tremblay, M.-E., Layé, S., & Nadjar, A. (2021). N-3 PUFA deficiency disrupts oligodendrocyte maturation and myelin integrity during brain development. *Glia*, 1–21. https://doi. org/10.1002/glia.24088

Li, J. (2015). Molecular regulators of nerve conduction - lessons from inherited neuropathies and rodent genetic models. *Experimental Neurology*, 267, 209–218. https://doi.org/10.1016/j.expneurol.2015.03.009

Li, G., Cui, S., Du, J., Liu, J., Zhang, P., Fu, Y., He, Y., Zhou, H., Ma, J., & Chen, S. (2018). Association of GALC, ZNF184, IL1R2 and ELOVL7 With Parkinson's Disease in Southern Chinese. *Frontiers in aging neuroscience*, 10, 402. https://doi.org/10.3389/fnagi.2018.00402

Lin, H., Magrane, J., Clark, E. M., Halawani, S. M., Warren, N., Rattelle, A., & Lynch, D. R. (2017). Early VGLUT1-specific parallel fiber synaptic deficits and dysregulated cerebellar circuit in the KIKO mouse model of Friedreich ataxia. *Disease models & mechanisms*, 10(12), 1529–1538.

Liu, J., Tang, T. S., Tu, H., Nelson, O., Herndon, E., Huynh, D. P., Pulst, S. M., & Bezprozvanny, I. (2009). Deranged calcium signaling and neurodegeneration in spinocerebellar ataxia type 2. *The Journal of neuroscience: the official journal of the Society for Neuroscience*, 29(29), 9148–9162. https://doi.org/10.1523/JNEUROSCI.0660-09.2009

Lombardi, M., Parolisi, R., Scaroni, F., Bonfanti, E., Gualerzi, A., Gabrielli, M., Kerlero de Rosbo, N., Uccelli, A., Giussani, P., Viani, P., Garlanda, C., Abbracchio, M. P., Chaabane, L., Buffo, A., Fumagalli, M., & Verderio, C. (2019). Detrimental and protective action of

microglial extracellular vesicles on myelin lesions: astrocyte involvement in remyelination failure. *Acta Neuropathologica*, 138(6), 987. https://doi.org/10.1007/S00401-019-02049-1

Lozada, L. E., Desai, A., Kevala, K., Lee, J. W., & Kim, H. Y. (2017). Perinatal Brain Docosahexaenoic Acid Concentration Has a Lasting Impact on Cognition in Mice. *The Journal of nutrition*, *147*(9), 1624–1630. https://doi.org/10.3945/jn.117.254607

Lu, H. C., & MacKie, K. (2016). An introduction to the endogenous cannabinoid system. *Biological Psychiatry*. https://doi.org/10.1016/j.biopsych.2015.07.028

Luchtman, D. W., Meng, Q., & Song, C. (2012). Ethyl-eicosapentaenoate (E-EPA) attenuates motor impairments and inflammation in the MPTP-probenecid mouse model of Parkinson's disease. *Behavioural Brain Research*, *226*(2), 386–396. https://doi.org/10.1016/J.BBR.2011.09.033

Luoma, A. M., Kuo, F., Cakici, O., Crowther, M. N., Denninger, A. R., Avila, R. L., Brites, P., & Kirschner, D. A. (2015). Plasmalogen phospho- lipids protect internodal myelin from oxidative damage. *Free Radical Biology & Medicine*, 84, 296–310. https://doi.org/10.1016/j.freeradbiomed.2015.03.012

Maganti, R. J., Hronowski, X. L., Dunstan, R. W., Wipke, B. T., Zhang, X., Jandreski, L., Hamann, S., & Juhasz, P. (2019). Defining changes in the spatial distribution and composition of brain lipids in the Shiverer and Cuprizone mouse models of myelin disease. *The Journal of Histochemistry and Cytochemistry*, 67(3), 203–219. https://doi.org/10.1369/0022155418815860

Magnusson, J. P., Zamboni, M., Santopolo, G., Mold, J. E., Barrientos-Somarribas, M., Talavera-Lopez, C., Andersson, B., & Frisén, J. (2020). Activation of a neural stem cell transcriptional program in parenchymal astrocytes. *ELife*, 9, 1–25. https://doi.org/10.7554/ELIFE.59733

Mancini, C., Hoxha, E., Iommarini, L., Brussino, A., Richter, U., Montarolo, F., Cagnoli, C., Parolisi, R., Morosini, D. I. G., Nicolò, V., Maltecca, F., Muratori, L., Ronchi, G., Geuna, S., Arnaboldi, F., Donetti, E., Giorgio, E., Cavalieri, S., Di Gregorio, E., ... Tempia, F. (2019). Mice harbouring a SCA28 patient mutation in AFG3L2 develop late-onset ataxia associated

with enhanced mitochondrial proteotoxicity. *Neurobiology of Disease*, 124, 14–28. https://doi.org/10.1016/j.nbd.2018.10.018

Manduca, A., Bara, A., Larrieu, T., Lassalle, O., Joffre, C., Layé, S., & Manzoni, O. J. (2017). Amplification of mGlu5-Endocannabinoid Signaling Rescues Behavioral and Synaptic Deficits in a Mouse Model of Adolescent and Adult Dietary Polyunsaturated Fatty Acid Imbalance. *The Journal of Neuroscience*, *37*(29), 6851 LP – 6868. https://doi.org/10.1523/JNEUROSCI.3516-16.2017

Manes, M., Alberici, A., Di Gregorio, E., Boccone, L., Premi, E., Mitro, N., Pasolini, M. P., Pani, C., Paghera, B., Perani, D., Orsi, L., Costanzi, C., Ferrero, M., Zoppo, A., Tempia, F., Caruso, D., Grassi, M., Padovani, A., Brusco, A., & Borroni, B. (2017). Docosahexaenoic acid is a beneficial replacement treatment for spinocerebellar ataxia 38. *Annals of Neurology*, 82(4), 615–621. https://doi.org/10.1002/ana.25059

Manes, M., Alberici, A., Di Gregorio, E., Boccone, L., Premi, E., Mitro, N., Pasolini, M. P., Pani, C., Paghera, B., Orsi, L., Costanzi, C., Ferrero, M., Tempia, F., Caruso, D., Padovani, A., Brusco, A., & Borroni, B. (2019). Long-term efficacy of docosahexaenoic acid (DHA) for Spinocerebellar Ataxia 38 (SCA38) treatment: An open label extension study. *Parkinsonism and Related Disorders*, 63(February), 191–194. https://doi.org/10.1016/j.parkreldis.2019.02.040

Marcus, J., Honigbaum, S., Shroff, S., Honke, K., Rosenbluth, J., & Dupree, J. L. (2006). Sulfatide is essential for the maintenance of CNS myelin and axon structure. *Glia*, 53(4), 372–381. https://doi.org/10. 1002/glia.20292

Marr, D. (1969). A theory of cerebellar cortex. *J. Physiol*. 202, 437–470. doi: 10. 1113/jphysiol.1969.sp008820

Matsuzaka, T., Shimano, H., Yahagi, N., Kato, T., Atsumi, A., Yamamoto, T., Inoue, N., Ishikawa, M., Okada, S., Ishigaki, N., Iwasaki, H., Iwasaki, Y., Karasawa, T., Kumadaki, S., Matsui, T., Sekiya, M., Ohashi, K., Hasty, A. H., Nakagawa, Y., Takahashi, A., … Yamada, N. (2007). Crucial role of a long-chain fatty acid elongase, Elovl6, in obesity-induced insulin resistance. *Nature medicine,* 13(10), 1193–1202. https://doi.org/10.1038/nm1662

McNamara, R. K., Schurdak, J. D., Asch, R. H., Peters, B. D., & Lindquist, D. M. (2018). Deficits in docosahexaenoic acid accrual during adolescence reduce rat forebrain White matter microstructural integrity: An in vivo diffusion tensor imaging study. *Developmental Neuroscience*, 40, 84–92.

McNamara, R. K., Szeszko, P. R., Smesny, S., Ikuta, T., DeRosse, P., Vaz, F. M., Milleit, B., Hipler, U.-C., Wiegand, C., Hesse, J., Amminger, G. P., Malhotra, A. K., & Peters, B. D. (2017). Polyunsatu- rated fatty acid biostatus, phospholipase A2 activity and brain white matter microstructure across adolescence. *Neuroscience*, 343, 423–433.

McLoughlin, H. S., Moore, L. R., Chopra, R., Komlo, R., McKenzie, M., Blumenstein, K. G., Zhao, H., Kordasiewicz, H. B., Shakkottai, V. G., & Paulson, H. L. (2018). Oligonucleotide therapy mitigates disease in spinocerebellar ataxia type 3 mice. *Annals of Neurology*, 84(1), 64–77. https://doi.org/https://doi.org/10.1002/ana.25264

Min, Y., Kristiansen, K., Boggs, J. M., Husted, C., Zasadzinski, J. A., & Israelachvili, J. (2009). Interaction forces and adhesion of supported myelin lipid bilayers modulated by myelin basic protein. *Proceedings of the National Academy of Sciences of the United States of America*, 106 (9), 3154–3159. https://doi.org/10.1073/pnas.0813110106

Minghetti, L., Salvi, R., Lavinia Salvatori, M., Ajmone-Cat, M. A., De Nuccio, C., Visentin, S., Bultel-Poncé, V., Oger, C., Guy, A., Galano, J.-M., Greco, A., Bernardo, A., & Durand, T. (2014). Nonenzymatic oxygenated metabolites of α-linolenic acid B1- and L1-phytoprostanes protect immature neurons from oxidant injury and promote differentiation of oligodendrocyte progenitors through PPAR-γ activation. *Free Radical Biology & Medicine*, 73, 41–50.

Miyakawa, H., Lev-Ram, V., Lasser-Ross, N., and Ross, W. N. (1992). Calcium transients evoked by climbing fiber and parallel fiber synaptic inputs in guinea pig cerebellar Purkinje neurons. *J. Neurophysiol*. 68, 1178–1189.

Mondal, K., Takahashi, H., II, J. C., Mar, N. Del, Li, C., Stephenson, D., Chalfant, C., Allegood, J., Cowart, L. A., Reiner, A., & Mandal, N. A. (2021). N-3 polyunsaturated fatty acids (n-3 PUFA) prevent traumatic brain injury (TBI)-mediated visual and motor deficits in mice by

suppressing ceramide biosynthesis. *Investigative Ophthalmology & Visual Science*, *62*(8), 3030–3030.

Moon, Y. A., Shah, N. A., Mohapatra, S., Warrington, J. A., and Horton, J. D. (2001). Identification of a mammalian long chain fatty acyl elongase regulated by sterol regulatory element-binding proteins. *J. Biol. Chem*. 276, 45358–45366. doi: 10.1074/jbc.M108413200

Moon, Y.-A., Hammer, R. E., and Horton, J. D. (2009). Deletion of ELOVL5 leads to fatty liver through activation of SREBP-1c in mice. *J. Lipid Res*. 50, 412–423. doi: 10.1194/jlr.M800383-JLR200

Moon, Y. A., Ochoa, C. R., Mitsche, M. A., Hammer, R. E., and Horton, J. D. (2014). Deletion of ELOVL6 blocks the synthesis of oleic acid but does not prevent the development of fatty liver or insulin resistance. *J. Lipid Res*. 55, 2597–2605. doi: 10.1194/jlr.M054353

Mueller, N., Sassa, T., Morales-Gonzalez, S., Schneider, J., Salchow, D. J., Seelow, D., Knierim, E., Stenzel, W., Kihara, A., Schuelke, M. (2019). De novo mutation in ELOVL1 causes ichthyosis, acanthosis nigricans, hypomyelination, spastic paraplegia, high frequency deafness and optic atrophy. *J. Med. Genet.* 56, 164–175.

Nagaraja, R. Y., Sherry, D. M., Fessler, J. L., Stiles, M. A., Li, F., Multani, K., Orock, A., Ahmad, M., Brush, R. S., Anderson, R. E., Agbaga, M. P., & Deák, F. (2021). W246G Mutant ELOVL4 Impairs Synaptic Plasticity in Parallel and Climbing Fibers and Causes Motor Defects in a Rat Model of SCA34. *Molecular Neurobiology*, *58*(10), 4921–4943. https://doi.org/10.1007/s12035-021-02439-1

Nedelescu, H. & Abdelhack, M. (2013). Comparative morphology of dendritic arbors in populations of Purkinje cells in mouse sulcus and apex. *Neural Plast*. 948587

Nelson, D. L., & Cox, M. M. (2017). *Lehninger principles of biochemistry (7th ed.).* W.H. Freeman.

Nguyen, L. N., Ma, D., Shui, G., Wong, P., Cazenave-Gassiot, A., Zhang, X., Wenk, M., R., Goh, E., L., K., Silver, D., L. (2014). Mfsd2a is a transporter for the essential omega-3 fatty acid docosahexaenoic acid. *Nature* 509, 503–506. doi: 10.1038/nature13241

Niemelä, P., Hyvönen, M. T., & Vattulainen, I. (2004). Structure and dynamics of sphingomyelin bilayer: Insight gained through systematic comparison to phosphatidylcholine. *Biophysical Journal*, 87(5), 2976– 2989. https://doi.org/10.1529/biophysj.104.048702

Norton, W. T., & Poduslo, S. E. (1973). Myelination in rat brain: Changes in myelin composition during brain maturation. *Journal of Neurochemistry*, 21 (4), 759–773. https://doi.org/10.1111/j.1471-4159.1973.tb07520.x

O'Brien, J. S., & Sampson, E. L. (1965). Lipid composition of the normal human brain: Gray matter, white matter, and myelin. *Journal of Lipid Research*, 6(4), 537–544.

Ohler, B., Graf, K., Bragg, R., Lemons, T., Coe, R., Genain, C., & Husted, C. (2004). Role of lipid interactions in autoimmune demyelination. *Biochimica et Biophysica Acta*, 1688(1), 10–17. https://doi.org/10. 1016/j.bbadis.2003.10.001

Okuda, A., Naganuma, T., Ohno, Y., Abe, K., Yamagata, M., Igarashi, Y., Kihara, A. (2010). Hetero-oligomeric interactions of an ELOVL4 mutant protein: implications in the molecular mechanism of stargardt-3 macular dystrophy. *Mol. Vis*. 16, 2438–2445.

Ouellet, M., Emond, V., Chen, C. T., Julien, C., Bourasset, F., Oddo, S., et al. (2009). Diffusion of docosahexaenoic and eicosapentaenoic acids through the blood- brain barrier: an in situ cerebral perfusion study. *Neurochem. Int.* 55, 476–482. doi: 10.1016/j.neuint.2009.04.018

Ozaki, K., Doi, H., Mitsui, J., Sato, N., Iikuni, Y., Majima, T., Yamane, K., Irioka, T., Ishiura, H., Doi, K., Morishita, S., Higashi, M., Sekiguchi, T., Koyama, K., Ueda, N., Miura, Y., Miyatake, S., Matsumoto, N., Yokota, T., Tanaka, F., … Ishikawa, K. (2015). A Novel Mutation in ELOVL4 Leading to Spinocerebellar Ataxia (SCA) With the Hot Cross Bun Sign but Lacking Erythrokeratodermia: A Broadened Spectrum of SCA34. *JAMA neurology*, 72(7), 797–805. https://doi.org/10.1001/jamaneurol.2015.0610

Palmer, L. M., Clark, B. A., Gründemann, J., Roth, A., Stuart, G. J., & Häusser, M. (2010). Initiation of simple and complex spikes in cerebellar Purkinje cells. *The Journal of physiology*, 588(Pt 10), 1709–1717. https://doi.org/10.1113/jphysiol.2010.188300

Patterson, E., Wall, R., Fitzgerald, G. F., Ross, R. P., & Stanton, C. (2012). Health implications of high dietary omega-6 polyunsaturated Fatty acids. *Journal of Nutrition and Metabolism*, *2012*. https://doi.org/10.1155/2012/539426

Pauter, A. M., Olsson, P., Asadi, A., Herslof, B., Csikasz, R. I., Zadravec, D., Jacobsson, A. (2014). Elovl2 ablation demonstrates that systemic DHA is endogenously produced and is essential for lipid homeostasis in mice. *J. Lipid Res*. 55, 718–728. doi: 10.1194/jlr.M046151

Perkins, E. M., Clarkson, Y. L., Sabatier, N., Longhurst, D. M., Millward, C. P., Jack, J., Toraiwa, J., Watanabe, M., Rothstein, J. D., Lyndon, A. R., Wyllie, D. J., Dutia, M. B., & Jackson, M. (2010). Loss of beta-III spectrin leads to Purkinje cell dysfunction recapitulating the behavior and neuropathology of spinocerebellar ataxia type 5 in humans. *The Journal of neuroscience: the official journal of the Society for Neuroscience*, *30*(14), 4857–4867. https://doi.org/10.1523/JNEUROSCI.6065-09.2010

Pifferi, F., Laurent, B. and Plourde, M. (2021) Lipid Transport and Metabolism at the Blood-Brain Interface: Implications in Health and Disease. *Front. Physiol*. 12:645646. doi: 10.3389/fphys.2021.645646

Plourde, M., and Cunnane, S. C. (2007). Extremely limited synthesis of long chain polyunsaturates in adults: implications for their dietary essentiality and use as supplements. *Appl. Physiol. Nutr. Metab.* 32, 619–634. doi: 10.1139/H07-034

Poling, J.S., Vicini, S., Rogawski, M.A., Salem, Jr N. (1996). Docosahexaenoic acid block of neuronal voltage-gated K+ channels: subunit selective antagonism by zinc. *Neuropharmacology* 35:969–982.

Pujol-Lereis, L. M. (2019). Alteration of sphingolipids in biofluids: Implications for neurodegenerative diseases. *International Journal of Molecular Sciences*, 20(14), 3564–3584. https://doi.org/10.3390/ijms20143564

Purves, D. (2004). *Neuroscience. 6th edition.* Sunderland, Mass: Sinauer Associates, Publishers.

Quarles, R. H., Macklin, W. B., & Morell, P. (2005). Myelin formation, structure and biochemistry. In S. Brady, G. Siegel, R. W. Albers, & D. Price (Eds.), *Basic neurochemistry: Molecular, cellular and medical aspects* (7th ed., pp. 51–71). Elsevier Academic Press.

Ramakrishnan, H., Hedayati, K. K., Lüllmann-Rauch, R., Wessig, C., Fewou, S. N., Maier, H., Goebel, H.-H., Gieselmann, V., & Eckhardt, M. (2007). Increasing sulfatide synthesis in myelin-forming cells of arylsulfatase A deficient mice causes demyelination and neurological symptoms reminiscent of human metachromatic leukodystrophy. *The Journal of Neuroscience*, 27(35), 9482–9490. https://doi.org/10.1523/ JNEUROSCI.2287-07.2007

Rinaldo, L., and Hansel, C. (2013). Muscarinic acetylcholine receptor activation blocks long-term potentiation at cerebellar parallel fiber-Purkinje cell synapses via cannabinoid signaling. *Proc. Natl. Acad. Sci*. U S A 110, 11181–11186. doi: 10.1073/pnas.1221803110

Rizzi, T. S., van der Sluis, S., Derom, C., Thiery, E., van Kesteren, R. E., Jacobs, N., Van Gestel, S., Vlietinck, R., Verhage, M., Heutink, P., & Posthuma, D. (2013). FADS2 Genetic Variance in Combination with Fatty Acid Intake Might Alter Composition of the Fatty Acids in Brain. *PLOS ONE*, 8(6), e68000. https://doi.org/10.1371/journal.pone.0068000

Robertson, R. C., Seira Oriach, C., Murphy, K., Moloney, G. M., Cryan, J. F., Dinan, T. G., Paul Ross, R., & Stanton, C. (2017). Omega-3 polyunsaturated fatty acids critically regulate behaviour and gut microbiota development in adolescence and adulthood. *Brain, behavior, and immunity*, *59*, 21–37. https://doi.org/10.1016/j.bbi.2016.07.145

Robinet, P., Fradagrada, A., Monier, M. N., Marchetti, M., Cogny, A., Moatti, N., Paul, J.-L., Vedie, B., Lamaze, C. (2006). Dynamin is involved in endolysosomal cholesterol delivery to the endoplasmic reticulum: role in cholesterol homeostasis. *Traffic* 7, 811–823. doi: 10.1111/j.1600-0854.2006.00435.x

Roccaro-Waldmeyer, D. M., Girard, F., Milani, D., Vannoni, E., Prétôt, L., Wolfer, D. P., et al. (2018). Eliminating the VGlut2-dependent glutamatergic transmission of parvalbumin-expressing neurons leads to deficits in locomotion and vocalization, decreased pain sensitivity, and increased dominance. *Front. Behav. Neurosci*. 12. doi:10.3389/fnbeh.2018.00146.

Rodríguez-Cueto, C., Benito, C., Fernández-Ruiz, J., Romero, J., Hernández-Gálvez, M., & Gómez-Ruiz, M. (2014a). Changes in CB(1) and CB(2) receptors in the post-mortem cerebellum of humans affected by spinocerebellar ataxias. *British journal of pharmacology*, 171(6), 1472–1489. https://doi.org/10.1111/bph.12283

Rodríguez-Cueto, C., Benito, C., Romero, J., Hernández-Gálvez, M., Gómez-Ruiz, M., & Fernández-Ruiz, J. (2014b). Endocannabinoid-hydrolysing enzymes in the post-mortem cerebellum of humans affected by hereditary autosomal dominant ataxias. *Pathobiology: journal of immunopathology, molecular and cellular biology*, 81(3), 149–159. https://doi.org/10.1159/000358127

Russo, R., Cattaneo, F., Lippiello, P., Cristiano, C., Zurlo, F., Castaldo, M., Irace, C., Borsello, T., Santamaria, R., Ammendola, R., Calignano, A., & Miniaci, M. C. (2018). Motor coordination and synaptic plasticity deficits are associated with increased cerebellar activity of NADPH oxidase, CAMKII, and PKC at preplaque stage in the TgCRND8 mouse model of Alzheimer's disease. *Neurobiology of Aging*, 68, 123–133. https://doi.org/10.1016/j.neurobiolaging.2018.02.025

Sacco, T., Boda, E., Hoxha, E., Pizzo, R., Cagnoli, C., Brusco, A., & Tempia, F. (2010). Mouse brain expression patterns of Spg7, Afg3l1, and Afg3l2 transcripts, encoding for the mitochondrial m-AAA protease. *BMC Neuroscience*, 11(1), 1–9. https://doi.org/10.1186/1471-2202-11-55/FIGURES/3

Saeedimasine, M., Montanino, A., Kleiven, S., & Villa, A. (2019). Role of lipid composition on the structural and mechanical features of axonal membranes: A molecular simulation study. *Scientific Reports*, 9(1), 8000. https://doi.org/10.1038/s41598-019-44318-9

Safo, P. K., & Regehr, W. G. (2005). Endocannabinoids control the induction of cerebellar LTD. *Neuron*. https://doi.org/10.1016/j.neuron.2005.09.020

Sailer, A., Scholz, S. W., Nalls, M. A., Schulte, C., Federoff, M., Price, T. R., Lees, A., Ross, O. A., Dickson, D. W., Mok, K., Mencacci, N. E., Schottlaender, L., Chelban, V., Ling, H., O'Sullivan, S. S., Wood, N. W., Traynor, B. J., Ferrucci, L., Federoff, H. J., Mhyre, T. R., … European Multiple System Atrophy Study Group and the UK Multiple System Atrophy Study

Group (2016). A genome-wide association study in multiple system atrophy. *Neurology*, 87(15), 1591–1598. https://doi.org/10.1212/WNL.0000000000003221

Sakers, K., Lake, A. M., Khazanchi, R., Ouwenga, R., Vasek, M. J., Dani, A., & Dougherty, J. D. (2017). Astrocytes locally translate transcripts in their peripheral processes. *Proceedings of the National Academy of Sciences of the United States of America*, 114(19), E3830–E3838. https://doi.org/10.1073/pnas.1617782114

Salvati, S., Malvezzi Campeggi, L., Corcos Benedetti, P., Di Felice, M., Gentile, V., Nardini, M., & Tomassi, G. (1993). Effects of dietary oils on fatty acid composition and lipid peroxidation of brain membranes (myelin and synaptosomes) in rats. *The Journal of Nutritional Biochemistry*, 4(6), 346–350. https://doi.org/https://doi.org/10.1016/0955-2863(93)90080-G

Salvati, S., Natali, F., Attorri, L., Di Benedetto, R., Leonardi, F., Di Biase, A., Ferri, F., Fortuna, S., Lorenzini, P., Sanchez, M., Ricceri, L., & Vitelli, L. (2008). Eicosapentaenoic acid stimulates the expression of myelin pro- teins in rat brain. *Journal of Neuroscience Research,* 86, 776–784.

Sarna, J. R., Marzban, H., Watanabe, M., Hawkes, R. (2006) Complementary stripes of phospholipase Cβ3 and Cβ4 expression by Purkinje cell subsets in the mouse cerebellum. *J. Comp. Neurol*. 496, 303–313.

Sassa, T., and Kihara, A. (2014). Metabolism of very long-chain fatty acids: genes and pathophysiology. *Biomol. Ther*. 22, 83–92. doi: 10.4062/biomolther.2014. 017

Schmidt, H., & Knösche, T. R. (2019). Action potential propagation and synchronisation in myelinated axons. *PLoS Computational Biology*, 15 (10), e1007004. https://doi.org/10.1371/journal.pcbi.1007004

Seebungkert, B., Lynch, J.W. (2002). Effects of polyunsaturated fatty acids on voltage-gated K+ and Na+ channels in rat olfactory receptor neurons. *Eur J Neurosci* 16:2085–2094.

Serhan, C. N., Chiang, N., Dalli, J., and Levy, B. D. (2014). Lipid mediators in the resolution of inflammation. *Cold Spring Harb. Perspect. Biol.* 7:a016311. doi: 10.1101/cshperspect.a016311

Sezgin, E., Levental, I., Mayor, S., & Eggeling, C. (2017). The mystery of membrane organization: Composition, regulation and roles of lipid rafts. *Nature Reviews. Molecular Cell Biology*, 18(6), 361–374. https:// doi.org/10.1038/nrm.2017.16

Shakkottai, V. G., do Carmo Costa, M., Dell'Orco, J. M., Sankaranarayanan, A., Wulff, H., & Paulson, H. L. (2011). Early changes in cerebellar physiology accompany motor dysfunction in the polyglutamine disease spinocerebellar ataxia type 3. *The Journal of neuroscience: the official journal of the Society for Neuroscience*, 31(36), 13002–13014. https://doi.org/10.1523/JNEUROSCI.2789-11.2011

Sherry, D. M., Hopiavuori, B. R., Stiles, M. A., Rahman, N. S., Ozan, K. G., Deak, F., Agbaga, M. P., & Anderson, R. E. (2017). Distribution of ELOVL4 in the Developing and Adult Mouse Brain. *Front. Neuroanat*, 11, 38. https://doi.org/10.3389/fnana.2017.00038

Shikama, A., Shinozaki, H., Takeuchi, Y., Matsuzaka, T., Aita, Y., Murayama, T., Sawada, Y., Piao, X., Toya, N., Oya, Y., Takarada, A., Masuda, Y., Nishi, M., Kubota, M., Izumida, Y., Nakagawa, Y., Iwasaki, H., Kobayashi, K., Yatoh, S., Suzuki, H., … Yahagi, N. (2015). Identification of human ELOVL5 enhancer regions controlled by SREBP. *Biochemical and biophysical research communications*, 465(4), 857–863. https://doi.org/10.1016/j.bbrc.2015.08.101

Shuvaev, A. N., Hosoi, N., Sato, Y., Yanagihara, D., & Hirai, H. (2017). Progressive impairment of cerebellar mGluR signalling and its therapeutic potential for cerebellar ataxia in spinocerebellar ataxia type 1 model mice. *The Journal of physiology*, 595(1), 141–164. https://doi.org/10.1113/JP272950

Simons, K. (2016). Cell membranes: A subjective perspective. *Biochimica et Biophysica Acta*, 1858(10), 2569–2572. https://doi.org/10.1016/j. bbamem.2016.01.023

Smeets, C. J. L. M., & Verbeek, D. S. (2016). Climbing fibers in spinocerebellar ataxia: A mechanism for the loss of motor control. In *Neurobiology of Disease* (Vol. 88). https://doi.org/10.1016/j.nbd.2016.01.009

Standring S. (2015). *Gray's Anatomy. The Anatomical Basis of Clinical Practice (41st Edition*). Elsevier.

Stephens, G. J. (2016). Does modulation of the endocannabinoid system have potential therapeutic utility in cerebellar ataxia? *J. Physiol.* 594, 4631–4641. doi:10.1113/JP271106.

Stoyas, C. A., Bushart, D. D., Switonski, P. M., Ward, J. M., Alaghatta, A., Tang, M., Niu, C., Wadhwa, M., Huang, H., Savchenko, A., Gariani, K., Xie, F., Delaney, J. R., Gaasterland, T., Auwerx, J., Shakkottai, V. G., & La Spada, A. R. (2020). Nicotinamide Pathway-Dependent Sirt1 Activation Restores Calcium Homeostasis to Achieve Neuroprotection in Spinocerebellar Ataxia Type 7. *Neuron*, *105*(4), 630-644.e9. https://doi.org/https://doi.org/10.1016/j.neuron.2019.11.019

Strata, P., and Rossi, F. (1998). Plasticity of the olivocerebellar pathway. *Trends Neurosci*. 21, 407–413.

Suminaite, D., Lyons, D. A., & Livesey, M. R. (2019). Myelinated axon physiology and regulation of neural circuit function. *Glia*, 67(11), 2050– 2062. https://doi.org/10.1002/glia.23665

Sun, C., Zou, M., Wang, X., Xia, W., Ma, Y., Liang, S., Hao, Y., Wu, L., & Fu, S. (2018). FADS1- FADS2 and ELOVL2 gene polymorphisms in susceptibility to autism spectrum disorders in Chinese children. *BMC Psychiatry* 18:283. doi: 10.1186/s12888- 018- 1868- 7

Sural-Fehr, T., & Bongarzone, E. R. (2016). How membrane dysfunction influences neuronal survival pathways in sphingolipid storage disorders. *Journal of Neuroscience Research*, 94(11), 1042–1048. https://doi. org/10.1002/jnr.23763

Takano, M., Hikishima, K., Fujiyoshi, K., Shibata, S., Yasuda, A., Konomi, T., Hayashi, A., Baba, H., Honke, K., Toyama, Y., Okano, H., & Nakamura, M. (2012). MRI characterization of paranodal junction failure and related spinal cord changes in mice. *PLoS One*, 7(12), e52904. https://doi.org/10.1371/journal.pone.0052904

Tan, C. Y., Virtue, S., Bidault, G., Dale, M., Hagen, R., Griffin, J. L., & Vidal-Puig, A. (2015). Brown Adipose Tissue Thermogenic Capacity Is Regulated by Elovl6. *Cell reports*, 13(10), 2039–2047. https://doi.org/10.1016/j.celrep.2015.11.004

Tapiero, H., Nguyen Ba, G., Couvreur, P., & Tew, K. D. (2002). Polyunsaturated fatty acids (PUFA) and eicosanoids in human health and pathologies. *Biomedicine and Pharmacotherapy*, 56(5), 215–222. https://doi.org/10.1016/S0753-3322(02)00193-2

Tempia, F., Miniaci, M. C., Anchisi, D., & Strata, P. (1998). Postsynaptic Current Mediated by Metabotropic Glutamate Receptors in Cerebellar Purkinje Cells. *Journal of Neurophysiology*, *80*(2), 520–528. https://doi.org/10.1152/jn.1998.80.2.520

Tempia, F., Alojado, M. E., Strata, P., & Knöpfel, T. (2001). Characterization of the mGluR(1)-mediated electrical and calcium signaling in Purkinje cells of mouse cerebellar slices. *Journal of neurophysiology*, 86(3), 1389–1397. https://doi.org/10.1152/jn.2001.86.3.1389

Thaxton, C., & Bhat, M. A. (2009). Myelination and regional domain differentiation of the axon. *Results and Problems in Cell Differentiation*, 48, 1–28. https://doi.org/10.1007/400_2009_3

Thomazeau, A., Bosch-Bouju, C., Manzoni, O., and Layé, S. (2017). Nutritional n-3 PUFA deficiency abolishes endocannabinoid gating of hippocampal long-term potentiation. *Cereb. Cortex* 27, 2571–2579. doi: 10.1093/cercor/bhw052

Tian, C., Fan, C., Liu, X., Xu, F., & Qi, K. (2011). Brain histological changes in young mice submitted to diets with different ratios of n-6/n-3 polyunsaturated fatty acids during maternal pregnancy and lactation. *Clinical Nutrition*, 30, 659–667.

Tvrdik, P., Westerberg, R., Silve, S., Asadi, A., Jakobsson, A., Cannon, B., Loison, G., & Jacobsson, A. (2000). Role of a new mammalian gene family in the biosynthesis of very long chain fatty acids and sphingolipids. *The Journal of cell biology*, 149(3), 707–718. https://doi.org/10.1083/jcb.149.3.707

van Meer, G., Voelker, D. R., & Feigenson, G. W. (2008). Membrane lipids: Where they are and how they behave. *Nature Reviews Molecular Cell Biology*, 9(2), 112–124. https://doi.org/10.1038/nrm2330

Van Woerden, G. M., Hoebeek, F. E., Gao, Z., Nagaraja, R. Y., Hoogenraad, C. C., Kushner, S. A., Hansel, C., De Zeeuw, C. I., & Elgersma, Y. (2009). betaCaMKII controls the direction of

plasticity at parallel fiber-Purkinje cell synapses. *Nature Neuroscience*, *12*(7), 823–825. https://doi.org/10.1038/NN.2329

Vaz, F. M., McDermott, J. H., Alders, M., Wortmann, S. B., Kölker, S., Pras-Raves, M. L., Vervaart, M. A. T., van Lenthe, H., Luyf, A. C. M., Elfrink, H. L., Metcalfe, K., Cuvertino, S., Clayton, P. E., Yarwood, R., Lowe, M. P., Lovell, S., Rogers, R. C., Deciphering Developmental Disorders Study, van Kampen, A., ... Banka, S. (2019). Mutations in PCYT2 disrupt etherlipid biosynthesis and cause a complex hereditary spastic paraplegia. *Brain*, 142(11), 3382–3397. https://doi.org/10.1093/brain/awz291

Venkataraman, K., & Futerman, A. H. (2000). Ceramide as a second messenger: Sticky solutions to sticky problems. *Trends in Cell Biology*, 10(10), 408–412. https://doi.org/10.1016/s0962-8924(00) 01830-4

Voogd, J. & Glickstein, M. (1998). The anatomy of the cerebellum. *Trends Neurosci*, *21*:370-375.

Vreugdenhil, M, Bruehl, C, Voskuyl, RA, Kang, JX, Leaf, A, Wadman, WJ. (1996). Polyunsaturated fatty acids modulate sodium and calcium currents in CA1 neurons. *Proc Natl Acad Sci* 93:12559–12563

Wadiche, J. I. & Jahr, C. E. (2005). Patterned expression of Purkinje cell glutamate transporters controls synaptic plasticity. *Nature Neurosci*. 8, 1329–1334

Wallis, J. G., Watts, J. L., & Browse, J. (2002). Polyunsaturated fatty acid synthesis: What will they think of next? Trends in Biochemical Sciences, 27(9), 467–473. https://doi.org/10.1016/S0968-0004(02)02168-0

Walter, J. T., Alviña, K., Womack, M. D., Chevez, C., & Khodakhah, K. (2006). Decreases in the precision of Purkinje cell pacemaking cause cerebellar dysfunction and ataxia. *Nature Neuroscience*, *9*(3), 389–397. https://doi.org/10.1038/nn1648

Witte, A. V., Kerti, L., Hermannstädter, H. M., Fiebach, J. B., Schreiber, S. J., Schuchardt, J. P., Hahn, A., & Flöel, A. (2014). Long- chain omega-3 fatty acids improve brain function and structure in older adults. *Cerebral Cortex*, 24, 3059–3068.

Xiao, Y., Li, X. (1999). Polyunsaturated fatty acids modify mouse hippocampal neuronal excitability during excitotoxic or convulsant stimulation. *Brain Res* 846:112. –121.

Xiao, J., Cerminara, N. L., Kotsurovskyy, Y., Aoki, H., Burroughs, A., Wise, A., K., Luo, Y., Marhall S. P., Sugihara, I., Apps, R., Lang, E.J. (2014) Systematic Regional Variations in Purkinje Cell Spiking Patterns. *PLOS ONE* 9(8): e105633. https://doi.org/10.1371/journal.pone.0105633

Yang, W., Geng, C., Yang, Z., Xu, B., Shi, W., Yang, Y., Tian, Y. (2020). Deciphering the roles of caveolin in neurodegenerative diseases: the good, the bad and the importance of context. *Ageing Res. Rev.* 62:101116.

Yassine, H. N., Braskie, M. N., Mack, W. J., Castor, K. J., Fonteh, A. N., Schneider, L. S., Harrington, M. G., & Chui, H. C. (2017). Association of docosahexaenoic acid supplementation with Alzheimer disease stage in Apolipoprotein e ϵ4 carriers: A review. *JAMA Neurology*, *74*(3), 339–347. https://doi.org/10.1001/jamaneurol.2016.4899

Yehuda, S., Rabinovitz, S., Carasso, R. L., Mostofsky, D.I. (2002) The role of polyunsaturated fatty acids in restoring the aging neuronal membrane. *Neurobiol. Aging*, 23 , pp. 843-853, 10.1016/S0197-4580(02)00074-X

Young, C, Gean, PW, Chiou, LC, Shen, YZ. (2000). Docosahexaenoic acid inhibits synaptic transmission and epileptiform activity in therat hippocampus. *Synapse* 37:90–94.

Zang, Y. and De Schutter, E. (2019) Climbing Fibers Provide Graded Error Signals in Cerebellar Learning. *Front. Syst. Neurosci*. 13:46. doi: 10.3389/fnsys.2019.00046

Zhang, K., Kniazeva, M., Han, M., Li, W., Yu, Z., Yang, Z., Li, Y., Metzker, M. L., Allikmets, R., Zack, D. J., Kakuk, L. E., Lagali, P. S., Wong, P. W., MacDonald, I. M., Sieving, P. A., Figueroa, D. J., Austin, C. P., Gould, R. J., Ayyagari, R., & Petrukhin, K. (2001). A 5-bp deletion in ELOVL4 is associated with two related forms of autosomal dominant macular dystrophy. *Nature genetics*, 27(1), 89–93. https://doi.org/10.1038/83817

Zhang, M., Li, C. C., Li, F., Li, H., Liu, X. J., Loor, J. J., Kang, X. T., & Sun, G. R. (2017). Estrogen promotes hepatic synthesis of long-chain polyunsaturated fatty acids by regulating

ELOVL5 at post-transcriptional level in laying hens. *International Journal of Molecular Sciences*, 18(7), 1–15. https://doi.org/10.3390/ijms18071405

Zheng, W., Kollmeyer, J., Symolon, H., Momin, A., Munter, E., Wang, E., Kelly, S., Allegood, J. C., Liu, Y., Peng, Q., Ramaraju, H., Sullards, M. C., Cabot, M., & Merrill, A. H., Jr. (2006). Ceramides and other bioactive sphingolipid backbones in health and disease: Lipidomic analysis, metabolism and roles in membrane structure, dynamics, signaling and autophagy. *Biochimica et Biophysica Acta*, 1758(12), 1864–1884. https://doi.org/10.1016/j.bbamem.2006.08.009

RINGRAZIAMENTI

Alla fine di questo lungo percorso di alti e bassi, momenti di estrema felicità e profondo sconforto, mi sento di aver imparato molte più cose su me stessa di quanto (naturalmente) ho fatto della vita di laboratorio. Ho scoperto di essere una che non molla mai, che quando anche si indispettisce per gli imprevisti riesce a trovare subito un rimedio. Molte delle cose che ho scoperto sono dovute alle persone meravigliose che ho incontrato sul mio percorso. Penso a Marco, il mio confidente, amico, amore che mi sa sempre calmare, fa prendere meno seriamente me stessa, mi sa capire, essendo la metà perfetta della mia mela che da tempo speravo di trovare. Penso alla mia famiglia del NICO che per sei anni mi ha aiutata a crescere. Primo tra tutti il laboratorio del professor Filippo Tempia, che mi ha permesso di seguire da vicino le mie passioni e farmi diventare in tutto e per tutto una neuroscienziata. Poi Eriola, amica, capa, mamma e sorella che mi ha motivata, aiutata, istruita con le cose che sa fare, mi ha dato fiducia e mi ha reso "impermeabile" a molte cose che nella vita prima mi avrebbero affossato. Tutti gli studenti che sono passati prima o dopo al laboratorio, a partire da Emilia e Federica, le mie prime vere studentesse, amiche e compagne di gioia condivisa. Francesco, il mio piccolo grande uomo, Linda, la mia amica del cuore, Chiara B, Elisabetta e Marianna. Le mie amiche, non solo colleghe, sempre pronte a piangere, ridere e offrire un dolce (o un caffè alla macchinetta) ad ogni evenienza: Roberta, Chiara LR, Sara, Valentina, Brigitta, Nino, Sofia, Chiara O, Gaby. Siete la motivazione per cui ogni giorno è anche un po' felice anche quando sono triste, siete il motivo del mio "BUONGIORNO" mattutino. Ci sono poi gli amici di sempre, che mi hanno accompagnato e sostenuto in ogni passo e anche questa volta so essere pronti dietro la porta a festeggiare con me un altro traguardo, penso a Erika, Maria, Federica, Alessia, Lucrezia, Daniela, Marco, ma anche Alessia Z, Valentina, Ilaria, Stefano e Giulia. Siete il pilastro che regge la mia vita, essendo l'amicizia uno dei valori a cui tengo maggiormente, la nostra vera e sincera, so che sarà immutabile negli anni. Infine, la mia famiglia che mi ha sostenuta sempre, essendo tutti i giorni orgogliosi di me, i miei genitori, mia sorella Alice, mio nonno Gianni, mio cugino Leonardo, i miei zii, le mie cugine Chiara e Valeria, le mie nonne sempre nel mio cuore. La famiglia è la radice da cui un fiore che poi sboccia quindi ogni mio successo è anche un successo vostro.